DEVELOPMENT OF A HUMAN STEM CELL-BASED BLOOD-BRAIN BARRIER MODEL AND ITS USE IN THE STUDY OF DRUG TRANSPORT IN ALZHEIMER'S DISEASE

by

Jennifer L. Mantle

A dissertation submitted to the Faculty of the University of Delaware in partial fulfillment of the requirements for the degree of Doctor of Philosophy in Chemical Engineering

Fall 2017

DEVELOPMENT OF A HUMAN STEM CELL-BASED BLOOD-BRAIN BARRIER MODEL AND ITS USE IN THE STUDY OF DRUG TRANSPORT IN ALZHEIMER'S DISEASE

by

Jennifer L. Mantle

Approved: _____
Eric M. Furst, Ph.D.
Chair of the Department of Chemical and Biomolecular Engineering

Approved: _____
Babatunde A. Ogunnaike, Ph.D.
Dean of the College of Engineering

Approved: _____
Ann L. Ardis, Ph.D.
Senior Vice Provost for Graduate and Professional Education

I certify that I have read this dissertation and that in my opinion it meets the academic and professional standard required by the University as a dissertation for the degree of Doctor of Philosophy.

Signed: _____

Kelvin H. Lee, Ph.D.
Professor in charge of dissertation

I certify that I have read this dissertation and that in my opinion it meets the academic and professional standard required by the University as a dissertation for the degree of Doctor of Philosophy.

Signed: _____

April M. Kloxin, Ph.D.
Member of dissertation committee

I certify that I have read this dissertation and that in my opinion it meets the academic and professional standard required by the University as a dissertation for the degree of Doctor of Philosophy.

Signed: _____

Millicent O. Sullivan, Ph.D.
Member of dissertation committee

I certify that I have read this dissertation and that in my opinion it meets the academic and professional standard required by the University as a dissertation for the degree of Doctor of Philosophy.

Signed: _____

John H. Slater, Ph.D.
Member of dissertation committee

ACKNOWLEDGMENTS

First I would like to thank Kelvin Lee for his guidance and support throughout the past five years. He has high standards that challenged me to be a better scientist, a more creative problem solver and a more effective communicator. Some of the most valuable lessons learned include how to craft a better story with the information at hand, that interesting things happen when taking calculated risks, how to say only what you mean, and how to have an effective meeting in ten minutes or less. I truly appreciate his encouragement and support of personal and professional development activities, including the IGERT program, K-12 outreach at DBI and attending conferences, which have enhanced my graduate school experience.

I would next like to thank my committee members, April Kloxin, Millie Sullivan and John Slater, for their constructive feedback, thoughtful discussion, helpful suggestions and interest in my work. I'm especially grateful for the professional and personal mentorship of April Kloxin as my IGERT coadvisor. She helped me with communication, provided a fresh perspective on my work and also helped me prepare for having a child, and it was helpful to have someone to talk to who understood the demands of the academic world.

I want to thank the members of the Lee Lab, both past and present, for enriching my graduate school experience, and providing experimental advice, insightful questions, discussion and feedback: Diane Wuest, Kristin Valente, Ben Kremkow, Amalie Tuerk Levy, Josephine Chiu, Maddy Macdonald Stinner, John Ruanos-Salguero, Michael Gallucci, Victoria Hunt, Nate Hamaker, Doug Nmagu, Lie

Min, Jongyoun Baik, Xiaolin Zhang, Jing Guo and Leila Choe. To the grad students that came before me, your guidance helped me understand how to succeed in the lab and you talked me out of countless ruts. A special thanks to Leila Choe for all her expertise in the lab and for trading stories about breaking everything we touch.

I am grateful to the National Science Foundation Integrative Graduate Education and Research Traineeship (IGERT) program in Systems Biology of Cells in Engineered Environments (award #1144726) and the DBI Townsend Outreach Fellowship for providing the funds that supported my research. I want to acknowledge a number of individuals who provided research, scientific and experimental knowledge; this work would not have been possible without their assistance. Diane Wuest trained me in the lab and passed down all her BBB knowledge. Lie Min developed, performed and analyzed the MRM assays for small molecule and Alzheimer's drugs. Leila Choe provided training and assistance with the Luminex, 2D gels and many other lab techniques. John Ruanos-Salguero has shared the fun of iPSC culture, kept my cells alive, and shared his NSC-astrocyte know-how. Jongyoun Baik shared his cell culture and molecular biology technique expertise. Allison Wing performed stem cell growth curves, helped troubleshoot and fed cells. Kyle Gomes helped start the 3D BBB work and helped develop the endocytosis assay. Chandran Sabanayagam performed AFM of Aβ. Jeff Caplan, Jean Ross and Mike Moore provided training, troubleshooting and assistance with confocal microscopy. Additionally, I'd like to thank all the staff at DBI, particularly Connie Brantley, Michele Kleinhomer and Allie Sethman as well as Kathie Young in Chemical Engineering for always being helpful and kind.

Participating and leading the K-12 outreach program at DBI has been one of the most fulfilling aspects of my graduate career. I am grateful to have had the opportunity to work with Katie Lakofksy and Catherine Stoner; developing and running Sussex Science night events, incorporating more experiments into tours and spending time driving down to Sussex (including borrowing oysters for the evening) are some of my favorite outreach memories. A special thanks to Jeff Caplan, Debbie Powell, Erin Bernberg, Bruce Kingham and Michele Kleinhomer for entertaining our crazy outreach ideas and for taking the time out of your day to make the program better.

I would not have survived grad school without my UD friends, particularly Kaleigh Reno, Amalie Levy, Kristin Valente, and Ryan Patet. All the coffee dates at Brew HaHa!, lunches on main street, homework sessions in the first floor lounge, pep talks, gingerbread house competitions and other adventures have made my time at UD special. I am also grateful for my lifelong friends Katie Thelian, Merry Yannace, Briana Wildemann, Jackie Weiss, Mike Weiss and Anthony Panetta for their love, support and friendship.

I am extremely grateful for the love and unwavering support of my parents, Jean and Bob. My mom has been the best listener and has spent a lot of vacation time and weekends at our house with Ella so I could finish this degree. My dad has a wonderful way of putting things in perspective and reminding me not to let the little things get to me. My brother Jimmy has had sound advice and when all else fails, a knack for making beer. I am also grateful for the love and support of my second family, Kathy, Elton, Kevin, Lisa, David, and Brynn. I want to thank members of my

extended family, including my grandmothers Frances and Blanche, my grandfathers Stephen and Eddie and my godmother Joanne for always believing in me.

My daughter Ella has completely changed my perspective in the past six months, has taught me to not take myself so seriously and has made me want to be a better person and role model for her in the years to come. I can't begin to express the amount of love and gratitude I feel for my husband, Tom. His support, discussion, pep talks, advice and sense of humor keep me grounded and moving forward. I love you both and am incredibly fortunate and grateful to have such a wonderful, caring and loving family.

TABLE OF CONTENTS

LIST OF TABLES

LIST OF FIGURES

ABSTRACT

There are currently no FDA-approved therapeutics that can slow, halt, or prevent Alzheimer's disease (AD) and only five approved drugs that treat the cognitive symptoms associated with AD. One of the key challenges with treating neurological diseases such as AD is delivery of systemically-administered therapeutics in the blood across the blood-brain barrier (BBB) into the brain. The BBB, composed of the endothelial cells that line cerebral capillaries, tightly regulates transport of molecules between the blood and the brain parenchyma and in doing so, severely limits the transport of therapeutics for neurological disease. Immunotherapies are an attractive class of therapeutic for AD due to their high target specificity and affinity however they generally exhibit notoriously low brain transport. Furthermore, while many immunotherapy drug candidates have shown efficacy in preclinical animal models, none have demonstrated disease-modifying effects in human clinical trials; studying transport of therapeutics *in vivo* in humans is challenging. Therefore, the goal of this research is to develop a human cell-based *in vitro* BBB model and to apply the model to study transport of therapeutics in AD.

An ideal BBB model is made from human brain microvascular endothelial cells (BMECs), forms a tight barrier with *in vivo*-like transport restriction, and can be modified to mimic normal or pathological states. In this work, we differentiate human induced pluripotent stem cells into BMECs as the basis for the *in vitro* model which are capable of physiologically-relevant barrier performance. The model was characterized by measuring transendothelial electrical resistance (TEER), small

molecule permeability, expression of BMEC-specific proteins and directional transport of a known substrate. We evaluated the permeabilities of several known small molecule drugs that can serve as benchmarks for the evaluation of new therapeutics, and validated the benchmarking system with the FDA approved AD drugs. We established a relationship between TEER and brain permeability of two different classes of drugs, suggesting fundamental differences between how small and large molecule therapeutics are transported.

While studying transport of therapeutics, it is also important to consider the effects of pathological states on the BBB. AD is often accompanied by increases in plasma-derived proteins found in the brain and changes to expression or activity of transport proteins. Furthermore, molecular transport can be affected by secondary insults such as inflammation. The effects of pathological states on specific features of the BBB as well as the molecular mechanisms of immunotherapeutic transport are poorly understood. We employed a neuroinflammation model and observed impaired barrier function as measured by a decrease in barrier tightness and an increase in antibody transport. This response is partially mitigated by the presence of astrocytes. These results suggest that a breakdown in trancellular transport precedes any increase in paracellular permeability in disease and provide a link neuroinflammation and specific aspects of BBB breakdown. The model was lastly used to gain fundamental insights into the transport behavior of immunotherapies through the use of inhibitors and probes of different endocytic routes in normal, neuroinflammation and AD models. IgG transport is a saturable process and different endocytic pathways are likely responsible for IgG uptake in normal and pathological conditions.

Models of the cells that comprise and surround the BBB can facilitate a more thorough understanding of disease progression, help identify new therapeutic targets, and can advance the development of new therapeutics for neurodegenerative diseases capable of reaching targets in the brain. These findings offer critical insights into the direct effects of pathological states on barrier function and demonstrate that this *in vitro* model can be applied to study the transport of different classes of therapeutics from the blood to the brain. Furthermore, these efforts provide a basis for future studies of transport of therapeutics at the BBB in disease, and this approach can be extended to the study of other neurological diseases and classes of therapeutics.

Chapter 1

INTRODUCTION

1.1 Motivation and Background

1.1.1 Challenges of Treating Alzheimer's Disease

Alzheimer's disease (AD) is a neurodegenerative disease that affects 5.5 million people in the United States, including 5.3 million people over the age of 65. AD is the most common form of dementia, accounting for 60-80% of all dementia cases, and is the fifth leading cause of death in for those 65 and older. This disease is a huge financial burden, with estimated costs for AD and other dementias reaching $259 billion in 2017, and this disease takes an emotional toll on caregivers and family members of those affected. Despite the prevalence of AD, there are only five drugs that are FDA approved to temporarily improve the cognitive symptoms of the disease, but there are no therapies to slow, halt, or prevent AD. Without the development of disease-modifying treatments that can cure or prevent AD, the number of individuals over the age of 65 living with AD is projected to increase to 7.1 million by the year 2025 and to 13.8 million by 2050 (Alzheimer's Association 2017).

Alzheimer's disease is characterized microscopically by the presence of extracellular Aβ plaques and intraneuronal neurofibrillary tangles composed of

hyperphosphorylated tau. Cerebral amyloid angiopathy (CAA), or the accumulation of Aβ in the walls of cerebral arteries and capillaries (Thal et al., 2008) is present in over 80% of AD cases and in 10-40% of the elderly without AD (Attems et al., 2005; Bell and Zlokovic, 2009). On a larger scale, AD leads to brain atrophy in the cortex and most severely in the hippocampus, as well as enlarged ventricles and white matter abnormalities (Tarasoff-Conway et al., 2015). While progression of AD is widely studied, the initial cause and events that accelerate the disease are not well defined and likely occur decades before the onset of cognitive decline (Sperling et al., 2011). The predominant theory of AD is the amyloid hypothesis, which postulates that disease progression and subsequent neurodegeneration is driven by an imbalance in production and clearance of Aβ peptides, which leads to accumulation in the brain. The contributions of tau and neuroinflammation are being increasingly recognized as important in disease progression as well (Heppner et al., 2015). The alternate two-hit vascular hypothesis posits that vascular changes that precede AD, including hypoperfusion and blood-brain barrier (BBB) dysfunction, may lead to an increase in Aβ production or impaired Aβ clearance (Marchesi, 2011; Zlokovic, 2011).

There are many challenges associated with developing an effective therapeutic for AD, which include the high cost of drug development, the long time needed to observe the effects of treatments on disease progression, and the presence of the BBB, which protects the brain and prevents the entry of nearly all therapeutics. Between 2002 and 2012, there were 244 drugs tested in clinical trials for AD and only one of those treatments eventually gained approval from the FDA. It is widely accepted that

about 98% of small molecule drugs and nearly 100% of large molecule drugs delivered systemically are excluded from the brain (Pardridge, 2005).

Current treatments for AD include three cholinesterase inhibitors (donepezil, galantamine, rivastigmine), one N-methyl-D-aspartate (NMDA) inhibitor (memantine), and one donepezil/memantine combination treatment. These small molecule drugs are used to treat the cognitive symptoms of AD, including memory, mood, behavior, and the ability to perform daily functions. These medications are symptomatic treatments that help stabilize symptoms for a limited time but they cannot prevent or reverse the neuronal death that occurs as AD progresses or prolong the lives of patients (Alzheimer's Association 2017). A small molecule drug must be less than 400-500 Da in size, lipophilic and must not be a substrate of any efflux pumps at the BBB to be able to successfully cross from the blood into the brain (Pardridge, 2012), which severely limits the pool of available molecules to treat neurological diseases such as AD.

Passive immunotherapy against Aβ is an attractive strategy for modifying the progression of AD as antibody-based drugs have high target specificity and can recruit the body's own immune cells to clear Aβ-immune complexes. A key challenge of using these large-molecule therapeutics to treat a neurodegenerative disease like AD is their relative inability to cross the BBB. There have been a number of immunotherapies in clinical trials (including bapineuzumab, solaneuzumab, Gammagard IVIG, gantenerumab, ponezumab, crenezumab, BAN2401, and aducanumab), each targeting a different Aβ epitope or aggregate conformation

however despite preclinical efficacy, no AD immunotherapies are currently FDA approved (Lannfelt et al., 2014). Aducanumab, the most recent and promising anti-Aβ antibody-based therapy, has shown effectiveness in a double-blind, placebo-controlled Phase1B randomized trial (Sevigny et al., 2016). This drug reduced brain Aβ plaques in a dose- and time-dependent fashion in patients with prodromal or mild AD, has entered Phase III trials and has received fast-track designation from the FDA. In contrast to other immunotherapies, in preclinical studies aducanumab had a brain:plasma ratio of 1.3%, which is an order of magnitude higher than the commonly reported 0.1% of systemically-administered antibody able to penetrate the brain (Yu and Watts, 2013). This class of therapeutics could benefit from improved transport to the brain however the mechanism of antibody transport across the BBB is not well understood.

1.1.2 Transport at the Blood-Brain Barrier

The BBB, composed of brain microvascular endothelial cells (BMECs) that line cerebral capillaries, tightly regulates the neuronal microenvironment. BMECs maintain brain homeostasis via tight junction complexes between cells, specific expression of solute carriers, and expression of ABC-type efflux transporters. Tight junctions between cells have a “gate” function as they restrict paracellular permeability as well as a “fence” function as they segregate the luminal and abluminal membranes of BMECs, enabling polarization (Abbott et al., 2006; Abbott et al., 2010).

BMECs are located in close proximity to other cell types of the so-called neurovascular unit (NVU; **Figure 1.1**); pericytes cover an estimated 30% of the abluminal endothelial surface and astrocyte endfeet processes cover an estimated 99% of the abluminal surface of BMECs (Mathiisen et al., 2010). These cells play an important role in the development of BBB-specific properties as well as the maintenance of the adult BBB. The crosstalk between these cell types occurs via soluble factors and possibly through direct cell-cell contact (Abbott et al., 2006). Neurons and microgia are also located in close proximity to BMECs, and secreted molecules from these cell types have the potential to impact barrier function as well.

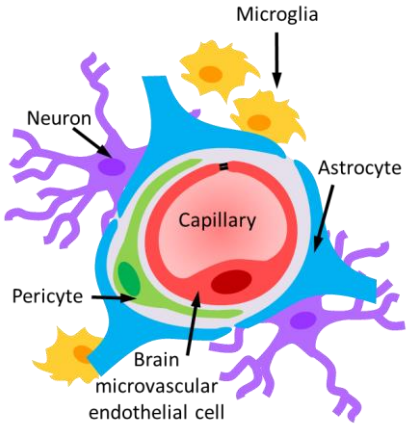

Figure 1.1. The neurovascular unit. The BBB is made of the brain microvascular endothelial cells that compose cerebral capillaries. Located in close proximity to these endothelial cells are pericytes and astrocytes that help maintain barrier function. Neurons and microglia are also located in close proximity to the NVU and can modulate barrier function as well.

A key feature that distinguishes the brain endothelium from other endothelium in the body is tightly controlled and often restrictive molecular transport. There are several different routes of transport across the BBB, depicted in **Figure 1.2**. Passive paracellular transport between cells is limited to hydrophilic molecules less than about 400 Da in size due to the presence of tight junctions. Some small lipophilic molecules are able to passively diffuse across the endothelial monolayer and drugs that treat CNS disorders often fall into this transport class. Solute carriers, such as the GLUT1 (glucose transporter 1) and LAT1 (L-system for large neutral amino acids) are responsible for moving nutrients across the BBB and can be bidirectional or can preferentially transport solutes in one direction. Efflux transporters, such as P-glycoprotein (P-gp), are generally located on the luminal membrane, where they move substances in the brain to blood direction. Many compounds that would otherwise passively diffuse across BMECs based on size and lipophilicity are substrates of efflux pumps and are instead excluded from the brain. Lastly, transcytosis across BMECs can occur via receptor-mediated transcytosis (e.g. transferrin and transferrin receptor), adsorptive-mediated transcytosis and non-specific fluid-phase macropinocytosis.

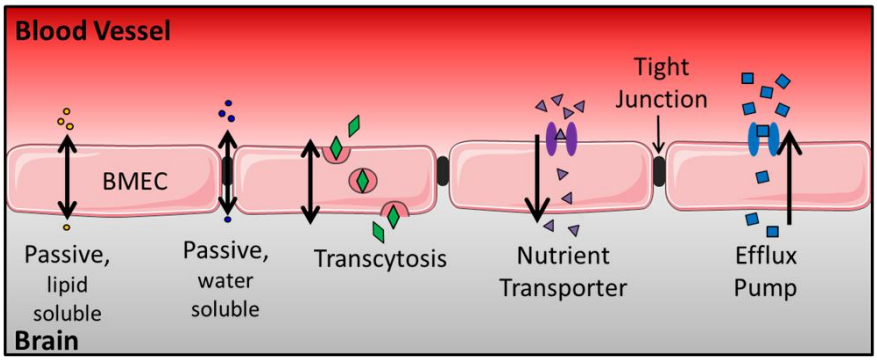

Figure 1.2. Transport routes across the BBB. Molecules can either be passively or actively transported across the BBB. Small hydrophilic molecules less than 400 Da may passively diffuse between cells while small lipophilic molecules may diffuse through cells. There are solute carriers responsible for nutrient transport across the BBB as well as efflux pumps that remove or exclude molecules from the brain. Lastly, transcytosis can be receptor-mediated, adsorptive, or via macropinocytosis, however this is not a major transport route compared to other endothelia in the body.

When developing a new therapeutic for AD or other neurological disorders, it is advantageous to understand the transport route from the blood to the brain. Immunotherapies are about three orders of magnitude larger (about 150 kDa) than the 400 Da size threshold for hydrophilic molecules to passively diffuse across the BBB, therefore these drugs must be transported through the cells. While receptor mediated transcytosis is responsible for transport of some specific compounds such as transferrin and insulin, transcytosis is not a major route of transport at the BBB. Compared to peripheral endothelium, BMECs have much lower levels of endocytosis and transcytosis, with only 1-10 vesicles per μm2 compared with 30-40 vesicles per μm2 in lung and intestinal capillary endothelium (Hamm et al., 2004; Ito et al., 1980; Stewart, 2000). Furthermore, there are no known transporters responsible for the transcytosis of antibodies. It is widely accepted that only 0.1% of an injected dose of

an antibody therapeutic will be able to penetrate the BBB, however questions still remain about how this small fraction is able to penetrate the BBB.

In AD, molecular transport mechanisms are altered which may affect treatment efficiency and distribution of a drug in the brain (Schenk and Vries, 2016). Vascular changes, such as a reduction in cerebral blood flow and BBB dysfunction may precede the onset of neurodegeneration and cognitive symptoms (Bell and Zlokovic, 2009). Studies have shown an increase in albumin and other blood-derived proteins in the cerebrospinal fluid of patients with AD (Erickson and Banks, 2013), indicative of increased BBB permeability. Studies have shown reduced expression of lipoprotein receptor related protein-1 (LRP1), responsible for reduced clearance of Aβ (Deane et al., 2009), reduced expression of GLUT1 leading to lower brain glucose uptake (Winkler et al., 2015), and reduced activity and expression of P-gp (Hartz et al., 2016) in AD. Furthermore, secondary events such as inflammation, both a risk factor and a contributor to disease progression (Heppner et al., 2015), may also alter transport properties at the BBB. Brain microvessels from AD patients secrete increased levels of inflammatory molecules such as tumor necrosis factor alpha (TNF-α) and interleukin (IL-6) compared to healthy individuals (Grammas and Ovase, 2001). Inflammation is known to increase macropinocytosis (Lim and Gleeson, 2011; Preston et al., 2014) and an increase in vesicular transcytosis has been shown in other pathological conditions such as hypoxia, ischemia, and injury (De Bock et al., 2016). How changes to transport might affect therapeutic delivery over the course of AD is not well understood.

1.1.3 *In Vitro* Blood-Brain Barrier Models

Before a new drug candidate can be approved by the FDA and marketed to patients, it must go through a series of preclinical *in vitro* and *in vivo* animal tests, followed by clinical trials for safety, dosing and efficacy. The process from discovery to final approval often takes at least ten years and is estimated to cost $2.56 billion (DiMasi et al., 2016). In particular for Alzheimer's disease, nearly all of the potential therapeutics that show efficacy in animal models have failed to show safety or clinical effect in human trials. Better preclinical models have the potential to ensure that only the most promising candidates go through development and clinical trials. *In vitro* models provide a simplified, tunable and more high-throughput way to study transport of therapeutics across the BBB in a cost effective way, when compared to *in vivo* models (Naik and Cucullo, 2012).

In vitro BBB models are most commonly constructed by growing monolayer of BMECs on a Transwell cell culture insert that is placed into a well filled with media. The monolayer of cells separates the model into the "blood" (top; luminal; apical) compartment and the "brain" (bottom; abluminal; basolateral) compartment (**Figure 1.3**). Molecules of interest can be introduced to either compartment and the amount transported can be quantified over time to investigate permeability, transport rate, or efflux ratio. Increasing layers of complexity can be added to the model via soluble factors in the media or coculture with other NVU cell types such as astrocytes, pericytes, neurons, or differentiating neural progenitor cells (Helms et al., 2016;

Lippmann et al., 2014; Nakagawa et al., 2007; Weidenfeller et al., 2007; Wuest and Lee, 2012).

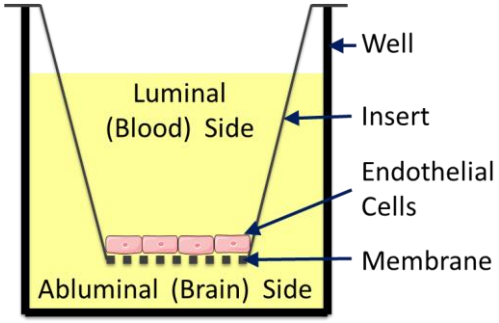

Figure 1.3. *In vitro* BBB model. BMECs are grown in a monolayer on a permeable membrane located within a Transwell cell culture insert. By placing the insert into a culture well, the monolayer of cells separates the model into "blood" and "brain" compartments.

An ideal *in vitro* BBB model recapitulates the barrier function and transport behavior of the *in vivo* BBB and allows for studies of tight junctions, transporters, enzymes, molecular trafficking and is suitable for permeability screening of new therapeutics (Helms et al., 2016). The quality of a BBB model is commonly assessed by measuring transendothelial electrical resistance (TEER), permeability of small tracer molecules such as sodium fluorescein (376 Da), Lucifer yellow (444 Da), sucrose (342 Da) and mannitol (180 Da), and expression BMEC-specific proteins. TEER greater than 1500 $\Omega \cdot cm^2$ is considered a minimum *in vivo* benchmark; this value is considerably higher than the TEER of 2-20 $\Omega \cdot cm^2$ expected in peripheral capillaries (Butt et al., 1990). Another verification of the presence of tight junctions is

the localization of proteins such as occludin and claudin-5 to the membranes between cells. High claudin-5 expression is indicative of a BBB phenotype and is essential for a tight barrier (Abbott et al., 2006). Lastly, bidirectional transport of substrates with and without inhibitors can verify both the functionality of transporters and the proper polarization of the cell monolayer.

BMECs can be sourced from primary cells, cell lines, or stem cells and can be from animal or human sources (1.1; Reviewed by Helms et al., 2016). Primary mouse and rat models typically have TEER values between 100-300 $\Omega \cdot cm^2$ although higher TEER values may be achieved with optimal conditions. Although these cells are relatively easy to source, multiple animals are required per experiment and the barrier is considerably looser than the *in vivo* BBB. A number of common drugs such as acetaminophen and caffeine have been shown to have higher permeability in an *in vitro* rat model compared to a human model, limiting the utility of rodent models to study transport of human therapeutics (Lacombe et al., 2011). BMECs from bovine or porcine sources yield considerably more cells per isolation and can achieve 1000-2000 $\Omega \cdot cm^2$ average TEER values in optimized conditions. Additionally, a quantitative proteomics comparison of isolated brain capillaries from multiple sources showed that porcine BMECs expressed ABC transporters and had a ratio of different efflux pumps more similar to monkey and human than rodent BMECs (Kubo et al., 2015). While these barrier properties are more desirable than primary rodent cells, large animal brains are not easily sourced. Lastly, in general primary cell isolation is time consuming, requires considerable expertise, and may still be variable between labs and

within the same lab. Helms et al. demonstrated that TEER values ranged from 327 to 2555 Ω·cm² across batches within the same study using bovine BMECs (Helms et al., 2014). Primary cultures from human sources would be ideal for studying transport of therapeutics, however these cells are challenging to obtain and are often isolated from surgical material (Bernas et al., 2010), which is not representative of healthy tissue (Wilhelm et al., 2011).

Table 1.1. TEER values for BBB models derived from primary, cell line, and stem cell sources. (Adapted from Helms et al., 2016)

	Primary murine	**Primary bovine**	**Primary human**	**Cell line murine**	**Cell line human**	**hiPSC-derived**
TEER (Ω·cm²)	100-300	1000-2000	n/a	< 50	30-50	2000+

Immortalized cell lines are often readily available and can be used for multiple passages, eliminating sourcing issues of primary cells. The mouse bEnd.3 cell line is commercially available however it rarely reaches TEER values greater than 50 Ω·cm² (Brown et al., 2007; Omidi et al., 2003). The cEND and cerebEND mouse cell lines can achieve TEER values as high as 1000 Ω·cm² with media additives (Blecharz et al., 2008) however species differences between mouse and human still remain. The immortalized human cell line hCMEC/D3 can be cultured for many passages and eliminates species differences however it suffers from low TEER values ranging from 30-50 Ω·cm². TEER can be improved through the incorporation of physiologically relevant shear stress or coculture with astrocytes and/or pericytes however it still

remains about an order of magnitude lower than the desired 1500 Ω·cm² *in vivo* threshold.

Differentiation from human stem cell sources provides an attractive alternative to primary cells and immortalized cell lines as these cells are of human origin, renewable in culture and exhibit an *in vivo*-like barrier phenotype. Lippmann et al. developed a technique to differentiate human induced pluripotent stem cells (hPSCs) into BMECs that express BMEC-specific proteins such as occludin, claudin-5, VE-cadherin, ZO-1, GLUT-1, and P-gp, have low permeability to sucrose and other small molecules, exhibit polarized transport of P-gp substrates, and have TEER values that exceed 2000 Ω·cm² (Lippmann et al., 2012; Lippmann et al., 2014). These hPSC-derived BMECs also respond to coculture with pericytes and a mixture of astrocytes and neurons differentiated from neural progenitor cells (NPCs; Lippmann et al., 2014). The hPSCs are cultured for nine days in unconditioned medium that allows codifferentiation of endothelial cells and neural cells, switched to an endothelial cell specific media for two days, and subcultured onto a substrate that selectively allows growth of endothelial cells, yielding a nearly 100% pure BMEC population after 11 days (Lippmann et al., 2012). This robust protocol successfully yields BMECs from multiple hPSC and embryonic stem cell sources (Appelt-Menzel et al., 2017; Katt et al., 2016; Lippmann et al., 2012; Lippmann et al., 2014; Patel et al., 2017). An *in vitro* BBB model using hPSC-derived BMECs is a promising tool for the study of human neurological disease and transport of therapeutics.

1.2 Project Goals

The goal of this work is to develop an *in vitro* BBB model system derived entirely from human stem cell sources and apply the model to understand transport of therapeutics in AD. This goal was accomplished through three specific objectives:

(1) *Develop and validate hPSC-derived in vitro BBB model*: hPSC culture and differentiation protocols were implemented and improved for consistent differentiation into BMECs with physiologically-relevant properties. The model was validated by measuring TEER, expression of BMEC-specific proteins, small molecule permeability and P-gp efflux as described in Chapter 2. Astrocytes derived from human neural stem cells were grown in coculture to demonstrate the interaction between BMECs and other cell types of the NVU in Chapter 3.

(2) *Demonstrate model utility for studying therapeutic transport in AD*: Different TEER thresholds were established as minimum criteria for studying both small and large molecule therapeutics in. The model was used to quantify blood-to-brain transport of the four FDA-approved drug substances used to treat the symptoms of AD as well as a model large molecule therapeutic in Chapter 2. Chapter 4 describes the use of inhibitors and probes of specific endocytic routes to gain a better understanding of the transport mechanisms of immunotherapies at the BBB.

(3*) Demonstrate model utility for studying disease stimuli in AD*: The model response to disease stimuli was characterized, including barrier integrity, transport behavior, and secretion of inflammatory cytokines. The contributions of BMECs and

astrocytes to these changes were investigated in Chapter 3. Relative changes in different endocytic routes were quantified in the presence of AD stimuli in Chapter 4.

REFERENCES

Abbott NJ, Patabendige AAK, Dolman DEM, Yusof SR, Begley DJ. 2010. Structure and function of the blood-brain barrier. Neurobiol. Dis. 37:13–25.

Abbott NJ, Rönnbäck L, Hansson E. 2006. Astrocyte-endothelial interactions at the blood-brain barrier. Nat. Rev. Neurosci. 7:41–53.

Alzheimer's Association. 2017. 2017 Alzheimer's disease facts and figures. Alzheimer's Dement.13:325-373.

Appelt-Menzel A, Cubukova A, Günther K, Edenhofer F, Piontek J, Krause G, Stüber T, Walles H, Neuhaus W, Metzger M. 2017. Establishment of a Human Blood-Brain Barrier Co-culture Model Mimicking the Neurovascular Unit Using Induced Pluri- and Multipotent Stem Cells. Stem Cell Reports 8:894–906.

Attems J, Jellinger KA, Lintner F. 2005. Alzheimer's disease pathology influences severity and topographical distribution of cerebral amyloid angiopathy. Acta Neuropathol. 110:222–231.

Bell RD, Zlokovic BV. 2009. Neurovascular mechanisms and blood-brain barrier disorder in Alzheimer's disease. Acta Neuropathol. 118:103–113.

Bernas M, Cardoso F, Daley S. 2010. Establishment of primary cultures of human brain microvascular endothelial cells: a new and simplified method to obtain cells for an in vitro model of the blood. Nat. Protoc. 5:1265–1272.

Blecharz KG, Drenckhahn D, Forster CY. 2008. Glucocorticoids increase VE-cadherin expression and cause cytoskeletal rearrangements in murine brain endothelial cEND cells. J. Cereb. Blood Flow Metab. 28:1139–1149.

Brown RC, Morris AP, O'Neil RG. 2007. Tight junction protein expression and barrier properties of immortalized mouse brain microvessel endothelial cells. Brain Res. 1130:17–30.

Butt AM, Jones HC, Abbott NJ. 1990. Electrical resistance across the blood-brain barrier in anaesthetized rats: a developmental study. J. Physiol. 429:47–62.

De Bock M, Van Haver V, Vandenbroucke RE, Decrock E, Wang N, Leybaert L. 2016. Into rather unexplored terrain—transcellular transport across the blood-brain barrier. Glia 64:1097–1123.

Deane R, Bell RD, Sagare A, Zlokovic BV. 2009. Clearance of amyloid-beta peptide across the blood-brain barrier: implication for therapies in Alzheimer's disease. CNS Neurol. Disord. Drug Targets 8:16–30.

DiMasi JA, Grabowski HG, Hansen RW. 2016. Innovation in the pharmaceutical industry: New estimates of R&D costs. J. Health Econ. 47:20–33.

Erickson MA, Banks WA. 2013. Blood–Brain Barrier Dysfunction as a Cause and Consequence of Alzheimer's Disease. J. Cereb. Blood Flow Metab. 33:1500–1513.

Grammas P, Ovase R. 2001. Inflammatory factors are elevated in brain microvessels in Alzheimer's disease. Neurobiol. Aging 22:837–842.

Hamm S, Dehouck B, Kraus J, Wolburg-Buchholz K, Wolburg H, Risau W, Cecchelli R, Engelhardt B, Dehouck MP. 2004. Astrocyte mediated modulation of blood-brain barrier permeability does not correlate with a loss of tight junction proteins from the cellular contacts. Cell Tissue Res. 315:157–166.

Hartz AMS, Zhong Y, Wolf A, LeVine H, Miller DS, Bauer B. 2016. Aβ40 Reduces P-Glycoprotein at the Blood-Brain Barrier through the Ubiquitin-Proteasome Pathway. J. Neurosci. 36:1930–1941.

Helms HC, Abbott NJ, Burek M, Cecchelli R, Couraud P-O, Deli MA, Förster C, Galla HJ, Romero IA, Shusta EV, Stebbins MJ, Vandenhaute E, Weksler B, Brodin B. 2016. In vitro models of the blood-brain barrier: An overview of commonly used brain endothelial cell culture models and guidelines for their use. J. Cereb. Blood Flow Metab. 36:862–890.

Helms HC, Hersom M, Kuhlmann LB, Badolo L, Nielsen CU, Brodin B. 2014. An Electrically Tight In Vitro Blood-Brain Barrier Model Displays Net Brain-to-Blood Efflux of Substrates for the ABC Transporters, P-gp, Bcrp and Mrp-1. AAPS J. 16:1046–1055.

Heppner FL, Ransohoff RM, Becher B. 2015. Immune attack: the role of inflammation in Alzheimer disease. Nat. Rev. Neurosci. 16:358–372.

Ito U, Ohno K, Yamaguchi T, Takei H, Tomita H, Inaba Y. 1980. Effect of hypertension on blood-brain barrier. Change after restoration of blood flow in post-ischemic gerbil brains. An electronmicroscopic study. Stroke. 11:606–611.

Katt ME, Xu ZS, Gerecht S, Searson PC. 2016. Human Brain Microvascular Endothelial Cells Derived from the BC1 iPS Cell Line Exhibit a Blood-Brain Barrier Phenotype. PLoS One 11.

Kubo Y, Ohtsuki S, Uchida Y, Terasaki T. 2015. Quantitative Determination of Luminal and Abluminal Membrane Distributions of Transporters in Porcine Brain Capillaries by Plasma Membrane Fractionation and Quantitative Targeted Proteomics. J. Pharm. Sci. 104:3060–3068.

Lacombe O, Videau O, Chevillon D, Guyot A-C, Contreras C, Blondel S, Nicolas L, Ghettas A, Bénech H, Thevenot E, Pruvost A, Bolze S, Krzaczkowski L, Prévost C, Mabondzo A. 2011. In vitro primary human and animal cell-based blood-brain barrier models as a screening tool in drug discovery. Mol. Pharm. 8:651–663.

Lannfelt L, Relkin NR, Siemers ER. 2014. Amyloid-β-directed immunotherapy for Alzheimer's disease. J. Intern. Med. 275:284–295.

Lim JP, Gleeson PA. 2011. Macropinocytosis: an endocytic pathway for internalising large gulps. Immunol. Cell Biol. 89:836–843.

Lippmann ES, Al-Ahmad A, Azarin SM, Palecek SP, Shusta EV. 2014. A retinoic acid-enhanced, multicellular human blood-brain barrier model derived from stem cell sources. Sci. Rep. 4:4160.

Lippmann ES, Azarin SM, Kay JE, Nessler RA, Wilson HK, Al-Ahmad A, Palecek SP, Shusta EV. 2012. Derivation of blood-brain barrier endothelial cells from human pluripotent stem cells. Nat. Biotechnol. 30:783–791.

Marchesi VT. 2011. Alzheimer's dementia begins as a disease of small blood vessels, damaged by oxidative-induced inflammation and dysregulated amyloid metabolism: implications for early detection and therapy. FASEB J. 25:5–13.

Mathiisen TM, Lehre KP, Danbolt NC, Ottersen OP. 2010. The perivascular astroglial sheath provides a complete covering of the brain microvessels: An electron microscopic 3D reconstruction. Glia 58:1094–1103.

Naik P, Cucullo L. 2012. In Vitro Blood–Brain Barrier Models: Current and Perspective Technologies. J. Pharm. Sci. 101:1337–1354.

Nakagawa S, Deli MA, Nakao S, Honda M, Hayashi K, Nakaoke R, Kataoka Y, Niwa M. 2007. Pericytes from brain microvessels strengthen the barrier integrity in primary cultures of rat brain endothelial cells. Cell. Mol. Neurobiol. 27:687–694.

Omidi Y, Campbell L, Barar J, Connell D, Akhtar S, Gumbleton M. 2003. Evaluation of the immortalised mouse brain capillary endothelial cell line, b.End3, as an in vitro blood-brain barrier model for drug uptake and transport studies. Brain Res. 990:95–112.

Pardridge WM. 2012. Drug Transport across the Blood–Brain Barrier. J. Cereb. Blood Flow Metab. 32:1959–1972.

Pardridge WM. 2005. The blood-brain barrier: Bottleneck in brain drug development. NeuroRX 2:3–14.

Patel R, Page S, Al-Ahmad AJ. 2017. Isogenic blood-brain barrier models based on patient-derived stem cells display inter-individual differences in cell maturation and functionality. J. Neurochem. 142:74–88.

Preston JE, Joan Abbott N, Begley DJ. 2014. Transcytosis of macromolecules at the blood-brain barrier. Adv. Pharmacol. 71: 147–163.

Schenk GJ, Vries HE De. 2016. Altered blood–brain barrier transport in neuro-inflammatory disorders. Drug Discov. Today Technol. 20:5–11.

Sevigny J, Chiao P, Bussière T, Weinreb PH, Williams L, Maier M, Dunstan R, Salloway S, Chen T, Ling Y, Gorman JO, Qian F, Arastu M, Li M, Chollate S, Brennan MS, Quintero-Monzon O, Scannevin RH, Arnold HM, Engber T, Rhodes K, Ferrero J, Hang Y, Mikulskis A, Grimm J, Hock C, Nitsch RM, Sandrock A. 2016. The antibody aducanumab reduces Aβ plaques in Alzheimer's disease. Nature 537:50–56.

Sperling RA, Aisen PS, Beckett LA, Bennett DA, Craft S, Fagan AM, Iwatsubo T, Jack CR, Kaye J, Montine TJ, Park DC, Reiman EM, Rowe CC, Siemers E, Stern Y, Yaffe K, Carrillo MC, Thies B, Morrison-Bogorad M, Wagster MV, Phelps CH. 2011. Toward defining the preclinical stages of Alzheimer's disease: Recommendations from the National Institute on Aging-Alzheimer's Association workgroups on diagnostic guidelines for Alzheimer's disease. Alzheimer's Dement. 7:280–292.

Stewart PA. 2000. Endothelial Vesicles in the Blood-Brain Barrier: Are They Related to Permeability? Cell. Mol. Neurobiol. 20:149–163.

Tarasoff-Conway JM, Carare RO, Osorio RS, Glodzik L, Butler T, Fieremans E, Axel L, Rusinek H, Nicholson C, Zlokovic BV., Frangione B, Blennow K, Ménard J, Zetterberg H, Wisniewski T, de Leon MJ. 2015. Clearance systems in the brain—implications for Alzheimer disease. Nat. Rev. Neurol. 11:457–470.

Thal DR, Griffin WST, de Vos RAI, Ghebremedhin E. 2008. Cerebral amyloid angiopathy and its relationship to Alzheimer's disease. Acta Neuropathol. 115:599–609.

Weidenfeller C, Svendsen CN, Shusta EV. 2007. Differentiating embryonic neural progenitor cells induce blood-brain barrier properties. J. Neurochem. 101:555–565.

Wilhelm I, Fazakas C, Krizbai IA. 2011. In vitro models of the blood-brain barrier. Acta Neurobiol. Exp. 71:113–128.

Winkler EA, Nishida Y, Sagare AP, Rege SV, Bell RD, Perlmutter D, Sengillo JD, Hillman S, Kong P, Nelson AR, Sullivan JS, Zhao Z, Meiselman HJ, Wenby RB, Soto J, Abel ED, Makshanoff J, Zuniga E, De Vivo DC, Zlokovic BV. 2015. GLUT1 reductions exacerbate Alzheimer's disease vasculo-neuronal dysfunction and degeneration. Nat. Neurosci. 18:521–530.

Wuest DM, Lee KH. 2012. Optimization of endothelial cell growth in a murine in vitro blood-brain barrier model. Biotechnol. J. 7:409–417.

Yu YJ, Watts RJ. 2013. Developing Therapeutic Antibodies for Neurodegenerative Disease. Neurotherapeutics 10:459–472.

Zlokovic BV. 2011. Neurovascular pathways to neurodegeneration in Alzheimer's disease and other disorders. Nat. Rev. Neurosci. 12:723–738.

Chapter 2

MINIMUM TRANSENDOTHELIAL ELECTRICAL RESISTANCE THRESHOLDS FOR THE STUDY OF SMALL AND LARGE MOLECULE DRUG TRANSPORT

2.1 Preface

This work was adapted from Mantle, Min and Lee (2016) with permission (see Appendix A). This chapter develops and validates the human stem cell-derived blood-brain barrier model and establishes minimum model criteria for studying transport of small and large molecule therapeutics. We wish to thank Abraham J. Al-Ahmad, Hannah K. Wilson, Matthew J. Stebbins, Eric V. Shusta, and Sean P. Palacek at the University of Wisconsin Madison for their instruction and discussion. Allison Wing performed cell counts on hPSCs in E8 and mTeSR1. This work was funded in part by the National Science Foundation (Award Number 1144726).

2.1.1 Abstract

A human cell-based *in vitro* model that can accurately predict drug penetration into the brain as well as metrics to assess these *in vitro* models are valuable for the development of new therapeutics. Here, human induced pluripotent stem cells (hPSCs) are differentiated into a polarized monolayer that express blood–brain barrier (BBB)-

specific proteins and have transendothelial electrical resistance (TEER) values greater than 2500 Ω·cm2. By assessing the permeabilities of several known drugs, a benchmarking system to evaluate brain permeability of drugs was established. Furthermore, relationships between TEER and permeability to both small and large molecules were established, demonstrating that different minimum TEER thresholds must be achieved to study the brain transport of these two classes of drugs. This work demonstrates that this hPSC-derived BBB model exhibits an *in vivo*-like phenotype, and the benchmarks established here are useful for assessing functionality of other *in vitro* BBB models.

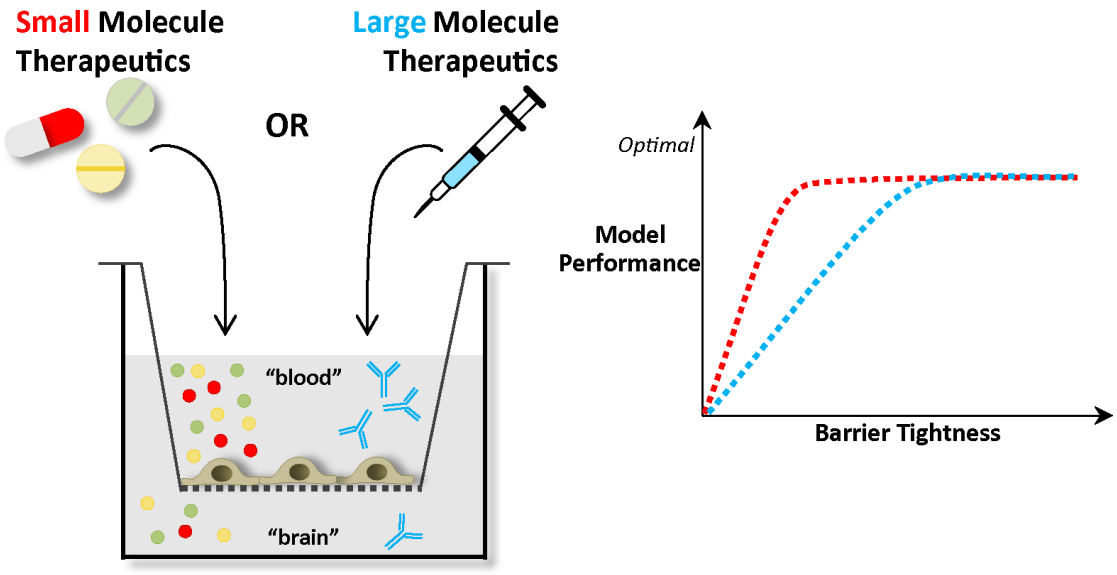

Figure 2.1. Chapter 2 overview schematic. The hPSC-derived BBB model consists of a monolayer of brain endothelial cells grown on a permeable membrane within a Transwell insert. By placing the insert into a culture well, the monolayer of cells separates the "blood" side (top) from the "brain" side (bottom). The hPSC-BBB model is useful for studying both small molecule therapeutics (red) and large molecule therapeutics (blue) such as antibodies. This work demonstrates that different thresholds of barrier tightness are required to study these two different classes of drugs, with a tighter barrier required to study large molecule therapeutics.

2.2 Introduction

Transport of therapeutics across the blood-brain barrier (BBB), which lies at the interface of the central nervous system (CNS) and the cerebral vasculature, is one of the key challenges prohibiting effective CNS disease treatment. A priori predictions of BBB permeability, such as Lipinski's Rule of Five (Lipinski et al., 1997), cannot fully capture the complexities of transport at the BBB based on molecular properties alone. Many *in vitro* models exist, including a model derived from induced pluripotent stem cells that is human-based, and physiologically-relevant (Lippmann et al., 2012;

Lippmann et al., 2014). However, an understanding of the properties of *in vitro* models, and how they relate to key *in vivo* properties, particularly small and large molecule drug permeability, is needed to use *in vitro* models in a predictive way.

The brain microvascular endothelial cells (BMECs) that line cerebral capillaries and compose the BBB exhibit many specialized properties that are often difficult to mimic *in vitro*. BMECs tightly regulate the neuronal microenvironment via tight junctions that restrict passive paracellular transport of hydrophilic molecules larger than 400 Da (Pardridge, 2012). In addition, BMECs contain specific transport systems to regulate active transcellular transport that allow entry of specific nutrients such as glucose, but exclude many small lipophilic compounds (Abbott et al., 2006; Abbott et al., 2010). Due to low rates of endocytosis and transcytosis activity at the BBB, large molecules such as proteins and peptides are generally excluded from the brain unless they are specifically transported via receptor mediated transcytosis (Abbott et al., 2006; Abbott et al., 2010). While murine, rat, bovine, porcine, and human primary and cell line models have been developed, these *in vitro* models may not properly mimic *in vivo* BBB properties or these cell types may not be commercially available and challenging to obtain (Helms et al., 2016). For example, existing models typically exhibit low transendothelial electrical resistance (TEER). The murine bEnd.3 (Brown et al., 2007; Omidi et al., 2003) and the human hCMC/D3 (Förster et al., 2008; Weksler et al., 2005) achieve TEER values below 50 Ω·cm2 and primary cell-based models (Wuest and Lee, 2012) rarely exceed 500 Ω·cm2 however in comparison, TEER values measured *in vivo* in rats are as high as 1500-6000 Ω·cm2

(Butt et al., 1990). Despite considerable progress towards developing *in vitro* BBB models, very few metrics exist to compare molecular transport in *in vitro* BBB models to *in vivo* BBB transport in humans.

With the goal of developing a physiologically-relevant, human, *in vitro* BBB model and establishing minimum model criteria, human induced pluripotent stem cells (hPSCs) are differentiated into BMECs as described by Lippmann et al. (Lippmann et al., 2012; Lippmann et al., 2014). A key step in reproducibly differentiating stem cells is maintenance of hPSCs in a pluripotent state. Previous studies have shown that human embryonic stem cells maintained in different media types and passaged via enzymatic vs. non enzymatic methods result in karyotypic changes (Buzzard et al., 2004; Draper et al., 2004; Mitalipova et al., 2005), changes to DNA methylation (Garitaonandia et al., 2015), and shifts in central carbon metabolism (Badur et al., 2015). To use this hPSC-derived BBB model for the screening of therapeutics, a better understanding of the transport behavior of well-studied drugs is required to serve as a benchmark for new drugs. Although *in vivo* permeability values of many drugs exist for rodents, these values are largely unavailable for humans.

In this work, the effects of two commonly-used hPSC maintenance media, mTeSRTM1 (Ludwig et al., 2006; Thomson and Ludwig, 2012) and TeSRTM-E8 (Chen et al., 2011), on stem cell growth rate and barrier function after differentiation into BMECs were investigated. After optimizing and evaluating the BBB phenotype of the differentiated cells, physiologically-relevant metrics for the *in vitro* hPSC-derived BBB model were established. The permeabilities of many small molecules

were measured using a multiplexed multiple reaction monitoring (MRM) assay to establish these benchmarks. Finally, distinct relationships between TEER and molecular transport of both small molecules and large proteins, two common classes of therapeutics, were established.

2.3 Materials and Methods

2.3.1 hPSC Culture and *In Vitro* Model Set Up

iPS(IMR90)-4 hPSCs (WiCell, Madison, WI; (Yu et al., 2007) were maintained on growth factor-reduced Matrigel (Fisher Scientific, Hampton, NH) in mTeSR1 medium or E8 medium (STEMCELL Technologies, Vancouver, BC, Canada) and passaged using Versene (Life Technologies, Carlsbad, CA) and mechanical dissociation. hPSCs were counted using the Trypan blue exclusion method and a hemocytometer (Fuchs Rosenthal, Horsham, PA). Cells were differentiated as described by Lippmann et al. (Lippmann et al., 2014) with the following modifications. After six days in unconditioned medium (UM; DMEM/Ham's F-12 (Life Technologies) containing 20% KnockOut Serum Replacement (Life Technologies), 1% MEM Non-Essential Amino Acid Solution (Life Technologies), 0.5% L-glutamine (Life Technologies) and 0.0015% β-mercaptoethanol (Sigma-Aldrich, St. Louis, MO), culture medium was switched to endothelial cell media (EC; Human Endothelial-SFM (HESFM; Life Technologies) supplemented with 1% platelet-poor derived serum (PDS; Alfa Aesar, Ward Hill, MA) and 200 ng/mL basic

fibroblast growth factor (bFGF; R&D Systems, Minneapolis, MN)) with 10 μM retinoic acid (RA; Sigma-Aldrich). After two days in EC with RA, differentiated BMECs were passaged using Versene and mechanical dissociation onto 24-well Transwell cell culture inserts (PET unless otherwise specified; 0.4 μm pores; Fisher Scientific) pre-treated for a minimum of four hours with 40% collagen IV (Sigma-Aldrich) and 10% fibronectin solution (Sigma-Aldrich). Cells were cultured on inserts for up to five days in EC medium,2 EC- medium (HESFM, 1% PDS),3 EC- with RA medium (ECSFM, 1% PDS, 1 μM RA) or enhanced medium (EM) (HESFM, 550 nM hydrocortisone, 312.4 μM adenosine 3',5'-cyclic monophosphate sodium salt (cAMP; Enzo Life Sciences, Farmingdale, NY), 17.4 μM phosphodiesterase inhibitor (Enzo Life Sciences), 5 μg/mL insulin (Sigma-Aldrich), 5 μg/mL transferrin (Sigma-Aldrich), 5 ng/mL sodium selenite (Sigma-Aldrich) and 1 μM RA).23 Alternately, differentiated BMECs were passaged onto glass-bottom 24-well plates (Cellvis, Mountain View, CA) coated with a 1:8 dilution of the collagen/fibronectin solution for immunocytochemistry experiments.

2.3.2 Immunocytochemistry and Confocal Microscopy

Cells were washed once with Dulbecco's phosphate-buffered saline (DPBS; Life Technologies) and fixed in 2% paraformaldehyde (Electron Microscopy Sciences, Hatfield, PA) in DPBS for 15 minutes. After three washes with DPBS, cells were permeabilized with 0.1% Triton X-100 in DPBS (Sigma-Aldrich) for 5 minutes and

blocked for 1 hour in 10% goat serum (Sigma-Aldrich) in DPBS. All antibody solutions (mouse anti-Claudin-5, rabbit anti-occludin, rabbit anti-ZO-1, mouse anti-GLUT-1; Life Technologies; mouse anti-P-gp; Fisher Scientific) were prepared in 10% goat serum in DPBS. Cells were incubated overnight at 4°C with 1 μg/mL (8 μg/mL for anti-P-gp) primary antibody solution. After three DPBS washes, cells were incubated for 1 hour with 4 μg/mL secondary antibody solution (AlexaFluor 488 conjugated goat anti-rabbit or AlexaFluor 488 conjugated goat anti-mouse; Life Technologies). Cells were washed three times in DPBS and incubated with 300 nM DAPI (Life Technologies) in DPBS for 10 minutes, followed by three DPBS washes and visualization. All immunocytochemistry was performed on cells after 2 days of culture on glass-bottom plates. Images were taken with a 40x water immersion objective on a Zeiss LSM 710 confocal microscope.

2.3.3 Transendothelial Electrical Resistance Measurements

Cell culture inserts were transferred to an Endohm-6 chamber (World Precision Instruments, Sarasota, FL) containing appropriate media and the overall resistance of the cell monolayer and membrane was measured using an EVOM2 Epithelial Volt Meter (World Precision Instruments). The resistance of a blank culture insert coated with collagen IV and fibronectin solution was measured and subtracted from each experimental value. The resulting value was multiplied by the membrane surface area to obtain the TEER value in Ω·cm2.

2.3.4 Sodium Fluorescein Permeability Measurements

To achieve different TEER values, cells were seeded at different densities and visually inspected for monolayer formation. After TEER measurements were complete, media was aspirated from the luminal and abluminal compartments, 0.1 mL of 100 μM sodium fluorescein (Sigma-Aldrich) in transport buffer, (10mM HEPES, 0.1% (w/v) bovine serum albumin, 4.5% (w/v) glucose; Sigma Aldrich) was added to the top compartment and 0.6 mL of transport buffer was added to the bottom compartment. 100 μL samples were collected from the bottom compartment every 15 minutes for 1 hour and transferred to a 96-well plate. 100 μL transport buffer were replaced in the bottom compartment. The 96-well plate was analyzed for fluorescence (excitation = 460 nm, emission = 515 nm) with a Spectra Max M5 spectrophotometer (Molecular Devices, Sunnyvale, CA). The solute permeability coefficient Ps (cm/s) was calculated using:

$$P_s = \frac{C_A * V_A}{t * S * C_L}$$

where CA is the abluminal concentration, VA is the abluminal volume, t is the amount of time, S is the surface area of the membrane and CL is the luminal concentration. The permeability of the cell monolayer was calculated by subtracting the inverse of the permeability of a blank insert coated with collagen and fibronectin from the inverse of the total permeability coefficient. Dilution due to removing and adding transport buffer in the abluminal compartment was also accounted for in the calculation (Deli et al., 2005).

2.3.5 IgG Quantification Assay

10 mg/mL Gammagard Liquid Immune Globulin Intravenous (Human) 10% (IVIG; Lot # LE12L017AB; Baxter, Westlake Village, CA) was added to the luminal compartment and 100 μL samples were collected from the abluminal compartment at 6, 12 and 24 hours and replaced with culture media. Transport of IgG antibodies was quantified using the Easy-Titer ® Human IgG Assay Kit (Thermo Fisher Scientific, Waltham MA) according to the manufacturer's protocol. Dilutions as well as blank permeability values were accounted for in permeability calculations.

2.3.6 P-glycoprotein Efflux Assay

The transport of the fluorescent P-glycoprotein (P-gp) substrate Rhodamine-123 (Sigma-Aldrich) was quantified in both the abluminal to luminal and the luminal to abluminal directions, with and without the P-gp inhibitor cyclosporin A (Sigma-Aldrich). All media was aspirated from top and bottom compartments and replaced with media containing 5 μM cyclosporin A or equivalent concentration DMSO (Sigma-Aldrich) as a control and incubated at 37°C for 1 hour. For luminal to abluminal studies, media in the top compartment was removed and replaced with media containing 10 μM Rhodamine 123 and inhibitor or control. For abluminal to luminal studies, media in the bottom compartment was removed and replaced with media containing 10 μM Rhodamine 123 and inhibitor or control. Every hour for three hours, 100 μL samples were collected and analyzed for fluorescence (excitation = 485

nm, emission = 530 nm) with the Spectra Max M5. To maintain constant volume, 100 μL of inhibitor or control media was replaced after each sample and dilutions were accounted for. Rates were calculated as the amount of Rhodamine 123 transported per unit time.

2.3.7 Drug Permeability Assay

All drugs (atenolol, caffeine, cimetidine, donepezil hydrochloride monohydrate, galantamine hydrobromide, hydroxyzine dihydrochloride, memantine hydrochloride, prazosin hydrochloride, propranolol hydrochloride, rivastigmine hydrogen tartrate, and trazodone hydrochloride; Sigma-Aldrich) were diluted to 1 mM in DMSO. Working drug solution was prepared by dissolving each drug to 10 μM in Ringer-HEPES buffer (Sigma-Aldrich) with 4.5% (w/v) glucose. After two days of growth in EC- media on Corning Transwell inserts (0.4 μM pores) and preliminary TEER measurements, the medium was removed and cells were incubated with 600 μL pre-warmed Ringer-HEPES buffer in the abluminal compartment and 100 μL pre-warmed working drug solution in the luminal compartment. Cells were incubated at 37°C and after 15 minutes, 50 μL samples were collected from the abluminal compartments and replaced with 50 μL of Ringer-HEPES buffer. Sample collection was repeated at 30, 40, 50, 60 and 90 minutes. All samples were stored at -20°C before an MRM assay was performed to quantify drug transport. Dilutions and permeability of a coated insert without cells were accounted for in the calculations.

2.3.8 Multiple Reaction Monitoring

LC-MRM analysis was performed on a QTRAP 2000 (AB Sciex, Foster City, CA) equipped with an Agilent 1100 HPLC (Agilent, Wilmington, DE). The abluminal drug permeability samples were supplemented with 1 μM amiloride (Sigma-Aldrich) as an internal standard and were centrifuged at 14,000 RPM for 5 minutes on an Eppendorf 5418 centrifuge (Eppendorf, Hauppauge, NY). 5 μL of the supernatant was injected onto a C18 reverse phase column (3 μm, 100 Å, 100 mm x 2 mm; Phenomenex, Torrance, CA) and gradient elution was performed with mobile phase A (0.1% formic acid in water; Avantor, Center Valley, PA) and B (0.1% formic acid in acetonitrile; Mallinckrodt Chemicals, St. Louis, MO) at a flow rate of 200 μL/min. For atenolol, caffeine, cimetidine, hydroxyzine, prazosin, propranolol, and trazodone, a program of 2% B for 9 min, 2-95% B in 6 min, and 95% B for 9 min was used to elute the analytes. For Alzheimer's disease drugs (donepezil, galantamine, memantine, rivastigmine), a program of 2% B for 6 min, 2-20% B in 1 min, 20% B for 6 min, 20-35% B in 1 min, 35% B for 2 min, 35-80% B in 3 min, 80% B for 2 min, 80-95% B in 1 min, 95% B for 3 min was used to elute the analytes. The eluted analytes were directly ionized with a TurboV™ source and data were acquired at 5500 V and 450°C in positive MRM mode. MRM assay parameters for each analyte, precursor (Q1) ion, product ion (Q3), decluster potential (DP), collision energy (CE), and dwell time are described in 2.1. Analytes with multiple transitions were treated as technical replicates

for quantification. MRM data were processed with Analyst 1.6.2 (AB Sciex) in Quant Mode. All measurements were made with both technical and biological duplicates.

Table 2.1. MRM Assay Parameters. Precursor ion (Q1), product ion (Q3), dwell time (ms), decluster potential (DP), collision energy (CE) shown for each compound.

Type	Compound	Q1 (m/z)	Q3 (m/z)	Dwell time (ms)	DP (v)	CE (v)
General	Atenolol	267.1	145	50	45	33
	Atenolol	267.1	190	50	45	20
	Caffeine	195.1	138.06	50	52	25
	Caffeine	195.1	110	50	52	30
	Cimetidine	253.2	95	50	45	37
	Cimetidine	253.2	117	50	45	22
	Hydroxyzine	375.2	201	50	55	27
	Hydroxyzine	375.2	166.2	50	55	55
	Prazosin	384.1	95	50	43	75
	Prazosin	384.1	231	50	43	75
	Propranolol	260.2	116	50	62	23
	Trazodone	372.2	176.2	50	45	31
	Trazodone	372.2	148	50	45	45
Alzheimer's drugs	Donepezil	380.3	91.1	50	70	30
	Rivastigmine	251.2	206.2	50	50	18
	Galantamine	288.2	213.1	50	50	30
	Galantamine	288.2	231.1	50	50	20
	Memantine	180.2	163.2	50	50	20
	Memantine	180.2	107.2	50	50	33
Internal standard	Amiloride	230.1	171	50	30	22
	Amiloride	230.1	115.9	50	30	42

2.3.9 Statistical Analysis

JMP® v11.0 (SAS Institute Inc. Cary, NC) was used for statistical analysis. Statistical evaluation of data was performed using Student's t-test and analysis of

variance (ANOVA) with $\alpha = 0.05$. Error bars represent standard error of the mean calculated over 3 independent experiments unless otherwise noted.

2.4 Results and Discussion

2.4.1 hPSCs Maintained in TeSR™-E8 and mTeSR™1 Exhibit Similar Growth and Differentiation

hPSC maintenance in a pluripotent state is an important step prior to differentiation into BMECs, therefore two widely-used media, TeSR™-E8 and mTeSR™1, were compared for hPSC growth rate and how well each media supported later differentiation into BMECs. The morphology of the cells maintained in the different media was similar (Figure 2.2, A), however the cells maintained in TeSR™-E8 appeared larger and colonies appeared more round with less jagged edges than those maintained in mTeSR™1. hPSCs maintained in TeSR™-E8 and mTeSR™1 media exhibit similar growth rates in a pluripotent state (Figure 2.2, B) and have similar properties after differentiation into BMECs. After the 11 day differentiation process into BMECs, cells sourced from the different hPSC media achieved similar peak TEER values of greater than 1,000 $\Omega \cdot cm^2$ (Figure 2.2, C).

These data provide a direct comparison of hPSCs in two feeder-free media and demonstrate the robustness and reproducibility of the differentiation of hPSCs into BMECs grown in either media. Stem cells maintained on mouse embryonic fibroblasts in standard unconditioned medium (Lippmann et al., 2012; Lippmann et al., 2014), on

matrigel in mTeSR™1 (Lippmann et al., 2012; Lippmann et al., 2014) and on matrigel in TeSR™-E8 (Katt et al., 2016) have been differentiated into BMECs but there have been no direct comparisons between methods. TeSR™-E8 is a cost-effective alternative to mTeSR™1 for the growth and differentiation of hPSCs into BMECs.

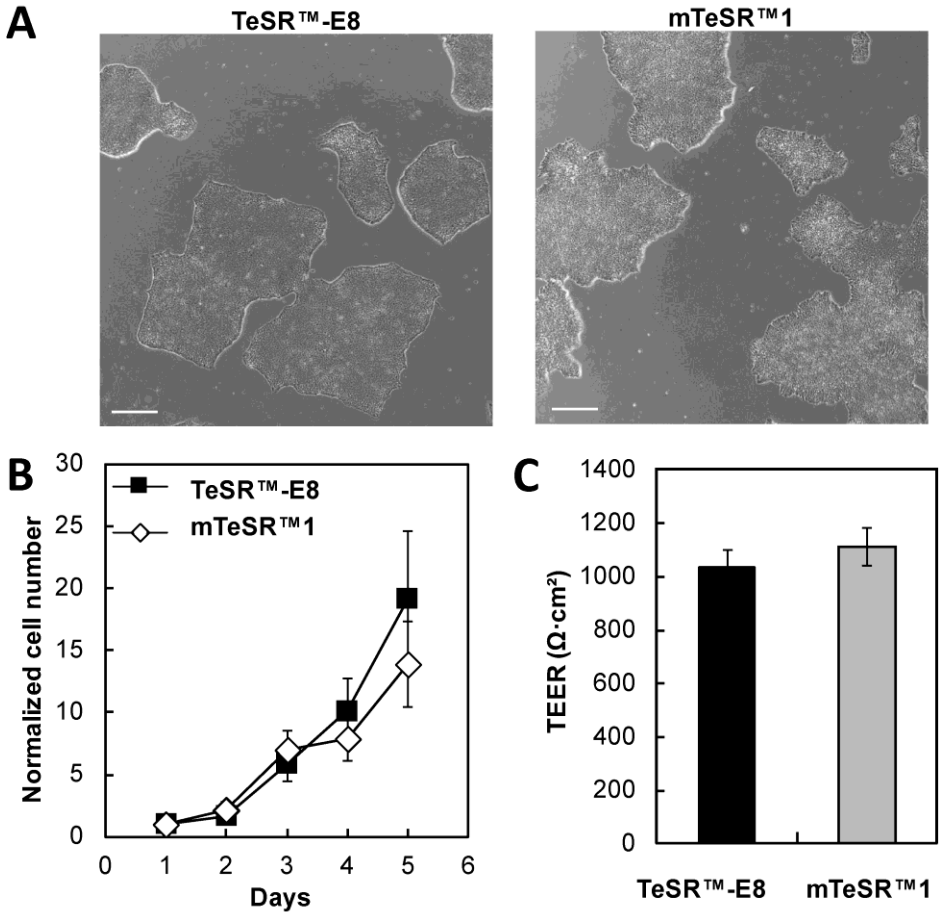

Figure 2.2. hPSCs maintained in mTeSR™1 and TeSR™-E8: growth rate and and TEER after differentiation. (A) hPSCs maintained in TeSR™-E8 (left) are larger and flatter than those maintained in mTeSR™1 (right; scale bars 400 μm). (B) Growth rates of hPSCs maintained in TeSR™-E8 and mTeSR™1 (n=8; mean ± SEM). Cell counts for each day were normalized to number of cells on Day 1. (C) TEER after differentiation of hPSCs maintained in both media types (n=9, biological & technical triplicate; mean ± SEM).

2.4.2 Differentiated BMECs Exhibit a Polarized BBB-like Phenotype in Monoculture

To properly mimic the characteristics of the BBB, hPSC-derived BMECs must form a polarized monolayer and express BBB-specific markers such as tight junction proteins and transporters. Immunocytochemistry of the tight junction proteins ZO-1, Occludin and Claudin-5 confirmed the presence and proper localization of tight junctions at the contact points between cells (Figure 2.3, A-C). The glucose transporter GLUT1 and the efflux pump P-gp are also expressed in the hPSC-BMECs (Figure 2.3, D, E) throughout cell membranes. The functional polarity of the hPSC-BMECs in monoculture was assessed by examining the directional transport of the P-gp substrate Rhodamine 123. The transport rate of Rhodamine 123 in the abluminal to luminal direction was four-fold greater than transport in the luminal to abluminal direction (Figure 2.4, A). When the cells were incubated with 5 μM of the P-gp inhibitor cyclosporin A, the transport rate in the abluminal to luminal direction decreased by 18% and transport rate in the luminal to abluminal direction increased by 35%.

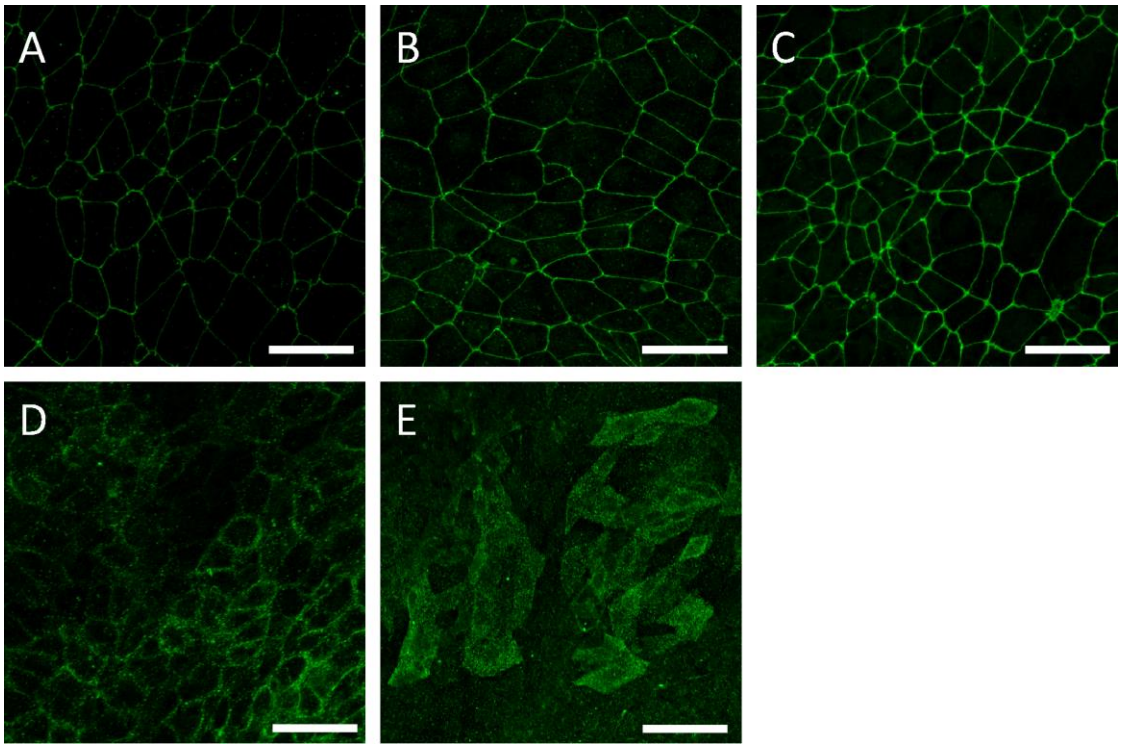

Figure 2.3. hPSC-derived BMECs express tight junction proteins and transporters. Differentiated hPSCs express the tight junction proteins Claudin 5 (A), Occludin (B), and ZO1 (C) localized to the junctions between cells. hPSC-BMECs also express the glucose transporter GLUT1 (D) and the efflux pump P-gp (E). Scale bars are 50 μm.

The directional transport of a P-gp substrate as well as the presence and proper localization of five BMEC markers confirms that the cells exhibit a BBB-like phenotype at the protein expression level. The P-gp activity assay revealed that this efflux pump is functional and preferentially transports substrate in the brain to blood direction. The ratio of transport rates (out: in) is consistent with a previous report of a Rhodamine 123 permeability ratio in iPSC-derived BMECs (Katt et al., 2016). In other cell line or primary models, BMECs are often cocultured with other cell types

from the neurovascular unit such as astrocytes, pericytes, and neurons, to improve barrier function and to impart polarization (Helms et al., 2016), however here the hPSC-BMECs are polarized without the need for additional cell types, which simplifies the model.

2.4.3 BMEC Media Impacts Barrier Integrity Over Time

Media additives are commonly used in BBB models to enhance barrier performance and the effects of these additives on peak barrier function and TEER over time are important to consider when choosing a media for a particular application. To study the impact of media additives on the physical barrier properties of BMECs, four different endothelial cell media were compared. The highest peak TEER values were achieved with the leanest media investigated (EC-). In addition, TEER was maintained more consistently over time by growth in media containing RA, and cells grown in media containing bFGF had the lowest overall TEER (Figure 2.4, B). The TEER of cells grown in EC- media peaked on Day 2 with a value of 2474 ± 65 Ω·cm², remained elevated for Day 3, and then began to decline at the highest rate. The second highest TEER was achieved by cells grown in EC- with RA, which peaked at 2125 ± 303 Ω·cm², remained elevated for Day 3, and declined slowly through Day 5. Cells grown in EM, the serum-free additive-heavy media, peaked on Day 3 with a TEER of 1739 ± 217 Ω·cm² although it remained elevated through the remainder of the experiment with no significant decline. The TEER of EC cells had the lowest peak of

the four media studied at 1062 ± 79 Ω·cm² on Day 2 and while it dropped on Day 3, it remained constant from Day 3 through Day 5.

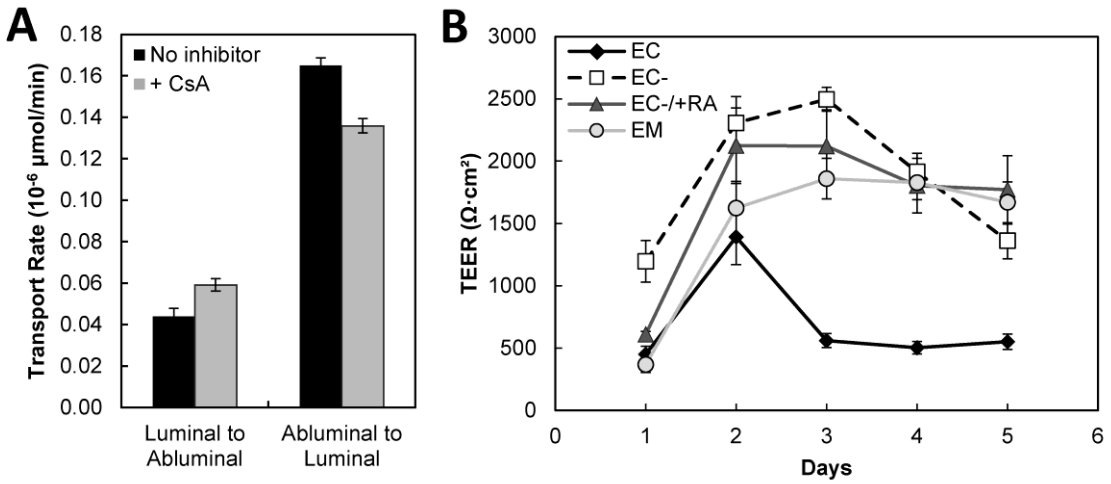

Figure 2.4. Barrier characterization of hPSC-derived BMECs. (A) The transport rate of the fluorescent P-gp substrate Rhodamine 123 in the abluminal to luminal direction and in the luminal to abluminal direction (black). With the addition of 5µM cyclosporin A, a P-gp inhibitor (gray), the transport rate in the luminal to abluminal direction increases ($p=0.0150$) and the transport rate in the abluminal to luminal direction decreases ($p = 0.0004$). (biological and technical triplicate). (B)TEER values over time for cells grown in EC-, EC-/+RA and EM media (biological duplicate, technical triplicate; mean ± SEM).

RA has been shown to be important for BBB development(Mizee et al., 2013), and for differentiation of high-performing BMECs (Lippmann et al., 2014). These results demonstrate that RA helped maintain barrier function over time but was not necessary for a high peak TEER. RA has also been shown to influence P-gp efflux activity (El Hafney et al., 1997) and while P-gp expression patterns change in the presence of RA (Figure 2.5), P-gp activity does not appear to be affected by the

absence of RA (Figure 2.6). Furthermore, cells achieved relatively high peak TEER that remained elevated over time in EM, which is a viable alternative for applications where a serum-free formulation is required, such as in a proteomic analysis of cells. All subsequent studies were performed on Day 2 using cells grown in EC- media because the highest TEER values were achieved.

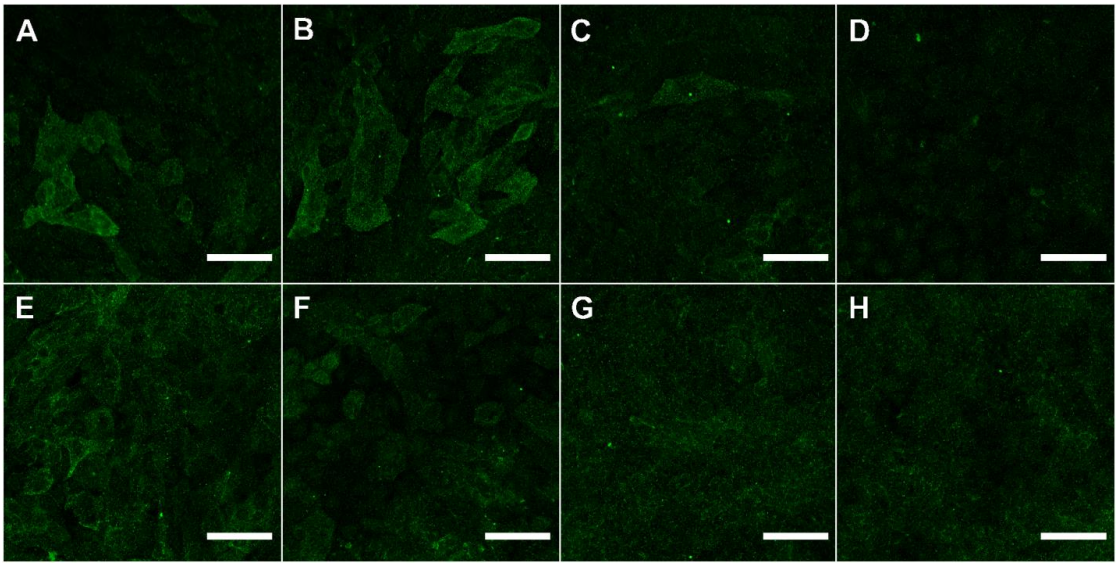

Figure 2.5. P-gp immunocytochemistry on cells grown in different BMEC media. BMECs cultured in EC media (A, B), EM (C, D), EC- medium (E, F), and EC- medium with RA (G, H) exhibit different P-gp staining patterns. Cells grown with RA (C-D, G-H) appear to have more consistent diffuse staining while cells grown without RA (A-B, E-F) have more intense staining patterns in individual cells.

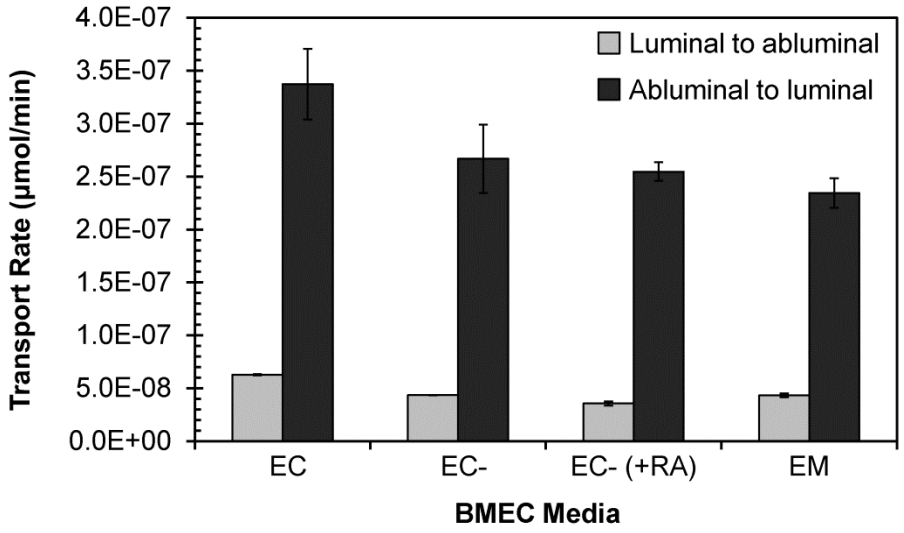

Figure 2.6. P-gp efflux activity of cells grown in different BMEC media. Cells grown in the four different BMEC media tested did not exhibit any statistically significant differences in P-gp efflux of Rhodamine 123.

2.4.4 Establishing Small Molecule Permeability Benchmarks

To use this hPSC-derived BBB model for the screening of new therapeutics, a better understanding of the transport behavior of known drugs (2.2) is required to serve as a benchmark for new drugs. A multiplexed MRM assay was employed to evaluate the permeabilities of seven small molecule drug substances with known transport behavior in mice to establish permeability benchmarks in the hPSC-derived BBB model (Figure 2.7). Atenolol, a small hydrophilic molecule, had the lowest permeability of $4.64 \pm 0.38 \cdot 10^{-6}$ cm/s. The two P-gp substrates cimetidine and hydroxyzine had permeability values of $7.84 \pm 0.38 \cdot 10^{-6}$ cm/s and $10.36 \pm 0.07 \cdot 10^{-6}$ cm/s respectively. The CNS-permeable drugs had permeability values ranging $16.36 \pm 3.33 \cdot 10^{-6}$ cm/s for hydroxyzine to $119.4 \pm 34.6 \cdot 10^{-6}$ cm/s for caffeine.

Table 2.2. Properties of drug compounds. Molecular weight, known CNS permeability, transport class, drug class and indication shown for each of molecules investigated.

Compound	MW (Da)	CNS Permeable	Transport Class	Drug Class	Indication
Atenolol	226	-	Passive, hydrophilic	Beta-blocker	High blood pressure
Cimetidine	252	-	Active, Efflux (P-gp)	Histamine H_2-receptor antagonist	Heartburn, peptic ulcers
Prazosin	420	-	Active, Efflux (P-gp)	Alpha-adrenergic blocker	High blood pressure, anxiety
Trazodone	408	+	Passive, lipophilic	Serotonin antagonist & reuptake inhibitor	Depression, anxiety
Caffeine	212	+	Passive, lipophilic	CNS stimulant	
Hydroxyzine	448	+	Passive, lipophilic	Antihistamine	Many, anxiety
Propranolol	296	+	Passive, lipophilic	Beta-blocker	High blood pressure
Donepezil	433	+	Unknown	Cholinesterase inhibitor	AD (all stages)
Memantine	216	+	Unknown	NDMA receptor blocker	Moderate to severe AD
Galantamine	368	+	Unknown	Cholinesterase inhibitor	Mild to moderate AD
Rivastigmine	400	+	Unknown	Cholinesterase inhibitor	Mild to moderate AD

Because hydrophilic drug molecules and P-gp substrates are considered to be CNS-impermeable, and hydrophobic drug molecules are considered to be CNS-permeable, the threshold for brain permeability in this model is $15 \cdot 10^{-6}$ cm/s. Lipinski's Rule of Five for CNS penetration predicts that all seven of these molecules are CNS permeable, which highlights the importance of complementing theoretical predictions with experimental observations (2.3). Experimentally, the permeabilities of

these seven drugs are comparable between the hPSC-BMECs and *in vivo* mouse data, demonstrating that CNS-impermeable drugs are restricted and CNS-permeable drugs are able to transport through the hPSC-BMECs. However, transport of drugs in the human *in vitro* BBB model is generally more restricted compared to mouse *in vivo* permeability data (Figure 2.8) (Nakagawa et al., 2009; Shayan et al., 2011). The differences between permeability values in human and mouse could be due to species differences, such as differences in lipid composition and differences in expression and activity of transporter proteins and enzymes (Deo et al., 2013).

Table 2.3. Lipinski's Rule of Five properties for the eleven molecules tested in the hPSC-derived BBB model. Criteria for a likely drug candidate include molecular weight ≤500, Oil/water partition coefficient (LogP) ≤5, Hydrogen bond donors ≤5, Hydrogen bond acceptors ≤10 and number of rotatable bonds ≤10 (Lipinski, et al., 1997). Further restrictions for CNS permeable drugs include molecular weight ≤400, LogP ≤5, Hydrogen bond donors ≤3, Hydrogen bond acceptors ≤7, and rotatable bonds ≤8 (Pajouhesh & Lenz, 2005). All the molecules tested pass both the general and more restrictive CNS Rule of Five. Values not within these constraints are shown in italics. Predicted molecular properties of all drugs were obtained from the DrugBank database.

Compound	MW (Da)	CNS?	Log P (≤ 5)	Hbond Donor (≤3)	Hbond acceptor (≤7)	Rotatable Bond (≤8)	Rule of 5?
Atenolol	226	-	0.57	3	4	8	Yes
Cimetidine	252	-	0.44	3	5	5	Yes
Prazosin	*420*	-	1.93	1	7	4	Yes
Trazodone	*408*	+	2.68	0	4	5	Yes
Caffeine	212	+	-0.24	0	3	0	Yes
Hydroxyzine	*448*	+	3.43	1	4	8	Yes
Propranolol	296	+	3.03	2	3	6	Yes
Donepezil	*433*	+	4.14	0	4	6	Yes
Memantine	216	+	3.31	1	1	0	Yes
Galantamine	368	+	1.39	1	4	1	Yes
Rivastigmine	400	+	2.45	0	2	5	Yes

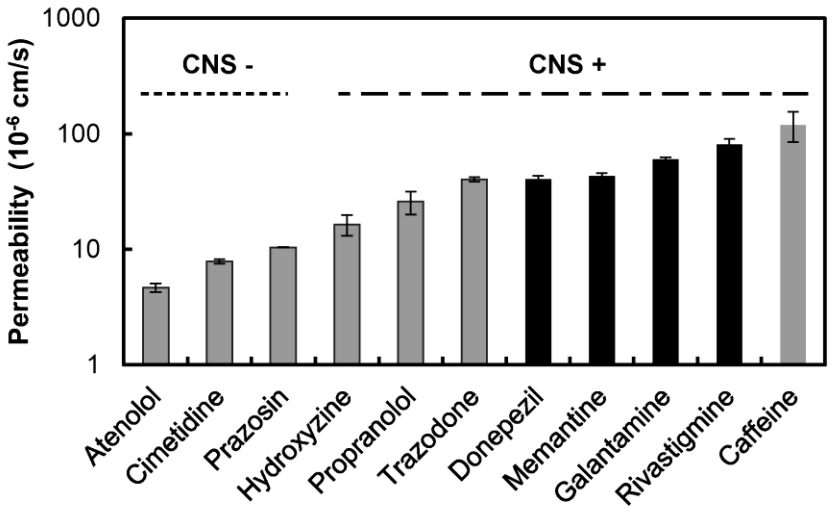

Figure 2.7. Permeability values for drugs measured by multiple reaction monitoring assay. Seven common drugs (gray) ordered from least to most permeable. The four Alzheimer's disease drugs (black) fall in the brain permeable region of the model. Atenolol, cimetidine, and prazosin are CNS impermeable and the remaining drugs are CNS permeable.

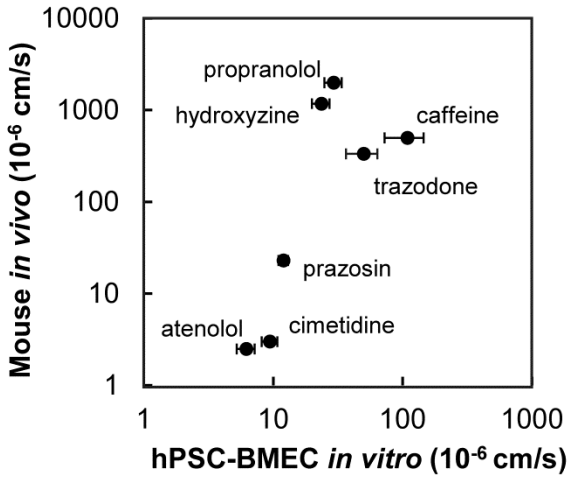

Figure 2.8. Comparison of drug permeability between *in vitro* hPSC-derived BMECs and *in vivo* mouse. The hPSC-BMEC model is generally more restrictive than the mouse in vivo BBB (Nakagawa et al., 2009; Shayan et al., 2012).

To validate the hPSC-BBB model benchmarks, permeabilities of the four FDA-approved small molecule drug molecules (donepezil, memantine, galantamine, and rivastigmine) to treat Alzheimer's disease symptoms were measured using a multiplexed MRM assay. The permeability values of these drugs ranged from $40.5 \pm 3.00 \cdot 10^{-6}$ for donepezil to $80.7 \pm 9.39 \cdot 10^{-6}$ cm/s for rivastigmine, suggesting these drugs are CNS-permeable (Figure 2.7).

Because the mechanism of action for these four drug molecules requires brain permeation, they were all expected to be CNS-permeable however comparable *in vivo* data are not publicly available for all four Alzheimer's drugs. Memantine permeability measured *in vitro* ($43.0 \pm 2.41 \cdot 10^{6}$ cm/s) is very close to the value of $55 \cdot 10^{6}$ cm/s measured *in vivo* in humans (Ametamey et al., 2002; Higuchi et al., 2015), further supporting the use of this model as a screening tool for therapeutics.

2.4.5 Transport Properties are Unchanged Above a Threshold TEER Value

The high TEER values achievable using the hPSC-BMEC model enabled the study of the relationship between molecular permeability in cells and varying degrees of barrier tightness ranging from very low TEER (200 $\Omega \cdot cm^2$) to very high TEER (3000 $\Omega \cdot cm^2$). Above a threshold TEER value of 500 $\Omega \cdot cm^2$, permeability to the small molecule sodium fluorescein remains constant at $3.31 \pm 0.24 \cdot 10^{-7}$ cm/s (Figure 2.9). When TEER is below this threshold value, permeability and TEER are inversely correlated, with the highest permeability occurring when TEER is lowest.

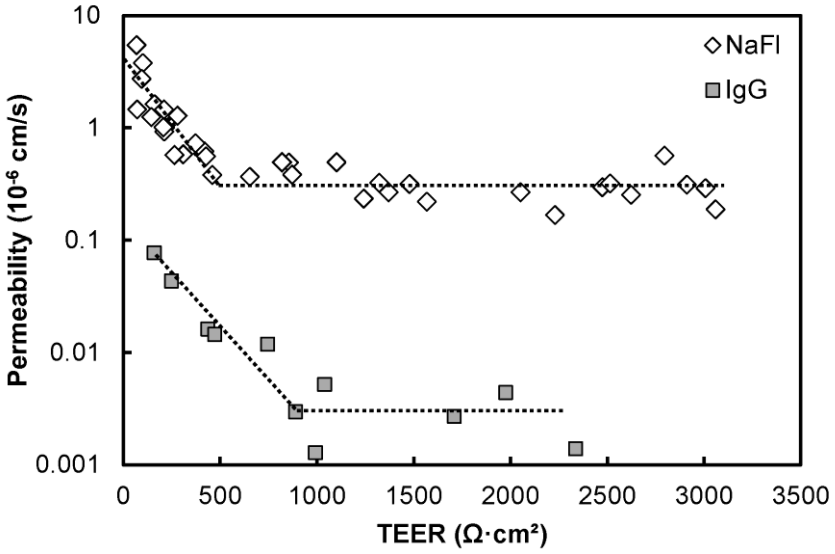

Figure 2.9. TEER threshold above which permeability does not change. Below a threshold TEER value, permeability and TEER are inversely correlated for both small and large molecules. Permeability of the small molecule sodium fluorescein (NaFl, white) does not change above a TEER value of 500 Ω·cm². Permeability of large IgG molecules (gray) does not change above a threshold TEER value of 900 Ω·cm². Dashed lines illustrate the inverse relationship between permeability and TEER at low TEER values and constant permeability above the threshold TEER.

These results are consistent with the notion that when screening permeability of small molecules, such as the 378 Da sodium fluorescein, a TEER value of 500 Ω·cm² is sufficient to ensure constant permeability. A similar permeability plateau at high TEER values has been observed for sucrose permeability in a primary porcine *in vitro* BBB model (Lohmann et al., 2002). TEER is a fast, easy, non-destructive method to assess barrier integrity prior to other experiments, and the desired value for *in vitro* models has been 1500 Ω·cm² (up to 6000 Ω·cm²) as measured *in vivo* in rats (Butt et al., 1990). Because sodium fluorescein is predominantly passively transported across the BBB, transcellular transport may potentially be responsible for the small

residual amount of sodium fluorescein transported to the abluminal compartment at high TEER.

Similar experiments were performed using human IgG molecules (MW 150 kDa) as a model of a large molecule drug. Permeability to IgGs was constant at 2.99 ± 0.64 $\cdot 10^{-9}$ cm/s above a TEER threshold of 900 $\Omega \cdot cm^2$ and was inversely correlated with TEER below this threshold. This permeability value is two orders of magnitude lower than sodium fluorescein permeability, and represents 0.034 ± 0.007 % of the initial dose in the luminal compartment crossing to the abluminal compartment after 6 hours.

The TEER threshold for constant IgG permeability was 900 $\Omega \cdot cm^2$, indicating that a tighter barrier is required to study antibody-based large molecule drugs and suggesting different routes of transport for sodium fluorescein and IgGs. There are no known transport receptors for IgGs and they are essentially excluded from the brain, with a widely accepted statistic of 0.1% of peripheral IgGs able to penetrate the brain (Yu and Watts, 2013). The 0.034% of initial IgG dose that crossed to the abluminal compartment after 6 hours is lower than this commonly accepted statistic but higher than peripherally administered human intravenous immunoglobulin measured in the murine cortex (0.009± 0.001%) (St-Amour et al., 2013). *In vivo* human IgG permeability data are not publicly available for comparison.

2.5 Conclusions

hPSC-derived BMECs are a robust, high throughput cell source for a human *in vitro* BBB model that can be used to screen new therapeutics, yielding over 100 experimental cases from a single 6-well plate of hPSCs. For comparison, only 40 inserts can be seeded from an optimized murine BMEC purification protocol requiring 10 individual animals (Wuest et al., 2013), therefore hPSCs are a renewable and high throughput source of BMECs when compared to primary cells. hPSC differentiation generates BMECs with an excellent barrier phenotype without the need for coculture to improve barrier properties. The small molecule benchmarks developed here are necessary for evaluating the permeability of new therapeutics with unknown transport properties as comparable *in vivo* data in humans often does not exist. Lastly, because of the high TEER values achievable using hPSC-derived BMECs, relationships between permeability and TEER of both a small molecule and a pharmaceutically-relevant class of large proteins were established. As long as TEER exceeds 500 $\Omega \cdot cm^2$, the model is useful for studying small molecule drugs, and if TEER is maintained above 900 $\Omega \cdot cm^2$, the model is useful for the study of large molecule drugs. This finding is a novel step towards establishing minimum criteria for *in vitro* BBB drug screening models, instead of relying on the gold standard of 1500 $\Omega \cdot cm^2$ as measured *in vivo* in rats. The permeability and TEER standards established in the hPSC-derived BBB *in vitro* model can be used as criteria to evaluate the integrity of

any *in vitro* BBB model. Furthermore, this model has the potential to be used to predict *in vivo* human permeability of both small and large molecule therapeutics.

REFERENCES

Abbott NJ, Patabendige AAK, Dolman DEM, Yusof SR, Begley DJ. 2010. Structure and function of the blood-brain barrier. Neurobiol. Dis. 37:13–25.

Abbott NJ, Rönnbäck L, Hansson E. 2006. Astrocyte-endothelial interactions at the blood-brain barrier. Nat. Rev. Neurosci. 7:41–53.

Ametamey SM, Bruehlmeier M, Kneifel S, Kokic M, Honer M, Arigoni M, Buck A, Burger C, Samnick S, Quack G, Schubiger PA. 2002. PET studies of 18F-memantine in healthy volunteers. Nucl. Med. Biol. 29:227–231.

Badur MG, Zhang H, Metallo CM. 2015. Enzymatic passaging of human embryonic stem cells alters central carbon metabolism and glycan abundance. Biotechnol. J. 10:1600–1611.

Brown RC, Morris AP, O'Neil RG. 2007. Tight junction protein expression and barrier properties of immortalized mouse brain microvessel endothelial cells. Brain Res. 1130:17–30.

Butt AM, Jones HC, Abbott NJ. 1990. Electrical resistance across the blood-brain barrier in anaesthetized rats: a developmental study. J. Physiol. 429:47–62.

Buzzard JJ, Gough NM, Crook JM, Colman A. 2004. Karyotype of human ES cells during extended culture. Nat. Biotechnol. 22:381–382.

Chen G, Gulbranson DR, Hou Z, Bolin JM, Probasco MD, Smuga-Otto K, Howden SE, Nicole R, Propson NE, Wagner R, Lee GO, Teng JMC, Thomson JA. 2011. Chemically defined conditions for human iPS cell derivation and culture. Nat. Methods 8:424–429.

Deli MA, Ábrahám CS, Kataoka Y, Niwa M. 2005. Permeability studies on in vitro blood-brain barrier models: Physiology, pathology, and pharmacology. Cell. Mol. Neurobiol. 25:59–127.

Deo AK, Theil FP, Nicolas JM. 2013. Confounding Parameters in Preclinical Assessment of Blood–Brain Barrier Permeation: An Overview With Emphasis on Species Differences and Effect of Disease States. Mol. Pharm. 10:1581–1595.

Draper JS, Smith K, Gokhale P, Moore HD, Maltby E, Johnson J, Meisner L, Zwaka TP, Thomson JA, Andrews PW. 2004. Recurrent gain of chromosomes 17q and 12 in cultured human embryonic stem cells. Nat. Biotechnol. 22:53–54.

Förster C, Burek M, Romero IA, Weksler B, Couraud P-O, Drenckhahn D. 2008. Differential effects of hydrocortisone and TNFalpha on tight junction proteins in an in vitro model of the human blood-brain barrier. J. Physiol. 586:1937–1949.

Garitaonandia I, Amir H, Boscolo FS, Wambua GK, Schultheisz HL, Sabatini K, Morey R, Waltz S, Wang YC, Tran H, Leonardo TR, Nazor K, Slavin I, Lynch C, Li Y, Coleman R, Romero IG, Altun G, Reynolds D, Dalton S, Parast M, Loring JF, Laurent LC. 2015. Increased risk of genetic and epigenetic instability in human embryonic stem cells associated with specific culture conditions. PLoS One 10.

El Hafney B, Chappey O, Piciottia M, Debraya M, Bovalb B, Rouxa F. 1997. Modulation of P-glycoprotein activity by glial factors and retinoic acid in an immortalized rat brain microvessel endothelial cell line. Neurosci. Lett. 236:107–111.

Helms HC, Abbott NJ, Burek M, Cecchelli R, Couraud PO, Deli MA, Förster C, Galla HJ, Romero IA, Shusta EV, Stebbins MJ, Vandenhaute E, Weksler B, Brodin B. 2016. In vitro models of the blood-brain barrier: An overview of commonly used brain endothelial cell culture models and guidelines for their use. J. Cereb. Blood Flow Metab. 36:862–890.

Higuchi K, Kitamura A, Okura T, Deguchi Y. 2015. Memantine transport by a proton-coupled organic cation antiporter in hCMEC/D3 cells, an in vitro human blood-brain barrier model. Drug Metab. Pharmacokinet. 30:182–187.

Katt ME, Xu ZS, Gerecht S, Searson PC. 2016. Human Brain Microvascular Endothelial Cells Derived from the BC1 iPS Cell Line Exhibit a Blood-Brain Barrier Phenotype. PLoS One 11.

Lipinski CA, Lombardo F, Dominy BW, Feeney PJ. 1997. Experimental and Computational Approaches to Estimate Solubility and Permeability in Drug Discovery and Development Settings. Adv. Drug Deliv. Rev. 23:3–25.

Lippmann ES, Al-Ahmad A, Azarin SM, Palecek SP, Shusta EV. 2014. A retinoic acid-enhanced, multicellular human blood-brain barrier model derived from stem cell sources. Sci. Rep. 4:4160.

Lippmann ES, Azarin SM, Kay JE, Nessler RA, Wilson HK, Al-Ahmad A, Palecek SP, Shusta EV. 2012. Derivation of blood-brain barrier endothelial cells from human pluripotent stem cells. Nat. Biotechnol. 30:783–791.

Lohmann C, Hüwel S, Galla H-J. 2002. Predicting Blood-Brain Barrier Permeability of Drugs: Evaluation of Different In Vitro Assays. J. Drug Target. 10:263–276.

Ludwig TE, Bergendahl V, Levenstein ME, Yu J, Probasco MD, Thomson JA. 2006. Feeder-independent culture of human embryonic stem cells. Nat. Methods 3:637–646.

Mitalipova MM, Rao RR, Hoyer DM, Johnson JA, Meisner LF, Jones KL, Dalton S, Stice SL. 2005. Preserving the genetic integrity of human embryonic stem cells. Nat. Biotechnol. 23:19–20.

Mizee MR, Wooldrik D, Lakeman KA, van het Hof B, Drexhage JA, Geerts D, Bugiani M, Aronica E, Mebius RE, Prat A, de Vries HE, Reijerkerk A. 2013. Retinoic Acid Induces Blood-Brain Barrier Development. J Neurosci 33:1660–1671.

Nakagawa S, Deli M a., Kawaguchi H, Shimizudani T, Shimono T, Kittel Á, Tanaka K, Niwa M. 2009. A new blood-brain barrier model using primary rat brain endothelial cells, pericytes and astrocytes. Neurochem. Int. 54:253–263.

Omidi Y, Campbell L, Barar J, Connell D, Akhtar S, Gumbleton M. 2003. Evaluation of the immortalised mouse brain capillary endothelial cell line, b.End3, as an in vitro blood-brain barrier model for drug uptake and transport studies. Brain Res. 990:95–112.

Pardridge WM. 2012. Drug Transport across the Blood–Brain Barrier. J. Cereb. Blood Flow Metab. 32:1959–1972.

Shayan G, Adamiak B, Relkin NR, Lee KH. 2012. Longitudinal analysis of novel Alzheimer's disease proteomic cerebrospinal fluid biomarkers during intravenous immunoglobulin therapy. Electrophoresis 33:1975–1979.

Shayan G, Choi YS, Shusta EV., Shuler ML, Lee KH. 2011. Murine in vitro model of the blood-brain barrier for evaluating drug transport. Eur. J. Pharm. Sci. 42:148–155.

St-Amour I, Paŕe I, Alata W, Coulombe K, Ringuette-Goulet C, Drouin-Ouellet J, Vandal M, Soulet D, Bazin R, Calon F. 2013. Brain bioavailability of human intravenous immunoglobulin and its transport through the murine blood-brain barrier. J. Cereb. Blood Flow Metab. 33:1–10.

Thomson JA, Ludwig TE. 2012. Primate Pluripotent Stem Cells Cultured in Medium Containing Gamma-aminobutyric Acid, Pipecolic Acid and Lithium. U.S. U.S. Patent 8,158,424.

Weksler BB, Subileau EA, Perrière N, Charneau P, Holloway K, Leveque M, Tricoire-Leignel H, Nicotra A, Bourdoulous S, Turowski P, Male DK, Roux F, Greenwood J, Romero IA, Couraud PO. 2005. Blood-brain barrier-specific properties of a human adult brain endothelial cell line. FASEB J. 19:1872–1874.

Wuest DM, Lee KH. 2012. Optimization of endothelial cell growth in a murine in vitro blood-brain barrier model. Biotechnol. J. 7:409–417.

Wuest DM, Wing AM, Lee KH. 2013. Membrane configuration optimization for a murine in vitro blood-brain barrier model. J. Neurosci. Methods 212:211–221.

Yu J, Vodyanik MA, Smuga-Otto K, Antosiewicz-Bourget J, Frane JL, Tian S, Nie J, Jonsdottir GA, Ruotti V, Stewart R, Slukvin II, Thomson JA. 2007. Induced pluripotent stem cell lines derived from human somatic cells. Sci. (New York, NY) 318:1917–1920.

Yu YJ, Watts RJ. 2013. Developing Therapeutic Antibodies for Neurodegenerative Disease. Neurotherapeutics 10:459–472.

Chapter 3

NEURAL STEM CELL-DERIVED ASTROCYTES MITIGATE THE INFLAMMATORY EFFECTS OF TNF-α AND IL-6 IN AN IPSC-BASED BLOOD-BRAIN BARRIER MODEL

3.1 Preface

In this chapter, the stem cell derived model is further expanded to include coculture with astrocytes differentiated from neural stem cells. The coculture model is used to investigate the effects of neuroinflammation on barrier function. This work was funded in part by the National Science Foundation (Award Number 1144726). We wish to thank John Ruanos-Salguero for his assistance with neural stem cell culture and differentiation.

3.1.1 Abstract

Abstract Inflammation can be a risk factor for neurodegenerative diseases such as Alzheimer's disease (AD) and may also contribute to the progression of AD. Here, we sought to understand how inflammation affects the properties of the brain microvascular endothelial cells (BMECs) that compose the blood-brain barrier (BBB), which is impaired in AD. A fully human *in vitro* BBB model with brain microvascular endothelial cells derived from induced pluripotent stem cells and neural stem cell (NSC)-derived astrocytes was used to investigate the effects of neuroinflammation on

barrier function. The cytokines TNF-α and IL-6 directly cause BBB dysfunction measured by a decrease in transendothelial electrical resistance, an increase in sodium fluorescein permeability, and a decrease in cell polarity, providing a link between neuroinflammation and specific aspects of BBB breakdown. NSC-derived astrocytes were added to the model and secreted cytokines and chemokines were quantified in monoculture and coculture both in the presence and absence of TNF-α and IL-6. Increased concentrations of pro-inflammatory cytokines known to be secreted by astrocytes or endothelial cells such as MCP-1, IL-8, IP-10, MIP-1β, IL-1 β, MIG, and RANTES peaked in inflammatory conditions when NSC-astrocytes were present. Despite the presence of several pro-inflammatory cytokines, the NSC-derived astrocytes mitigated the effects of inflammation measured by a restoration of transendothelial electrical resistance and IgG permeability. These results also suggest a breakdown in transcellular transport that precedes any increase in paracellular permeability in neuroinflammation. This model has the potential to resolve questions about neurodegenerative disease progression and delivery of therapeutics to the brain.

3.2 Introduction

Alzheimer's disease (AD) is a neurodegenerative disease that is the most common cause of dementia. AD pathology is characterized by extracellular amyloid-β (Aβ) plaques and neurofibrillary tangles in neurons which together lead to neuronal death and cognitive loss. Once believed to be a secondary response in AD, there is

increasing evidence that inflammation also contributes to AD progression (reviewed by Heppner, Ransohoff, & Becher, 2015). Both systemic inflammation (e.g. from chronic disease) and central nervous system inflammation (e.g. after traumatic brain injury) can be risk factors for AD (Holmes et al., 2009; Kyrkanides et al., 2011; Mayeux et al., 1993).

Tumor necrosis factor alpha (TNF-α) and interleukin (IL)-6 are two of the most commonly studied cytokines with respect to neuroinflammation in AD. A meta-analysis by Brosseron et al. (2014) revealed a correlation between increased TNF-α and IL-6 blood or cerebrospinal fluid (CSF) in patients with severe AD compared to patients with mild cognitive impairment (MCI) or less severe AD (although several studies reviewed by Brosseron et al. revealed no correlation). Additionally, brain microvessels from patients with AD have been shown to secrete increased levels of inflammatory molecules, including IL-6 and TNF-α, compared with age matched healthy individuals (Grammas and Ovase, 2001).

In addition to neuroinflammation, vascular pathology may also contribute to AD. Human and animal model studies suggest that dysfunction of the blood-brain barrier (BBB) plays a critical role in the progression of AD and may precede the onset of neurodegeneration and cognitive decline (Bell and Zlokovic, 2009). The blood-brain barrier comprises the brain microvascular endothelial cells (BMECs) that line cerebral capillaries and these BMECs restrict and control the movement of molecules between the blood and the brain. Together with other cells of the neurovascular unit

(NVU) such as astrocytes and pericytes, BMECs tightly regulate the neuronal microenvironment for proper function (Abbott et al., 2006).

Considerable progress has been made towards modeling the NVU *in vitro*, particularly from human stem cell sources, which mitigate availability and variability issues inherent to primary cell sources. BMECs derived from human induced pluripotent stem cells (iPSCs) exhibit an *in vivo*-like barrier phenotype, characterized by the presence of BMEC-specific proteins, functional and polarized molecular transport via proteins such as P-glycoprotein, high transendothelial electrical resistance (TEER), and low permeability to most molecules (Lippmann et al., 2012; Lippmann et al., 2014). The addition of other cell types of the NVU, such as astrocytes and pericytes (Lippmann et al., 2014), iPSC-derived astrocytes and neurons (Canfield et al., 2017), differentiating neural progenitor cells (Lim et al., 2007; Lippmann et al., 2011; Weidenfeller et al., 2007) and neural stem cells (NSCs) (Appelt-Menzel et al., 2017) improve the barrier phenotype of BMECs grown *in vitro*. Such *in vitro* BBB models can be used with different levels of complexity to elucidate contributions of different cell types and to further understanding of how different cell types can mitigate or exacerbate neurodegenerative disease.

This work aims to investigate the effects of neuroinflammation and crosstalk between cells of the NVU towards understanding the contributions of these two factors on BBB function in neurodegenerative diseases such as AD. Through the use of an *in vitro* model system with all cell components entirely derived from human stem cells, we first investigated the effects of inflammation via TNF-α and IL-6 on the

barrier properties of iPSC-derived BMECs (Lippmann et al., 2012; Lippmann et al., 2014; Stebbins et al., 2016). Human NSC-derived astrocytes (Kleiderman et al., 2016) were added to the *in vitro* model and molecular crosstalk between NSC-astrocytes and BMECs in inflammation via secretion of cytokines and chemokines was measured. Finally, we investigated the ability of NSC-derived astrocytes to mitigate the effects of inflammation on the barrier function of the BBB.

3.3 Materials and Methods

3.3.1 NSC Culture and Differentiation

iPSC-derived BC1 HIP™ Neural Stem Cells (MTI-GlobalStem) were maintained on 6-well plates (Corning, Corning, NY) coated with a 1:200 solution of Corning2Geltrex™ LDEV-Free Reduced Growth Factor Basement Membrane Matrix (Thermo Fisher Scientific) in Dulbecco Modified Eagle's Medium:Nutrient Mixture F-12 (DMEM/F12) with HEPES (Thermo Fisher Scientific) and incubated at room temperature for 1 hour prior to use. NSCs were maintained in NSC Maintenance Medium (NSCMM) consisting of NeuralX NSC Medium (MTI-GlobalStem) with GS22 Neural Supplement (50X; MTI-GlobalStem), MEM Non-Essential Amino Acids (100X; Thermo Fisher Scientific), and Glutagro (100X; Corning), supplemented with 20 ng/mL Human FGF2 Recombinant Protein (MTI-GlobalStem). Medium was changed every other day and cells were passaged every 3-4 days at 95% confluence

using StemPro Accutase (Thermo Fisher Scientific) and seeded at a density of 2x105 cells/cm2.

To differentiate NSCs into astrocytes, 24-well plates (for coculture; Corning) or 8-well chambered coverglass (for immunocytochemistry; Celvis) were pretreated with 10 μg/mL poly-L-ornithine hydrobromide (Sigma-Aldrich) at 37 °C for 1 hour, rinsed with Dulbecco's Phosphate Buffered Saline (DPBS; Thermo Fisher Scientific), and incubated with 1% laminin (Sigma-Aldrich) at 37 °C for 1 hour. NSCs were dissociated using StemPro Accutase and seeded on pretreated plates or coverglass chambers at a density of $5x10^5$ cells/cm^2. Medium was switched to astrocyte differentiation medium (ADM), consisting of NSCMM supplemented with 20 ng/mL bone morphogenetic protein 4 (BMP4; R&D Systems). Media changes occurred every other day until coculture with BMECs was initiated after 5-10 days.

3.3.2 iPSC-BMEC Differentiation and Model Set Up

iPS(IMR90)-4 iPSCs (WiCell) (Yu et al., 2007) were maintained and differentiated as previously described (Lippmann et al., 2014; Mantle et al., 2016). Briefly, iPSCs were maintained in mTeSR1 medium (STEMCELL Technologies) on 6-well plates coated with 83.3 μg/mL growth factor-reduced Matrigel (Thermo Fisher Scientific) in DMEM/F-12. Cells were passaged every 3-5 days using Versene (Thermo Fisher Scientific) and mechanical dissociation. Cells were differentiated as described by (Lippmann et al., 2014; Mantle et al., 2016). Differentiated BMECs (Day

9) were passaged to 24-well Transwell cell culture inserts (PET; 0.4 μm pores; Fisher Scientific) pretreated for a minimum of four hours with 40% collagen IV (Sigma-Aldrich) and 10% fibronectin (Sigma-Aldrich). The Transwell inserts were placed into 24-well plates or 24-well plates containing differentiated astrocytes for coculture, and all medium was switched to endothelial cell medium consisting of human endothelial cell serum free medium (Thermo Fisher Scientific) supplemented with 1% platelet-poor derived serum (EC- media). Experiments were performed after 48 hours of coculture unless otherwise noted.

To mimic neuroinflammation, cells were incubated with 10 ng/mL of recombinant human TNF-α (R&D Systems), 10 ng/mL IL-6 (R&D Systems), or 10 ng/mL each of both cytokines (inflammatory media). Cytokines were added to the media after BMECs were incubated for 24 hours on inserts.

3.3.3 NSC-Astrocyte Immunocytochemistry and Confocal Microscopy

All solutions were prepared in DPBS. NSCs at different stages of differentiation on 8-well chambered coverglass were washed once with DPBS and fixed using 2% paraformaldehyde (Electron Microscopy Sciences) for 15 minutes. Following three DPBS washes, the cells were permeabilized with 0.1% Triton X-100 (Sigma-Aldrich) for 5 minutes and blocked in 10% goat serum (Sigma-Aldrich) for 1 hour. Cells were incubated with primary antibody solution (mouse anti-glial fibrillary acidic protein (GFAP) and mouse anti-nestin purchased from Thermo Fisher

Scientific; mouse anti-nestin purchased from Abcam; Table 3.1) overnight at 4 °C on an orbital shaker. The cells were rinsed twice with 1% goat serum and incubated with secondary antibody solution at room temperature for 1 hour on an orbital shaker. Cells were rinsed twice with 1% goat serum and stored in DPBS at 4 °C until imaging. Fifteen minutes prior to imaging, one drop of NucBlue Fixed Cell ReadyProbes Reagent (ThermoFisher Scientific) was added to each chamber. Images were taken with a 20x objective on a Zeiss LSM 710 confocal microscope (Zeiss).

Table 3.1. **Antibodies used in immunocytochemistry of NSC-astrocytes**

1° Antibody	Dilution	2° Antibody	Conc (μg/mL)
Mouse anti-Nestin	1:500	Goat anti-mouse AlexaFluor 568	5
Chicken anti-Vimentin	1:5000	Goat anti-chicken AlexaFluor 488	5
Rabbit anti-GFAP	1:1000	Goat anti-rabbit AlexaFluor 647	1

3.3.4 Transendothelial Electrical Resistance (TEER) Measurements

Cell culture inserts containing BMECs were transferred to an Endohm-6 chamber (World Precision Instruments) containing EC- media. An EVOM2 Epithelial Volt Meter (World Precision Instruments) was used to measure the resistance of the cell monolayer and membrane. To calculate the TEER value, the measured resistance of a blank treated Transwell insert was subtracted from each experimental measured value and then multiplied by the membrane surface area.

3.3.5 Sodium Fluorescein Permeability Assay

Media in the bottom compartment was aspirated and replaced with 600 µL transport buffer, consisting of 10 mM HEPES, 0.1% (w/v) bovine serum albumin and 4.5% (w/v) glucose (Sigma-Aldrich). Media in the top compartment was aspirated and replaced with 100 µL of 100 µM sodium fluorescein (Sigma-Aldrich) in transport buffer. Samples were collected every 15 minutes for 1 hour by removing 100 µL from the bottom compartment and transferring it to a 96-well plate. 100 µL transport buffer was replaced in the bottom compartment to maintain constant volume. A Spectra Max M5 microplate reader (Molecular Devices) was used to analyze the 96-well plate for fluorescence (excitation = 460 nm, emission = 515 nm). The solute permeability coefficient P_s was calculated using the equation,

$$P_s = \frac{C_A * V_A}{t * S * C_L}$$

where C_A and C_L are the abluminal and luminal concentrations respectively, V_A is the abluminal volume, t is the time and S is the surface area of the membrane. The inverse of the permeability of a blank treated insert was subtracted from the inverse of P_s to obtain the permeability of the cell monolayer. Dilution due to sample removal and addition of transport buffer to maintain volume was accounted for in the calculation (Deli et al., 2005).

3.3.6 P-glycoprotein Efflux Assay

The transport rate of the fluorescent P-glycoprotein (P-gp) substrate Rhodamine 123 (Sigma-Aldrich) was measured in the luminal to abluminal and abluminal to luminal directions. All medium was aspirated from both compartments and replaced with EC- media in the receiving compartments and EC- media containing 10 μM Rhodamine 123 in the donor compartments. Samples of 100 μL were collected in a 96-well plate every hour for three hours. Medium was replaced to maintain constant volume and dilutions were accounted for in the calculations. The amount of Rhodamine 123 transported per unit time was calculated as the transport rate in each direction. The efflux ratio was calculated by dividing the rate in the abluminal to luminal direction by the rate in the luminal to abluminal direction.

3.3.7 IgG Quantification Assay

BMECs were grown in monoculture or coculture, cytokines or control media were added on Day 1 of coculture. On Day 2, 10 mg/mL Gammagard Liquid Immune Globulin Intravenous (Human) 10% (IVIG; Lot # LE12L017AB; Baxter) was added to the luminal compartment and cells were incubated at 37 °C for 6 hours. Abluminal samples were collected and stored at -20 °C until quantification. The Easy-Titer ® Human IgG Assay Kit (Thermo Fisher Scientific) was used according to the manufacturer's protocol to quantify the amount of IgG in the abluminal compartment after 6 hours.

3.3.8 Cytokine Quantification by Luminex

BMECs were grown in monoculture or coculture, 10 ng/mL each of TNF-α and IL-6 were added to appropriate wells on Day 1. On Day 2 media from the abluminal compartments were collected and stored at -20 °C until analysis. The Cytokine 25-Plex Human Panel (Thermo Fisher Scientific) assay and Luminex 100/200 system (Thermo Fisher Scientific) were used according to the manufacturer's instructions to quantify cytokines and chemokines in the abluminal samples. Samples were diluted 1:2 per the instructions. All measurements below the limit of detection were treated as a concentration of 0 pg/mL for statistical analysis.

3.3.9 Experimental Design and Statistical Analyses

JMP® v13.0 (SAS Institute Inc.) was used for statistical analysis. Statistical evaluation of data was performed using Student's t-test and analysis of variance (ANOVA) with $\alpha = 0.05$. To determine statistical significance of the effects of coculture and TNF-α/IL-6 media on TEER, IgG transport and Luminex assay results, a least squares fit was performed. Error bars in figures represent standard error of the mean calculated over three independent experiments unless otherwise noted.

3.4 Results

3.4.1 TNF-α and IL-6 Treatment Impairs Barrier Integrity

To investigate the effects of inflammation directly on the endothelial cells of the BBB, iPSC-derived BMECs were incubated with IL-6, TNF-α or both cytokines for 24 hours. TEER, a measure of barrier integrity, was unchanged after the addition of IL-6 alone but was reduced by 13% and 16% after the addition of TNF-α and both cytokines respectively (Figure 3.1, A; unpaired t-test; $p = 0.033$ and $p = 0.007$). Permeability to sodium fluorescein, a measure of paracellular permeability, was 2- to 2.5-fold higher than the control with the addition of inflammatory cytokines (Figure 3.1, B; unpaired t-test; $p = 0.005$, $p = 0.021$ and $p = 0.048$). Transport of the fluorescent P-gp substrate Rhodamine 123 was measured in both the luminal to abluminal and abluminal to luminal directions (Figure 3.1, C). The efflux ratio, or the ratio of the amount transported out of the brain compartment to the amount transported into the brain compartment, decreased in the presence of inflammatory cytokines. The efflux ratio in the cells in the inflammation cases was about 40% lower than the control case and is evidence for a loss in polarity in BMECs. Together, these results suggest that the cytokines TNF-α and IL-6 can directly impair BBB integrity.

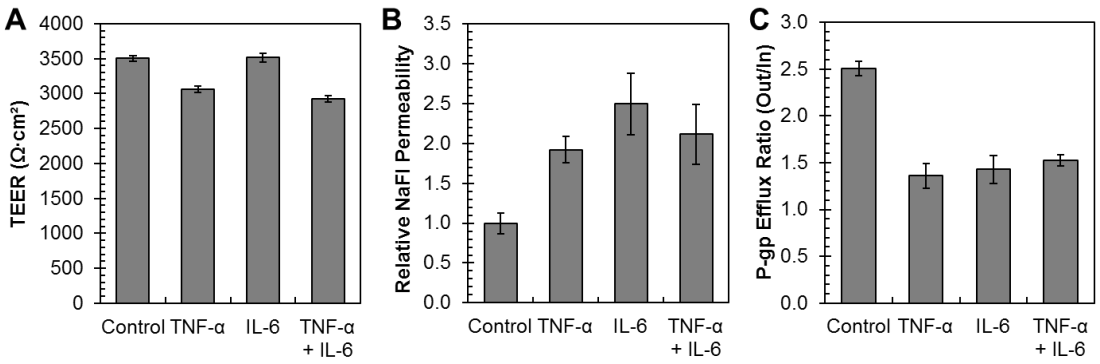

Figure 3.1: Barrier integrity with inflammation. Barrier integrity of iPSC-BMECs after incubation with the cytokines TNF-α and IL-6 measured by (A) TEER (B) sodium fluorescein permeability (normalized to the control) and (C) efflux ratio (abluminal to luminal transport rate/luminal to abluminal transport rate) of the P-gp substrate Rhodamine 123. (n=4; two biological replicates and two independent experiments; data represents the mean ± standard error of the mean)

3.4.2 Coculture With NSC-Derived Astrocytes Improves TEER

Crosstalk between BMECs and other cell types of the NVU *in vivo* is important for maintaining a properly functioning BBB therefore to investigate this crosstalk between cell types, astrocytes were differentiated from NSCs. Immunocytochemistry was used to characterize the cells both before and after differentiation. NSCs expressed nestin, an NSC marker, and vimentin, often used as an astrocyte marker, but lacked GFAP expression, a mature astrocyte marker (Figure 3.2, A, top). After five days of differentiation, the cells still showed expression of nestin, had increased intensity of vimentin expression and a subpopulation of cells also expressed GFAP (Figure 3.2, A, bottom). Cell morphology changed by day 5 from

NSC to the more astrocyte characteristic phenotype with a star shape and endfoot processes.

After 5-10 days of differentiation, NSC-derived astrocytes were cocultured with iPSC-derived BMECs for a fully human coculture model of the BBB. With the addition of NSC-astrocytes, BMECs had a 15% increase in TEER over the monoculture case (Figure 3.2, B). This effect was consistent for NSCs differentiated for five or ten days (data not shown) and therefore a differentiation time of five days was used for all subsequent experiments.

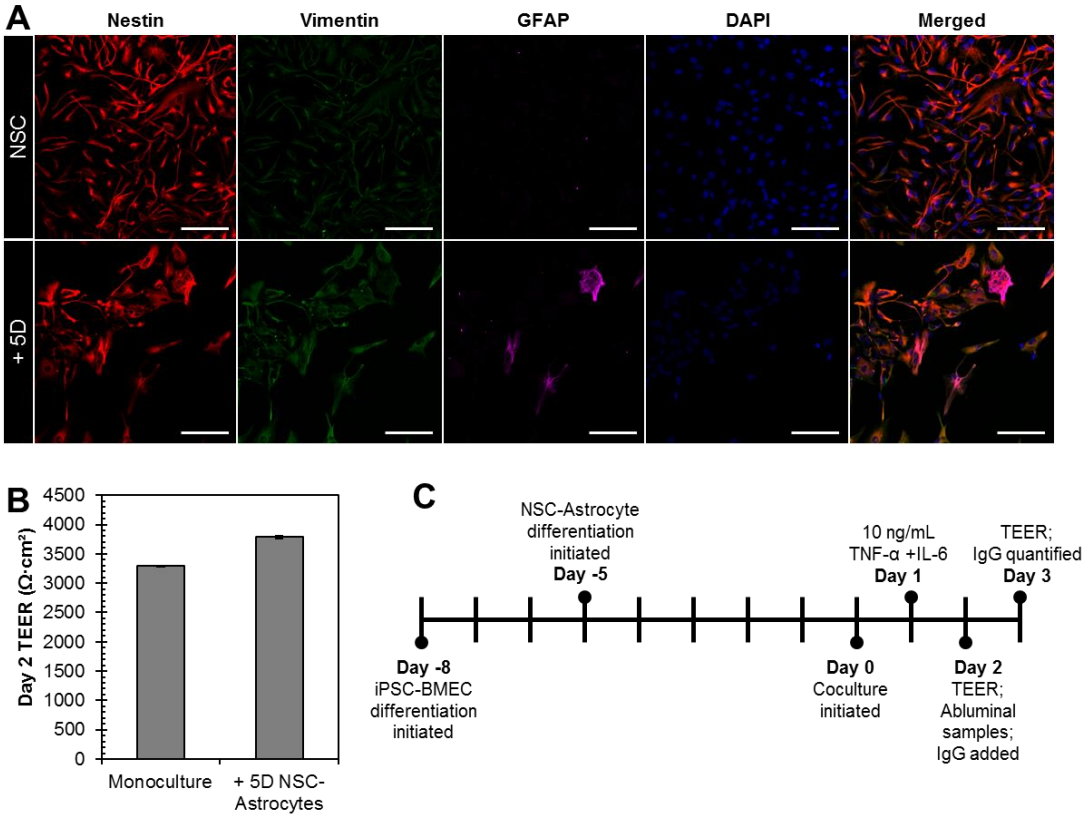

Figure 3.2. NSC-astrocyte characterization. (A) NSCs (top) and cells that have been differentiated for five days (bottom) immunostained for nestin (red), vimentin (green), and GFAP (magenta). Nuclei stained with DAPI (blue). Scale bars 100 μm. (B) Representative Day 2 TEER of BMECs cocultured with 5 day differentiated (+5D) NSC-Astrocytes and monoculture without astrocytes (n = 3; representative figure; data represents the mean ± standard error of the mean; p = 0.0004). (C) iPSC differentiation into BMECs was initiated first, followed by NSC differentiation into astrocytes in parallel. On Day 0, coculture was initiated by passaging the differentiated BMECs onto transwell inserts and placing them into 24-well plates containing the differentiated astrocytes. Cytokines were added one day after coculture initiation and experiments were carried out 24 and 48 hours later.

3.4.3 Cytokine and Chemokine Crosstalk Between BMECs and NSC-Astrocytes

BMECs were grown in monoculture or coculture with NSC-derived astrocytes, and 10 ng/mL each of TNF-α and IL-6 were added in the inflammation cases. After 24

hours, abluminal media was collected and 25 cytokines and chemokines were quantified using a Luminex multiplexed assay (Figure 3.2, C). Of the 25 analytes, 17 were quantified in at least one culture condition. Two were present in all cases (monocyte chemotactic protein 1; MCP-1; interferon gamma-induced protein 10; IP-10), two were present only in the inflammation cases (IL-8 and interferon alpha; IFN-α), six were measured only when NSC-astrocytes were present (IL-2R, IL-4, IL-7, IL-12, monokine induced by gamma interferon; MIG; macrophage inflammatory protein 1 alpha; MIP-1α; IL-6, and TNF-α) and four were detected in the inflammation coculture case only (IFN-γ, IL-1β, MIP-1β, RANTES). Nine analytes were below the limit of quantitation (Eotaxin, IL-1RA, IL-2, IL-5, IL-10, IL-13, IL-15 and IL-17).

MCP-1, a chemokine commonly associated with inflammation in neurodegenerative disease and injury, was measured in all cases (Figure 3.3, A). There was a 24- and 33-fold increase of MCP-1 from monoculture to coculture in the control and inflammation cases respectively. Additionally, there was a 6- and 8-fold increase in MCP-1 concentration from the control to inflammatory conditions in monoculture and coculture cases respectively. Here, MCP-1 is secreted by BMECs (and potentially astrocytes as well) and both coculture and inflammation elevate MCP-1 levels, although coculture has a greater effect. A second chemokine, interferon gamma-induced protein 10 (IP-10) was measured in all cases (Figure 3.3, B). There was an approximately 50-fold increase in IP-10 levels in the coculture with TNF-α and IL-6 case over the controls.

The two cytokines, IL-8 and IFN-α, were measured only in the inflammatory conditions, in both monoculture and coculture (Figure 3.3, C). With the presence of NSC-astrocytes, IL-8 concentration increased 71-fold over the monoculture conditions. There was a 10-fold increase in IFN-α concentration between the monoculture and coculture cases as well. These two cytokines are secreted by BMECs in response to TNF-α and IL-6 and we hypothesize their expression is exacerbated in response to other soluble factors present in coculture.

The largest group of cytokines was measured in the coculture cases only, both in the control and inflammatory conditions (Figure 3.3, D). The highest levels of cytokines were measured in the inflammation cases, with increases ranging from 1.2 to 4-fold for MIP-1α and MIG over the control. This group of cytokines is likely able to be secreted by NSC-astrocytes, or is secreted by endothelial cells in response to a factor only present when NSC-astrocytes are present.

A group of five cytokines were only detected with inflammation in coculture (Figure 3.3, E). This group included IFN-γ, IL-1β, MIP-1β, and RANTES. Of these cytokines, IFN-γ and IL-1β concentrations were low and very close to the LOQ while MIP-1β and RANTES were detected at higher levels of 22 and 296 pg/mL respectively.

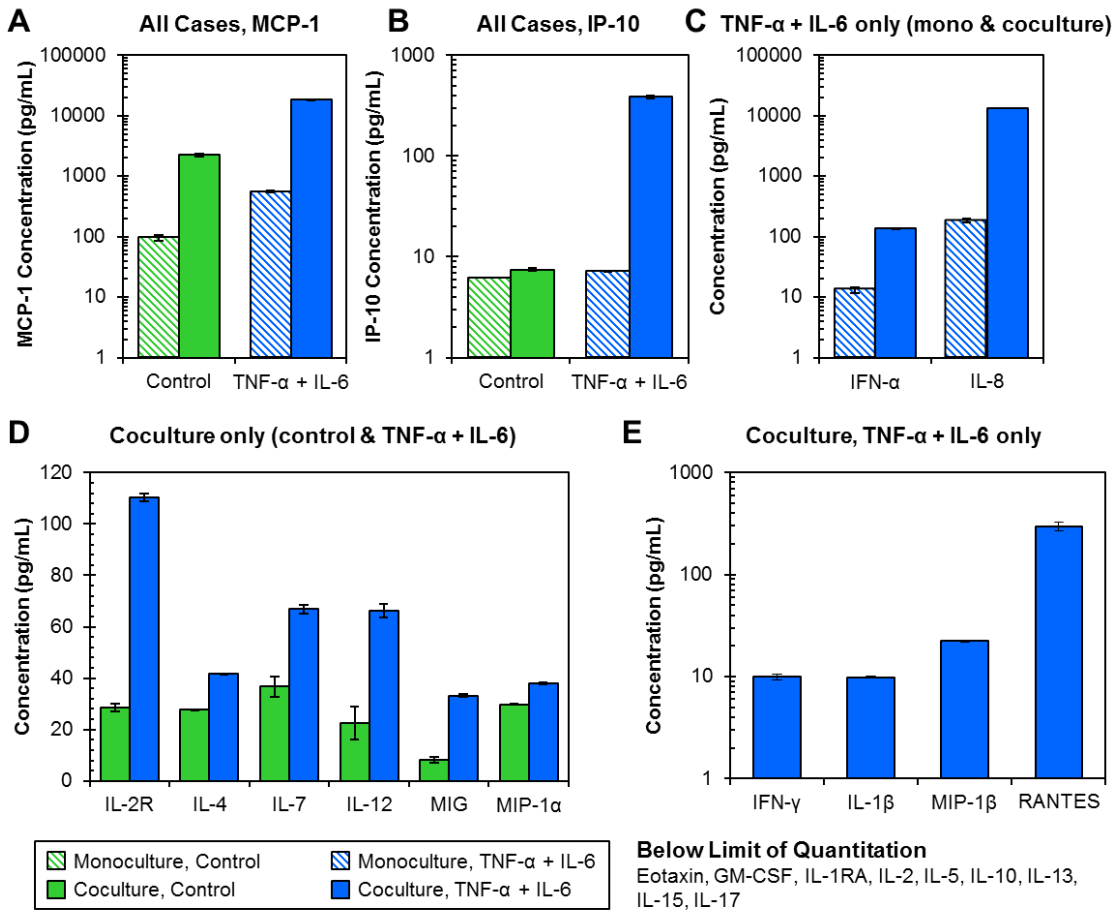

Figure 3.3. Concentrations of cytokines and chemokines measured by Luminex assay. Abluminal concentrations of 25 human cytokine and chemokines were measured after 24 hours of incubation with TNF-α and IL-6 or control media for cells grown in monoculture or coculture. Of the 25 cytokines assayed, 17 were measured in at least one case above the limit of quantitation. (A) MCP-1 and (B) IP-10 were measured in all four cases tested. (C) IFN-α and IL-8 were measured in the inflammatory cases for both monoculture and coculture. (D) Six cytokines were measured only in coculture cases with both control and inflammation media. (E) Four cytokines were measured only in the coculture wells with TNF-α and IL-6 media and were below the limit of quantitation in the other three cases.

3.4.4 NSC-Derived Astrocytes Mitigate Barrier Dysfunction Associated with TNF-α and IL-6 Inflammation

TEER of BMECs in monoculture or coculture with NSC-astrocytes was measured 24 and 48 hours after the addition of cytokine or control media to assess barrier integrity (Figure 3.4). For BMECs in monoculture, there was a 21% difference at 24 hours between the control and inflammatory conditions. In contrast, in coculture over the same timeframe, the TEER in inflammatory conditions was 12% lower than the control. This difference between monoculture and coculture is more significant 48 hours after the addition of TNF-α and IL-6 where the difference between TEER in control and inflammatory case was 56% for monoculture, but remained similar at 13% in coculture.

TEER values for monoculture cells dropped 17% and 54% between Day 2 and Day 3 for control and inflammatory conditions respectively, revealing that the addition of cytokines induces a barrier breakdown that is exacerbated with time in this model. In contrast, TEER values for coculture cells dropped 7.1% for the control and 8.5% for inflammatory conditions, suggesting that NSC-derived astrocytes help maintain BBB function during inflammation.

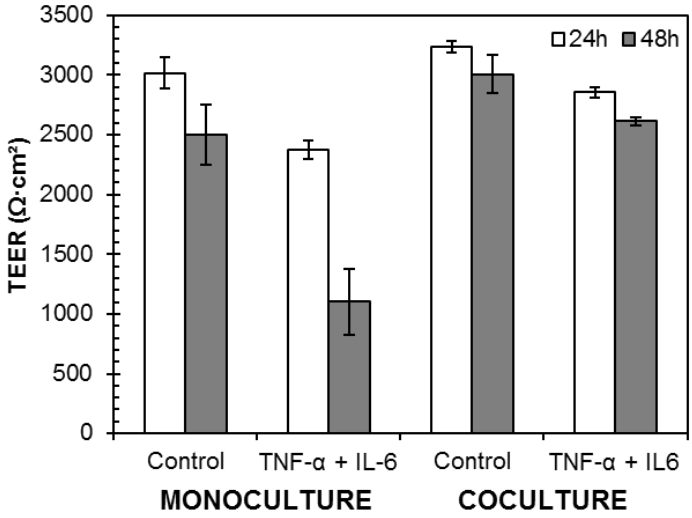

Figure 3.4. TEER of BMECs grown in monoculture or coculture with NSC-derived astrocytes with TNF-α and IL-6. iPSC-derived BMECs were grown in monoculture or coculture with NSC-derived astrocytes and TEER was measured 24 (white) and 48 (gray) hours after the addition of TNF-α and IL-6 or control media. (n=6; three biological replicates and two independent experiments; mean ± standard error of the mean)

IgG transport across the BBB was quantified as a second measure of barrier integrity. IgG extravasation is often used as an *in vivo* measure of barrier integrity after disease or injury. After 24 hours of incubation with cytokine or control media, 10 mg/mL IgGs were added to the luminal compartment to mimic plasma levels and quantified in the abluminal compartment 24 hours later. The amount of IgG transported from the luminal to abluminal compartment was affected by both inflammation and culture conditions (Figure 3.5; least squares fit; $p = 0.0204$ & $p = 0.0305$ respectively). The amount of IgG transported in monoculture with inflammation was about 2.8-fold higher than the monoculture control (unpaired t-test; $p = 0.0489$). However both the control and TNF-α/IL-6 cases in coculture were not

statistically different than the monoculture control. With BMECs alone, there is an increase in IgG transport in inflammation and this increase is mitigated by the presence of NSC-astrocytes.

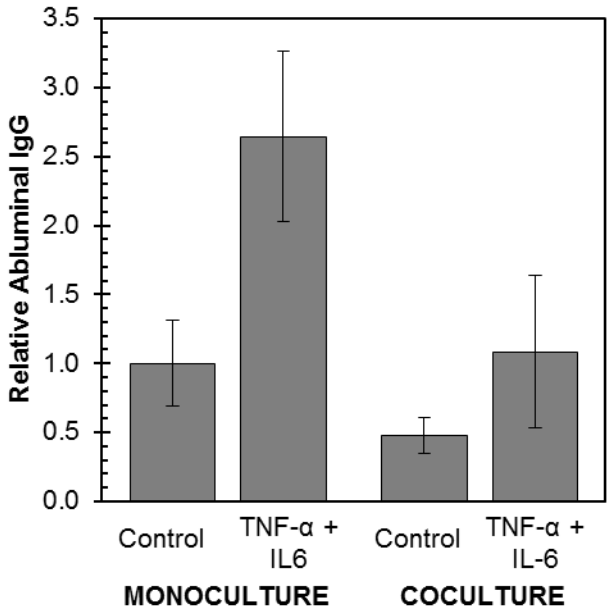

Figure 3.5. Luminal to abluminal IgG transport in coculture with TNF-α and IL-6. iPSC-derived BMECs were grown in monoculture or coculture with NSC-derived astrocytes and incubated with cytokine media or control media for 24 hours before 10mg/mL IVIG was added to the luminal compartment. Abluminal IgG concentration was measured at 24 hours. (n=6; three biological replicates and two independent experiments; mean ± standard error of the mean)

3.5 Discussion

In vitro BBB models facilitate the study of transport phenomena at the cellular level and allow for different levels of complexity through the incorporation of different cell types. To investigate the effects of astrocytes on BMECs during

inflammation, we used a fully human BBB model with cells derived entirely from stem cell sources. iPSCs were differentiated into BMECs while in parallel NSCs were differentiated into astrocytes and these two cell types were combined in a non-contact coculture. The NSC-derived astrocytes expressed two astrocytic markers vimentin and GFAP, however these cells still expressed the NSC marker nestin. Kleiderman et al., (2016) have shown that both NSCs and astrocytes derived from mouse embryonic stem cells express nestin, although a decrease in expression levels is indicative of a differentiated state. Despite a heterogeneous population of cells, these NSC-astrocytes still had a profound effect on the barrier properties of the BMECs as measured by an improvement in TEER.

Before investigating the effects of NSC-derived astrocytes on the BBB in inflammation, a baseline response was first established using BMECs alone. Although the reduction in TEER was significant in the presence of TNF-α, TEER values of 3000 $\Omega \cdot cm^2$ are high and are still within an expected *in vivo* range of 1500-6000 $\Omega \cdot cm^2$ (Butt et al., 1990). Additionally, these values around 3000 $\Omega \cdot cm^2$ exceed the minimum TEER transport threshold of 500 $\Omega \cdot cm^2$, above which paracellular permeability of small molecules, such as sodium fluorescein, does not change (Mantle et al., 2016). Therefore, it is unexpected to see a significant 2- to 2.5-fold increase in sodium fluorescein permeability in the presence of IL-6 and TNF-α. These results, coupled with a decrease in polarity as measured by a decreased P-gp efflux ratio, are consistent with transcellular transport increases in inflammation prior to a significant breakdown of paracellular permeability. An increase in vesicular transcytosis without a

breakdown in paracellular permeability has been shown in other pathological conditions such as hypoxia, ischemia, and injury (De Bock et al., 2016). Additionally, it is clear that TNF-α and IL-6 act directly on the cells of the BBB and can cause barrier dysfunction.

Another potential contribution to barrier dysfunction in disease is additional pro-inflammatory molecules that are secreted by astrocytes or BMECs in response to inflammation. During insults such as infection, inflammation, trauma, and neurodegeneration, astrocytes can enter a reactive state that results in local pro-inflammatory conditions (Broux et al., 2015). In the presence of inflammatory media in coculture, there was a significant increase in the number and concentration of several cytokines and chemokines that are well-known for their pro-inflammatory properties.

For every cytokine detected, the highest levels were measured in the coculture inflammation case when crosstalk between the two cell types was possible. Astrocytes are known to secrete pro-inflammatory MCP-1, IP-10, MIP-1β, IL-1 β, MIG, and RANTES, as well as IL-15, IL-17 and anti-inflammatory IL-10, which were below LOQ (Sofroniew, 2015; Wang et al., 2014; Williams et al., 2009; Xia et al., 2000). BMECs can also be a source of pro-inflammatory chemokines including MCP-1, IL-8, IP-10 and RANTES, which are important for immune cell recruitment to the brain (reviewed by Ransohoff, Schafer, Vincent, Blachère, & Bar-Or, 2015). MCP-1 is a chemokine responsible for recruitment of leukocytes to the brain, it can compromise BBB integrity through reorganization of tight junction proteins, and increased levels

of MCP-1 are associated with neurodegeneration and neuroinflammation (Yao and Tsirka, 2014). Additionally, MCP-1 has been shown to be upregulated in the CSF of patients with MCI and AD (Brosseron et al., 2014). IP-10 is also responsible for immune cell recruitment to the brain and can be secreted by both astrocytes and endothelial cells (Shimizu et al., 2015). MIP-1β is known to be expressed by a subpopulation of astrocytes in AD in coordination with IP-10 (Xia et al., 2000). IL-1β is known to increase BBB permeability via the downregulation of SHH in astrocytes (Wang 2014). MIG has been shown to be elevated in the plasma of AD patients compared to patients with MCI and healthy controls (Lee et al., 2008). Finally, several cytokines detected in this study including IL-1β, MCP-1 and IL-8 (as well as IL-6 and TNF-α) have been shown to be present in higher levels in microvessels from patients with AD compared to age matched controls (Grammas and Ovase, 2001; Grammas and Ovase, 2002). The results from these studies are consistent with known key molecules in inflammation associated with neurodegenerative disease.

There were several cytokines and chemokines detected that are not commonly associated with astrocytes or endothelial cells in AD or neuroinflammation, namely IFN-α, IL-2R, and IL-7. Other cytokines identified are more commonly associated with microgila, including MIP-1α, IL-4, and IL-12. MIP-1α was detected in both coculture conditions however it is known to be expressed by microglia *in vitro* in response to aggregated $A\beta_{1\text{-}42}$ (Lue et al., 2001). Levels of the anti-inflammatory IL-4 were slightly elevated in inflammation coculture compared to the control and were not detected in either monoculture case. Overexpression of IL-4 in the hippocampus of a

mouse model of AD resulted in increased deposition of Aβ, while an earlier study showed that CNS overexpression of IL-4 attenuated AD progression in a mouse model (Kiyota et al., 2010) so the role of this cytokine in disease is still unclear. IL-12 is part of the inflammatory response to Aβ and associated with a pro-inflammatory microglial state (Heppner et al., 2015). This *in vitro* coculture model could potentially be used to identify new molecular mechanisms in inflammation and neurodegenerative disease.

Despite the presence of many pro-inflammatory cytokines and chemokines and only one potentially anti-inflammatory cytokine, NSC-astrocytes mitigated the barrier dysfunction associated with TNF-α and IL-6 incubation. While TEER values in inflammation were lower in both monoculture and coculture when compared to the controls, the presence of NSC-astrocytes mitigated the effects of inflammation over time and helped to maintain barrier integrity. TEER in all cases remained above the 1000 $\Omega \cdot cm^2$ large molecule transport threshold, above which the permeability of large molecules, including IgGs, does not change (Mantle et al., 2016). However in monoculture with TNF-α and IL-6, there is a significant increase in IgG transport across the BBB, which is not present in the coculture case. These data further support the hypothesis that transcellular permeability is compromised before paracellular permeability in inflammatory conditions.

3.6 Conclusions

These results demonstrate that the cytokines TNF-α and IL-6 act directly on the BMECs of the BBB and a transcellular breakdown occurs before paracellular permeability is impaired. This effect is mitigated by the presence of NSC-derived astrocytes, even though there is a significant increase in several pro-inflammatory cytokines known to impair BBB function. This model mimics cellular responses to inflammation at the BBB and can provide a way to study the contributions of individual cell types to disease progression. These results highlight the complex nature of inflammation in neurodegenerative disease and suggest a delicate balance of soluble factors that impact the function of the BBB.

REFERENCES

Abbott NJ, Rönnbäck L, Hansson E. 2006. Astrocyte-endothelial interactions at the blood-brain barrier. Nat. Rev. Neurosci. 7:41–53.

Appelt-Menzel A, Cubukova A, Günther K, Edenhofer F, Piontek J, Krause G, Stüber T, Walles H, Neuhaus W, Metzger M. 2017. Establishment of a Human Blood-Brain Barrier Co-culture Model Mimicking the Neurovascular Unit Using Induced Pluri- and Multipotent Stem Cells. Stem Cell Reports 8.

Bell RD, Zlokovic BV. 2009. Neurovascular mechanisms and blood-brain barrier disorder in Alzheimer's disease. Acta Neuropathol. 118:103–113.

Brosseron F, Krauthausen M, Kummer M, Heneka MT. 2014. Body Fluid Cytokine Levels in Mild Cognitive Impairment and Alzheimer's Disease: A Comparative Overview. Mol. Neurobiol.50:534–544.

Broux B, Gowing E, Prat A. 2015. Glial regulation of the blood-brain barrier in health and disease. Semin. Immunopathol. 37:577–590.

Butt AM, Jones HC, Abbott NJ. 1990. Electrical resistance across the blood-brain barrier in anaesthetized rats: a developmental study. J. Physiol. 429:47–62.

Canfield SG, Stebbins MJ, Morales BS, Asai SW, Vatine GD, Svendsen CN, Palecek SP, Shusta EV. 2017. An isogenic blood-brain barrier model comprising brain endothelial cells, astrocytes, and neurons derived from human induced pluripotent stem cells. J. Neurochem. 140:874–888.

De Bock M, Van Haver V, Vandenbroucke RE, Decrock E, Wang N, Leybaert L. 2016. Into rather unexplored terrain—transcellular transport across the blood-brain barrier. Glia 64:1097–1123.

Deli MA, Ábrahám CS, Kataoka Y, Niwa M. 2005. Permeability studies on in vitro blood-brain barrier models: Physiology, pathology, and pharmacology. Cell. Mol. Neurobiol. 25:59–127.

Grammas P, Ovase R. 2001. Inflammatory factors are elevated in brain microvessels in Alzheimer's disease. Neurobiol. Aging 22:837–842.

Grammas P, Ovase R. 2002. Cerebrovascular transforming growth factor-β contributes to inflammation in the Alzheimer's disease brain. Am. J. Pathol. 160:1583–1587.

Heppner FL, Ransohoff RM, Becher B. 2015. Immune attack: the role of inflammation in Alzheimer disease. Nat. Rev. Neurosci. 16:358–372.

Holmes C, Cunningham C, Zotova E, Woolford J, Dean C, Kerr S, Culliford D, Perry VH. 2009. Systemic inflammation and disease progression in Alzheimer disease. Neurology 73:768–74.

Kiyota T, Okuyama S, Swan RJ, Jacobsen MT, Gendelman HE, Ikezu T. 2010. CNS expression of anti-inflammatory cytokine interleukin-4 attenuates Alzheimer's disease-like pathogenesis in APP+PS1 bigenic mice. FASEB J. 24:3093–3102.

Kleiderman S, Sá JV., Teixeira AP, Brito C, Gutbier S, Evje LG, Hadera MG, Glaab E, Henry M, Sachinidis A, Alves PM, Sonnewald U, Leist M. 2016. Functional and phenotypic differences of pure populations of stem cell-derived astrocytes and neuronal precursor cells. Glia 64:695–715.

Kyrkanides S, Tallents RH, Miller JH, Olschowka ME, Johnson R, Yang M, Olschowka JA, Brouxhon SM, O'Banion MK. 2011. Osteoarthritis accelerates and exacerbates Alzheimer's disease pathology in mice. J. Neuroinflammation 8:112.

Lee KS, Chung JH, Lee KH, Shin MJ, Oh BH, Hong CH. 2008. Bioplex analysis of plasma cytokines in Alzheimer's disease and mild cognitive impairment. Immunol. Lett. 121:105–109.

Lim JC, Wolpaw AJ, Caldwell MA, Hladky SB, Barrand MA. 2007. Neural precursor cell influences on blood-brain barrier characteristics in rat brain endothelial cells. Brain Res. 1159:67–76.

Lippmann ES, Weidenfeller C, Svendsen CN, Shusta EV. 2011. Blood-brain barrier modeling with co-cultured neural progenitor cell-derived astrocytes and neurons. J. Neurochem. 119:507–520.

Lippmann ES, Al-Ahmad A, Azarin SM, Palecek SP, Shusta EV. 2014. A retinoic acid-enhanced, multicellular human blood-brain barrier model derived from stem cell sources. Sci. Rep. 4:4160.

Lippmann ES, Azarin SM, Kay JE, Nessler RA, Wilson HK, Al-Ahmad A, Palecek SP, Shusta EV. 2012. Derivation of blood-brain barrier endothelial cells from human pluripotent stem cells. Nat. Biotechnol. 30:783–791.

Lue LF, Rydel R, Brigham EF, Yang LB, Hampel H, Murphy GM, Brachova L, Yan S Du, Walker DG, Shen Y, Rogers J. 2001. Inflammatory repertoire of Alzheimer's disease and nondemented elderly microglia in vitro. Glia 35:72–79.

Mantle JL, Min L, Lee KH. 2016. Minimum Transendothelial Electrical Resistance Thresholds for the Study of Small and Large Molecule Drug Transport in a Human in Vitro Blood-Brain Barrier Model. Mol. Pharm. 13:4191–4198.

Mayeux R, Ottman R, Tang MX, Noboa-Bauza L, Marder K, Gurland B, Stern Y. 1993. Genetic susceptibility and head injury as risk factors for Alzheimer's disease among community-dwelling elderly persons and their first-degree relatives. Ann Neurol 33:494–501.

Ransohoff RM, Schafer D, Vincent A, Blachère NE, Bar-Or A. 2015. Neuroinflammation: Ways in Which the Immune System Affects the Brain. Neurotherapeutics 12:896–909.

Shimizu F, Nishihara H, Sano Y, Takeshita Y, Takahashi S, Maeda T, Takahashi T, Abe M, Koga M, Kanda T. 2015. Markedly increased IP-10 production by blood-brain barrier in neuromyelitis optica. PLoS One 10.

Sofroniew MV. 2015. Astrocyte barriers to neurotoxic inflammation. Nat. Rev. Neurosci. 16:249–263.

Stebbins MJ, Wilson HK, Canfield SG, Qian T, Palecek SP, Shusta EV. 2016. Differentiation and characterization of human pluripotent stem cell-derived brain microvascular endothelial cells. Methods 101:93–102.

Wang Y, Jin S, Sonobe Y, Cheng Y, Horiuchi H, Parajuli B, Kawanokuchi J, Mizuno T, Takeuchi H, Suzumura A. 2014. Interleukin-1β induces blood-brain barrier disruption by downregulating sonic hedgehog in astrocytes. PLoS One 9:e110024.

Weidenfeller C, Svendsen CN, Shusta EV. 2007. Differentiating embryonic neural progenitor cells induce blood-brain barrier properties. J. Neurochem. 101:555–565.

Williams R, Yao H, Dhillon NK, Buch SJ. 2009. HIV-1 Tat co-operates with IFN-gamma and TNF-alpha to increase CXCL10 in human astrocytes. PLoS One 4:e5709.

Xia MQ, Bacskai BJ, Knowles RB, Qin SX, Hyman BT. 2000. Expression of the chemokine receptor CXCR3 on neurons and the elevated expression of its ligand IP-10 in reactive astrocytes: in vitro ERK1/2 activation and role in Alzheimer's disease. J. Neuroimmunol. 108:227–235.

Yao Y, Tsirka SE. 2014. Monocyte chemoattractant protein-1 and the blood-brain barrier. Cell. Mol. Life Sci. 71:683–697.

Yu J, Vodyanik MA, Smuga-Otto K, Antosiewicz-Bourget J, Frane JL, Tian S, Nie J, Jonsdottir GA, Ruotti V, Stewart R, Slukvin II, Thomson JA. 2007. Induced pluripotent stem cell lines derived from human somatic cells. Science 318:1917–1920.

Chapter 4

IGG TRANSPORT INCREASES AT THE BLOOD-BRAIN BARRIER DURING ALZHEIMER'S DISEASE AND NEUROINFLAMMATION

4.1 Preface

In this chapter, inhibitors and probes of different endocytic routes are used to characterize the transport mechanisms of IgGs across the blood-brain barrier. Changes to blood-brain barrier transport in disease are also investigated. This work was funded in part by the National Science Foundation (Award Number 1144726).

4.1.1 Abstract

Immunotherapies are a promising strategy for the treatment of neurological diseases such as Alzheimer's disease (AD) however it is widely accepted that less than 0.1% of the injected dose of a therapeutic antibody can reach the brain due to the presence of the blood-brain barrier (BBB). Additionally, transport of molecules at the BBB is altered in disease, which has the potential to affect the mechanism of entry to the brain as well as the quantity delivered. To better understand transport of immunotherapies at the BBB in disease, an *in vitro* BBB model derived from human induced pluripotent stem cells (iPSCs) was employed to investigate the endocytic uptake route of IgG. Uptake of fluorescently labeled IgGs at the BBB is a saturable

process, with less IgG uptake after pretreatment with a physiologically-relevant concentration of unlabeled IgGs. Inhibition of clathrin-mediated endocytosis, caveolar endocytosis and macropinocytosis demonstrated that macropinocytosis is a major transport route for IgGs at the BBB. Disease stimuli were added to the model to mimic AD ($A\beta_{1-40}$ and $A\beta_{1-42}$) and accompanying neuroinflammation (TNF-α and IL-6), which resulted in an increase in IgG uptake and transport. Lastly, we observed increases in caveolar endocytosis in the AD model, which may be responsible for the increase in IgG uptake in disease. This work presents an iPSC-derived BBB model that responds to disease stimuli with physiologically relevant changes to molecular transport and can be used to understand fundamental questions about transport mechanisms of immunotherapies in health and neurodegenerative disease.

4.2 Introduction

Alzheimer's disease (AD) is estimated to affect 5.5 million Americans in 2017, and despite the prevalence of AD there are only five FDA-approved small molecule symptomatic drugs and no disease-modifying or preventive therapeutics (Alzheimer's Association 2017). Immunotherapies are being developed and tested for the treatment of neurological diseases such as AD because of their advantages such as target specificity and affinity. More specifically, passive immunization against the amyloid β (Aβ) that composes extracellular senile plaques is an attractive strategy for the treatment of AD progression (Lannfelt et al., 2014). Despite preclinical promise, these

treatments have largely failed to have a disease-modifying effect and have yet to gain FDA approval, although there are some promising candidates in the pipeline. Aducanumab is the most recent anti-Aβ antibody and has been shown to reduce brain Aβ plaques in a dose- and time-dependent fashion in a double-blind placebo-controlled Phase 1B randomized trial and has entered Phase III trials (Sevigny et al., 2016). Questions still remain about the quantity of immunotherapeutics capable of overcoming the blood-brain barrier (BBB) to reach the brain in sufficient concentrations to have a measurable effect. The BBB is a bottleneck in development of drugs for central nervous system (CNS) disorders, as the challenge of transporting a large molecule drug across this barrier makes it difficult to translate therapeutics from the lab to the clinic (Pardridge, 2005).

The BBB comprises the brain microvascular endothelial cells (BMECs) that line cerebral capillaries and maintains brain homeostasis through a number of different mechanisms. Tight junctions prevent paracellular transport of hydrophilic molecules larger than 400 Da while some small lipophilic molecules are able to passively diffuse across the BBB. Efflux pumps effectively remove many compounds from the brain, including small lipophilic molecules that might otherwise passively diffuse across BMECs (Abbott et al., 2006; Abbott et al., 2010). Transcytosis of molecules through BMECs is limited in part by low levels of endocytosis at the BBB compared with other endothelium, with only 1-15 vesicles per μm^2 compared to 30-40 vesicles per μm^2 in lung and intestinal capillary endothelium (Ito et al., 1980; Stewart, 2000).

Because of the presence of tight junctions between BMECs, large molecules such as immunotherapeutics must be transcytosed from the blood to the brain, and the initial uptake of these molecules at the BBB can occur through several different mechanisms (

Table 4.1). Clathrin-mediated endocytosis is the most well-studied, classified by clathrin-coated pits that are 60-200 nm in size (Preston et al., 2014) and responsible for endocytosis of ligand-receptor pairs (i.e. transferrin and transferrin receptor). Caveolar endocytosis, which is classified by 50-100 nm flask-shaped vesicles formed from lipid raft domains of the plasma membrane, can also play a role in endocytosis of ligand-receptor pairs and in adsorptive-mediated endocytosis (Preston et al., 2014). However, caveolar endocytosis is not a major endocytic mechanism at the BBB and moreover it has been shown that suppression of this transport route is required for proper BBB function (Andreone et al., 2017). Macropinocytosis is a nonspecific bulk engulfment of extracellular fluid and these irregularly shaped vesicles can be 200 nm to 5 μm in size. It is not well understood which specific endocytic route is responsible for IgG transport across the BBB, and this knowledge could inform the development of more effective therapeutics.

Table 4.1. Endocytic pathways at the BBB.

Type of Uptake	Inhibitor	Probe	Characteristics
Clathrin-mediated (Deane et al., 2009; von Kleist et al., 2011)	Pitstop2	Transferrin	60-200 nm Clathrin-coated round vesicles Ligand-receptor pairs (i.e. transferrin & transferrin receptor) Changes to specific receptors in AD (i.e. reduced LRP1)
Caveolar (Andreone et al., 2017; Claudio, 1996; Haley and Lawrence, 2016; Knowland et al., 2014)	Nystatin	Cholera Toxin B Subunit (CTB)	50-100 nm Flask-shaped vesicles, lipid rafts Ligand-receptor pairs and adsorptive-mediated endocytosis Suppression required for BBB function Increased after stroke and in AD
Macropinocytosis (Lim and Gleeson, 2011)	Amiloride	10 kDa Dextran	200 nm-5μm Irregularly-shaped vesicles Nonspecific bulk engulfment of extracellular fluid Increased in inflammation

Different mechanisms of molecular transport at the BBB are altered in AD, which may also affect distribution of therapeutics in the brain and treatment efficiency (Schenk and Vries, 2016). For example, clinical studies have shown an increase in albumin, a blood-derived protein, in the cerebrospinal fluid in patients with AD and vascular dementia (Erickson and Banks, 2013), indicative of a leaky BBB. There is also a well characterized reduction in clearance of Aβ across the BBB via decreases in the expression of low-density lipoprotein receptor related protein-1 (LRP1) (Deane et al., 2009) in AD. Other studies have shown reductions in the glucose transporter

GLUT1 (Winkler et al., 2015) and reduced expression and activity of the efflux pump P-glycoprotein (Hartz et al., 2016) in AD. Secondary events may also alter transport properties; inflammation is both a risk factor and an early event in AD (Heppner et al., 2015) and is known to increase macropinocytosis (Lim and Gleeson, 2011; Preston et al., 2014). What remains largely unknown is how different aspects of AD affect transport routes at the BBB and how these changes might affect the delivery of large molecule therapeutics.

In vitro models are useful tools to study the transport of immunotherapies, as well as the effects of different aspects of disease, at the BBB. Our previous work has shown that there are different transendothelial electrical resistance (TEER) thresholds required for studying small and large molecule drugs and demonstrated the utility of the model for assessing permeability of small molecule therapeutics (Mantle et al., 2016). Because many new therapeutics for AD and other brain diseases are large molecule immunotherapies, there is a need for *in vitro* BBB models that can be used to quantify large molecule drug transport, understand specific transport routes, and identify changes to transport that occur in disease. Therefore, this work aims to use an *in vitro* BBB model derived from human induced pluripotent stem cells (iPSCs) (Lippmann et al., 2012; Lippmann et al., 2014) to elucidate the transport mechanisms of IgG across BMECs in disease. Intravenous immunoglobulin (IVIG), or pooled IgGs from healthy donors, was used as a model large molecule therapeutic. First, the transport behavior of IgGs in the *in vitro* model was characterized and compared to *in vivo* experiments. Next, small molecule inhibitors of different endocytic pathways

were used to identify the most likely IgG transport route. Two simple disease models were developed using Aβ isoforms to mimic AD and the cytokines tumor necrosis factor α (TNF-α) and interleukin 6 (IL-6) to mimic inflammation and changes to IgG transport and transport routes were evaluated.

4.3 Materials and Methods

4.3.1 Materials

Human $A\beta_{1-40}$ (DAEFRHDSGYEVHHQKLVFFAEDVGSNKGAIIGLMV-GGVV) and $A\beta_{1-42}$ (DAEFRHDSGYEVHHQKLVFFAEDVGSNKGAIIGLMVGG-VVIA) were purchased from AnaSpec (Freemont, CA, USA). Phenol-free Ham's F-12 media with L-glutamine was purchased from Caisson Laboratories (North Logan, UT, USA). Hexafluoro-2-propanol, anhydrous dimethyl sulfoxide, collagen IV, fibronectin, donkey serum, NaCl, Triton X-100, sodium deoxycholate, sodium dodecyl sulfate, TRIS, amiloride, nystatin, and Cholera Toxin B Subunit FITC conjugate were purchased from Sigma-Aldrich (St. Louis, MO, USA). The iPS(IMR90)-4 cell line was purchased from WiCell (Madison, WI, USA). mTeSR-1 medium was purchased from STEMCELL Technologies (Vancouver, BC, Canada). 6-well plates, 24-well Transwell inserts (PET; 0.4 μm pores), Transwell companion plates, and 96-well plates were purchased from Thomas Scientific (Swedesboro, NJ, USA). Growth factor-reduced Matrigel, DMEM/F-12, Versene, donkey anti-rabbit AlexaFluor-488, 4', 6-Diamidino-2-Phenylindole, Dihydrochloride (DAPI), goat anti-

mouse Alexa Fluor-488, Dulbecco's Phosphate Buffered Saline (DPBS), Easy-Titer® Human IgG Assay Kit, Dextran Texas Red 10 kDa, Transferrin from human serum Texas Red conjugate, and human endothelial cell serum free medium (ECSFM) were purchased from Thermo Fisher Scientific (Waltham, MA, USA). Rabbit anti FcRn was purchased from Santa Cruz Biotechnology (Dallas, TX, USA). Recombinant human TNF-α and recombinant human IL-6 were purchased from R&D Systems (Minneapolis, MN, USA). A MicroPlate Genie was purchased from Scientific Industries Inc. (Bohemia, NY, USA). A Spectra Max M5 microplate reader was purchased from Molecular Devices (Sunnyvale, CA, USA). Gammagard Liquid Immune Globulin Intravenous (Human) 10% (Lot # LE12L017AB) was purchased from Baxter (Westlake Village, CA, USA). Pitstop 2 was purchased from AbCam (Cambridge, UK). Platelet poor derived serum (PDS) was purchased from Alfa Aesar (Ward Hill, MA, USA). Paraformaldehyde solution, 16% was purchased from Electron Microscopy Sciences (Hatfield, PA, USA).

4.3.2 $A\beta_{1-40}$ and $A\beta_{1-42}$ Preparation

Human $A\beta_{1-40}$ and $A\beta_{1-42}$ were aggregated into oligomeric form (Dahlgren et al., 2002; Stine et al., 2003). Briefly, peptides were dissolved to 1 mM in hexafluoro-2-propanol, aliquoted, dried, and stored at -20 °C until use. To prepare oligomeric Aβ, peptides were dissolved to 5 mM in anhydrous dimethyl sulfoxide. Peptide solution

was diluted to 100 μM in ice cold phenol-free Ham's F-12 media with L-glutamine and incubated at 4 °C for 24 hours.

4.3.3 BMEC Differentiation, Culture and Disease Models

iPS(IMR90)-4 iPSCs (Yu et al., 2007) were maintained as previously described (Lippmann et al., 2014; Mantle et al., 2016). Briefly, iPSCs were grown in mTeSR-1 medium on 6-well plates coated with growth-factor reduced Matrigel and passaged every 3-5 days using Versene and mechanical dissociation. Cells were differentiated as previously described (Lippmann et al., 2012; Lippmann et al., 2014). On Day 9 of differentiation, cells were passaged to 24-well Transwell inserts coated with a solution of 40% collagen IV and 10% fibronectin in water. Alternately, cells were passaged to 96-well plates pretreated with a 1:8 dilution of the collagen/fibronectin solution in water. On Day 10 of differentiation, $A\beta_{1-40}$ or $A\beta_{1-42}$ were added to the abluminal compartment to achieve a final concentration of 5 μM to mimic AD. Alternately, to mimic neuroinflammation, cells were incubated with 10 ng/mL TNF-α, 10 ng/mL IL-6 or 10 ng/mL each of both cytokines. All experiments were performed on Day 11 (Figure 4.1).

4.3.4 IgG Uptake Assay

BMECs were passaged to 96 well plates on Day 9 of differentiation (Figure 4.1). On Day 11, 0.025 mg/mL fluorescently conjugated antibody (goat anti-mouse

Alexafluor-488) was added to appropriate wells and incubated at 37 °C for one hour. Media was aspirated and cells were rinsed twice with ice cold DPBS. After two washes, 100 μL lysis buffer (RIPA buffer), consisting of 150 mM NaCl, 1% (v/v) Triton X-100, 0.5% (w/v) sodium deoxycholate, 0.1% (w/v) sodium dodecyl sulfate and 50 mM TRIS in water, was added to the cells for 5 minutes. The plate was shaken on a MicroPlate Genie for an additional 5 minutes. The fluorescence of each well was quantified using a Spectra Max M5 microplate reader with excitation = 490 nm and emission = 525 nm. A standard curve was used to calculate ng of antibody transported based on the fluorescence detected.

4.3.5 IgG Transport Assay

To quantify IgG transport across the BBB model, IVIG was added to the luminal compartment at 10 mg/mL unless otherwise noted (Figure 4.1). Cells were incubated for 6 hours at 37 °C and abluminal samples were collected and stored at -20 °C. Abluminal IgG concentrations were quantified using the Easy-Titer ® Human IgG Assay Kit according to the manufacturer's protocol.

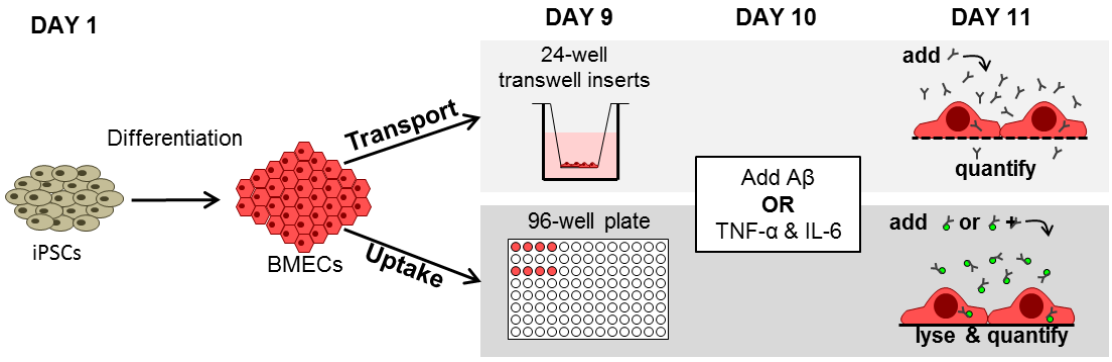

Figure 4.1. Experimental Overview. After nine days of differentiation, iPSC-BMECs are passaged for transport or uptake experiments. Aβ or cytokines are added on Day 10. To measure transport, IgGs are added to the luminal compartment and measured in the abluminal compartment after six hours. To measure uptake, fluorescently labeled IgGs (or unlabeled IVIG and fluorescent IgGs) are added to the cells and fluorescence is quantified after cell lysis.

4.3.6 FcRn Immunocytochemistry

Differentiated BMECs were grown on an 8-well chambered coverglass coated in a 1:8 dilution of collagen/fibronectin solution. After two days of growth, cells were washed three times with cold DPBS and fixed with 2% paraformaldehyde in DPBS for 15 minutes. Cells were washed three times with DPBS and permeabilized with 0.1% Trition X-100. Cells were washed twice with DPBS and blocked in 10% donkey serum in DPBS for one hour at room temperature. Cells were then incubated with primary antibody solution (4 μg/mL Rabbit anti-FcRn and 1% donkey serum in DPBS) on an orbital shaker for 12 hours at 4 °C. Cells were rinsed twice with 1% donkey serum in DPBS and incubated with secondary antibody solution (donkey anti-rabbit AlexaFluor-488 and 1% donkey serum in DPBS) at room temperature for one hour. Cells were rinsed twice with 1% donkey serum in DPBS, incubated with 300 nM

DAPI for 10 minutes, and washed three times with DPBS. Images were taken with a 20x objective on a Zeiss LSM 710 confocal microscope.

4.3.7 Endocytic Route Inhibition

Nystatin, an inhibitor of caveolar endocytosis (Schnitzer et al., 1994), Pitstop 2, an inhibitor of clathrin-mediated endocytosis (von Kleist et al., 2011), and amiloride, an inhibitor of macropinocytosis (Lim and Gleeson, 2011), were dissolved in DMSO, aliquoted and stored at -20 °C until use. Working concentrations were selected such that barrier integrity remained intact after incubation, as measured by TEER. Cells were grown on 24-well inserts (transport) or 96-well plates (uptake), all media were aspirated, and media containing appropriate inhibitors were added to the wells (Nystatin: 5 μg/mL; Pitstop 2: 10 μM; Amiloride: 100 μM). Cells were incubated with inhibitor media for 30 minutes prior to the addition of IgGs.

4.3.8 Transport Route Probes

Cholera Toxin B Subunit (CTB)-FITC conjugate was dissolved to 0.5 mg/mL in sterile water, aliquoted and stored at 4 °C until use. Dextran, Texas Red, 10 kDa was stored at 10 mg/mL at -20 °C until use. Transferrin from human serum Texas Red conjugate was stored at 5mg/mL at 4 °C until use. All probes were diluted in endothelial cell medium (EC; human endothelial cell serum free medium supplemented with 1% PDS) such that the total volume added to each well was the

same. Differentiated BMECs were grown on a 96-well plate and probes were added at a concentration of 50 μg/mL. Cells were incubated at 37 °C for one hour. Media were aspirated, cells were rinsed twice with ice cold DPBS and cold RIPA buffer was added to each well for 5 minutes. The plate was mixed on a MicroPlate Genie for an additional 5 minutes and fluorescence of each well was quantified using a Spectra Max 5 (FITC: excitation 490 nm, emission 525 nm; Texas Red: excitation 595 nm, emission 615 nm).

4.4 Results

4.4.1 IgG Transport Characterization

BMECs were grown on Transwell inserts and different amounts of IgG ranging from 0.5 to 20 mg/mL were added to the luminal compartment of the *in vitro* BBB model and quantified in the abluminal compartment after six hours (Figure 4.2, A). As luminal starting IgG concentration increased, the concentration detected in the abluminal compartment also increased until a starting concentration of about 7.5 mg/mL. Between 7.5 mg/mL and 20 mg/mL starting luminal IgG, the amount transported into the abluminal compartment after six hours is constant, consistent with a saturable IgG transport process through the BBB. To further probe the nature of IgG transport, BMECs were grown in 96 well plates and preincubated with 15 mg/mL unlabeled IgGs. After 15 minutes, fluorescently labeled IgG was added and the relative IgG uptake was quantified. The amount of fluorescent IgG uptake was

reduced by 72% in the cells that had been preincubated with unlabeled IgGs (Figure 4.2, B), also consistent with the notion that IgG uptake is a saturable process.

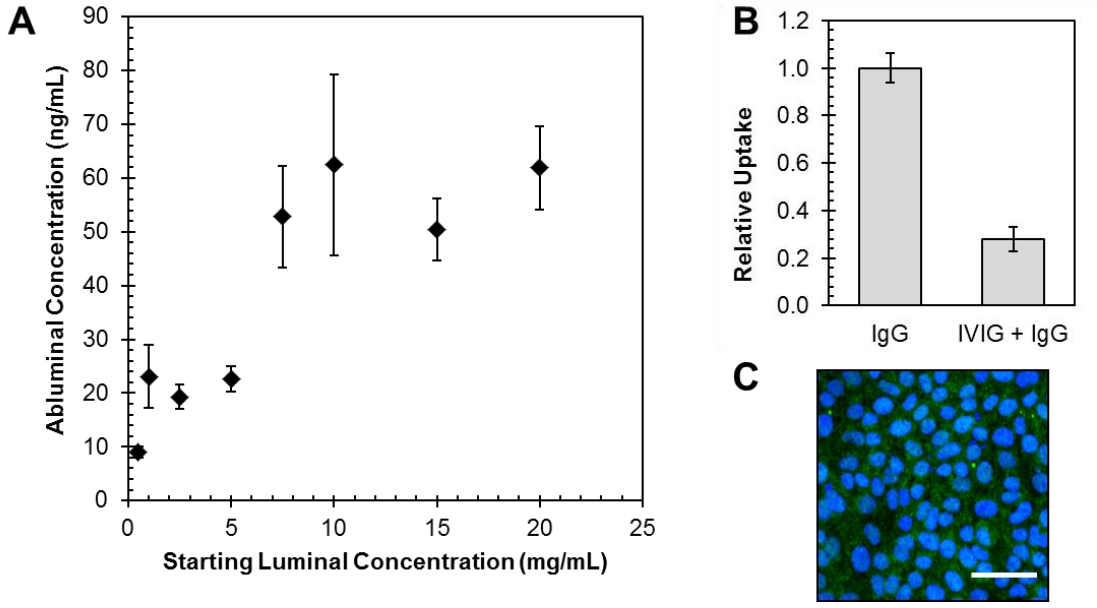

Figure 4.2. IgG transport characteristics in iPSC-BMECs. (A) Amount of IgG transported from luminal to abluminal chambers after six hours with different starting luminal concentrations. Each point represents the mean ± standard error of the mean over at least two independent experiments (n = at least 4; except 2.5 and 15 mg/mL (n = 2; one experiment)). (B) Uptake of AlexaFluor (AF)-488 labeled IgG, in the presence and absence of 15 mg/mL unlabeled IgGs (p = 3.4E-7). Data are normalized to uptake in the IgG only cells and each bar represents the mean ± standard error of the mean over two independent experiments (n=8). (C) FcRn (green) and DAPI (blue) staining of iPSC-derived BMECs. Scale bar is 50 μM.

4.4.2 IgG Uptake and Transport Occurs Via Macropinocytosis

BMECs were preincubated with inhibitors of different endocytic pathways including caveolar, clathrin-mediated and macropinocytosis. Nystatin was used to

inhibit caveolar endocytosis, Pitstop2 was used as an inhibitor of clathrin-mediated endocytosis, and amiloride was used to inhibit macropinocytosis. Both IgG uptake (Figure 4.3, A) and IgG transport across the BMEC monolayer after six hours (Figure 4.3, B) were quantified. IgG uptake was about 50% less than the control with the addition of amiloride ($p = 0.0001$), suggesting that IgG uptake is via nonspecific macropinocytosis. Luminal to abluminal IgG transport follows the same trend as IgG uptake and is reduced about 40% with the addition of amiloride, however this change is not statistically significant ($p = 0.054$). There were no statistically-significant changes with the addition of Pitstop2 or Nystatin in either uptake or transport, suggesting that clathrin-mediated endocytosis and caveolar endocytosis are not primary transport routes for IgGs across the BBB.

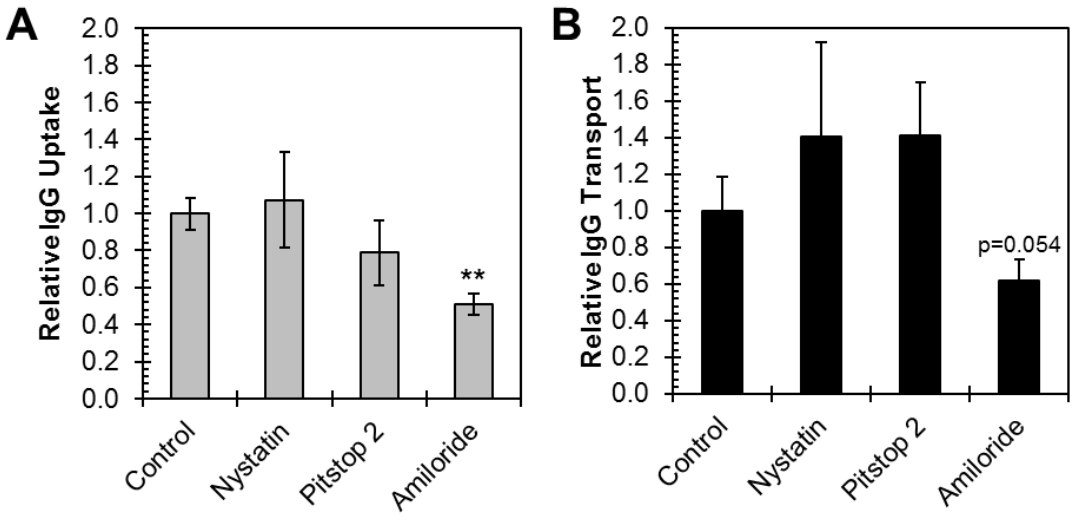

Figure 4.3. IgG uptake and transport with inhibition of endocytic routes. (A) IgG uptake after one hour (n = 9) and (B) luminal to abluminal IgG transport after six hours (right; n = 7) in the presence of endocytic route inhibitors. Nystatin inhibits caveolar endocytosis, Pitstop 2 is an inhibitor of clathrin-mediated endocytosis and amiloride is an inhibitor of macropinocytosis. Data are normalized to uptake or transport in the control cells and bars represent the mean ± standard error of the mean across three independent experiments. (** $p < 0.01$)

4.4.3 IgG Uptake and Transport Alterations in Disease Models

In neurodegenerative disease and brain injury there is evidence for increased vesicular transport across the BBB before any breakdown in the paracellular barrier (De Bock et al., 2016), therefore IgG transport and uptake experiments were performed in two disease states to quantify these changes. To mimic AD, BMECs were incubated with 5 μM $A\beta_{1-40}$, the primary component of vascular plaques in cerebral amyloid angiopathy that often accompanies AD, or $A\beta_{1-42}$, the primary component of neuritic plaques associated with neurodegeneration in AD. IgG uptake

(Figure 4.4, A) increased 12% with $A\beta_{1-40}$ ($p = 0.024$) and 45% with $A\beta_{1-42}$ ($p = 7.23E-6$). IgG transport through the BMEC monolayer (Figure 4.5, A) increased 126% over the control with $A\beta_{1-42}$ ($p = 0.0281$) and increased 22% over the control with $A\beta_{1-40}$ ($p = 0.0649$), although this increase was not statistically significant.

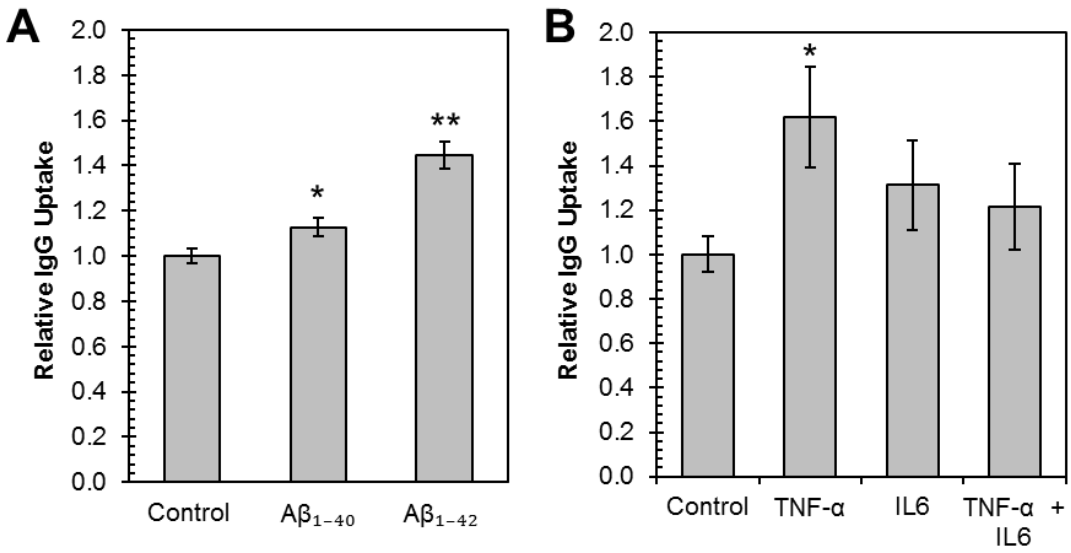

Figure 4.4. IgG uptake in disease models. (A) Cells were preincubated for 24 hours with 5 μM Aβ to mimic AD (n=8) or (B) 10 ng/mL cytokines to mimic neuroinflammation (n=10). IVIG was added to the luminal compartment and quantified after six hours. Data are normalized to the uptake in the control cases and each bar represents the mean ± standard error of the mean across three independent experiments. (* $p < 0.05$ and ** $p < 0.01$)

To mimic more general neuroinflammation that accompanies neurodegenerative disease or brain injury, BMECs were incubated with either 10 ng/mL IL-6, TNF-α or 10 ng/mL of both cytokines. These cytokines are two of the most commonly studied cytokines in neuroinflammation and increases in

cerebrospinal fluid levels of TNF-α and IL-6 are correlated with AD (Brosseron et al., 2014). IgG uptake (Figure 4.4, B) increased 62% in the presence of TNF-α ($p = 0.0233$). IgG uptake also increased 20-30% in the presence of IL-6 and both cytokines although these increases were not statistically significant. IgG transport across the BBB (Figure 4.5, B) was 86% higher when BMECs were incubated with both TNF-α and IL-6, compared to the control ($p = 0.0262$). These results demonstrate that this *in vitro* model can respond to disease stimuli with physiologically-relevant changes to molecular transport.

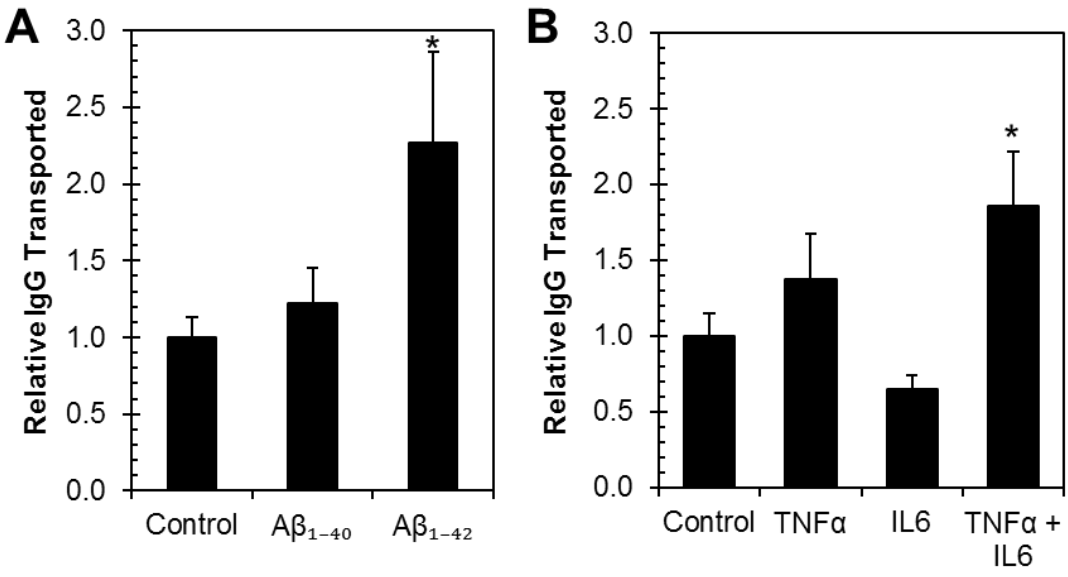

Figure 4.5. IgG Transport in disease models. (A) Cells were preincubated for 24 hours with 5 μM Aβ to mimic AD (left; n=12) or (B) 10 ng/mL cytokines to mimic neuroinflammation (right; n=7). BMECs were then incubated with a fluorescently labeled IgG and IgG uptake was quantified by fluorescence after one hour. Data are normalized to the uptake in the control cases and each bar represents the mean ± standard error of the mean across three independent experiments. (* $p < 0.05$)

4.4.4 Changes to Transport Routes in Disease Models

Given the observations that 1) IgG transport is likely via nonspecific macropinocytosis and 2) IgG transport increases in some disease states, we sought to understand changes to transport mechanisms in disease that could be responsible for the increase in IgG transport and transcellular breakdown. To investigate which transport routes are affected by disease states, BMEC uptake of fluorescent probes with known transport routes was quantified (Figure 4.6). The cases investigated included no treatment (control), inflammation with both TNF-α and IL-6, and incubation with $A\beta_{1-42}$. CTB was used as a probe of caveolar endocytosis, transferrin was used as a probe of clathrin-mediated endocytosis and 10 kDa dextran was used as a probe of macropinocytosis. CTB uptake increased 13% with inflammation ($p = 0.03$), indicating a small increase in caveolar endocytosis in inflammation, but no changes to the other routes. Uptake of CTB increased 78% with $A\beta_{1-42}$ ($p = 9.5E-7$) and uptake of 10 kDa dextran increased 32% ($p = 3.2E-5$). Caveolar endocytosis and macropinocytosis both increased in the AD model, however there was a greater increase in caveolar endocytosis. There were no changes to the amount of transferrin transported in either the inflammation or the AD models, which implies no changes to the clathrin-mediated endocytic pathway. These results are consistent with an increase in molecular uptake at the BBB in disease that is due to an increase in caveolar endocytosis.

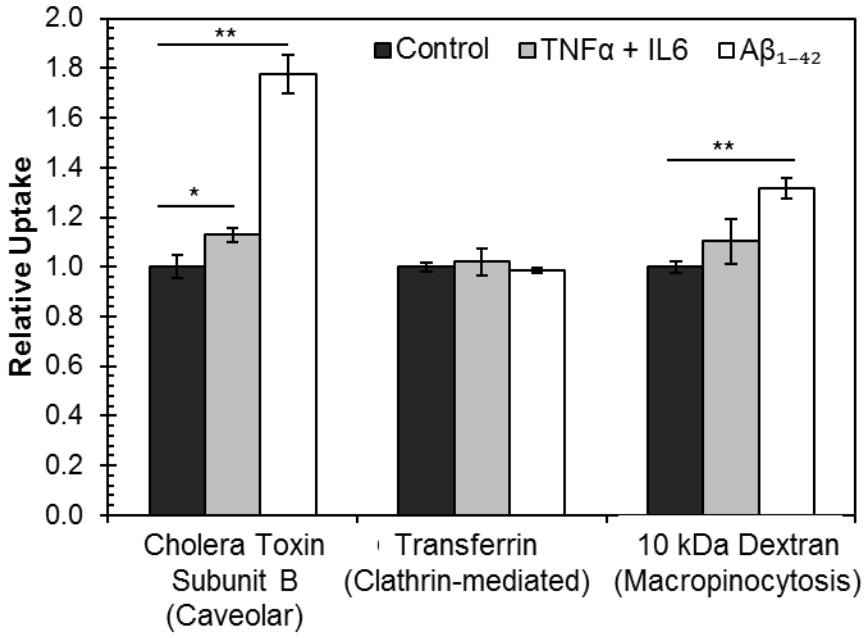

Figure 4.6. Changes to endocytic routes in disease. iPSC-derived BMECs were preincubated for 24 hours with 5 μM $A\beta_{1-42}$ to mimic AD or 10 ng/mL of each cytokine to mimic neuroinflammation. Fluorescently labeled probes of caveolar endocytosis, clathrin-mediated endocytosis and macropinocytosis were added to the cells and uptake was quantified via fluorescence after one hour. Data are normalized to uptake in the control cells for each pathway and each bar represents the mean ± standard error of the mean across three independent experiments (n=9; * $p < 0.05$ and ** $p < 0.01$)

4.5 Discussion

To study the transport of IgGs at the BBB, BMECs were differentiated from human iPSCs and grown on Transwell inserts to create an *in vitro* BBB model. We first sought to characterize the transport of IgGs across the *in vitro* BBB model to validate consistency with *in vivo* data. Previous work in our lab has shown that with a starting concentration of 10 mg/mL in the luminal compartment, 0.034% crosses into the abluminal compartment after six hours (Mantle et al., 2016). This figure falls

between the widely accepted statistic of 0.1% of peripheral IgGs able to penetrate the brain (Yu and Watts, 2013) and 0.009% of peripherally administered IVIG measured in the murine brain (St-Amour et al., 2013). Here we show that IgG transport across the *in vitro* BBB is a saturable process, with saturation occurring at a physiologically relevant IgG concentration around 7.5 mg/mL (plasma IgG concentrations typically range from 7-20 mg/mL (Cassidy et al., 1974)). Beyond this threshold concentration, abluminal IgG concentration remained about 60 ng/mL after six hours despite the addition of higher concentrations of IgG in the luminal compartment. When preincubated with unlabeled IgGs, uptake of fluorescent IgGs was reduced 72% compared to BMECs not preincubated with IgGs. This IgG transport behavior is consistent with a previous report that showed similar transport saturation with a 76-79% reduction in IgG transport across the *in vivo* guinea pig BBB in the presence of 4 mg/mL unlabeled IgG (Zlokovic et al., 1990). Lastly, iPSC-derived BMECs express FcRn, believed to be important for IgG transport at the BBB (Deane et al., 2005; Schlachetzki et al., 2002; Zhang and Pardridge, 2001). It has been hypothesized that FcRn is responsible for reverse transcytosis of IgGs in the brain to blood direction (Zhang and Pardridge, 2001) and studies have shown it to be present at the BBB (Schlachetzki et al., 2002). FcRn may also play a role in the mechanism of action of anti-Aβ mAbs by mediating the clearance of IgG-Aβ-immune complexes from the brain to the blood (Deane et al., 2005; Zhang and Pardridge, 2001).Combined, these results demonstrate that the iPSC-derived BBB model mimics the *in vivo* BBB with respect to properties relevant to IgG transport at the BBB.

Having established that the *in vitro* model mimics *in vivo* IgG transport, we next sought to gain insight into the endocytic mechanism responsible for IgG uptake and transcytosis through BMCs. Both IgG uptake and transcytosis are reduced after the addition of amiloride, an inhibitor of nonspecific macropinocytosis, but uptake and transport are unchanged with inhibitors of clathrin-mediated and with inhibitors of caveolar endocytosis. Studies in Caco-2 human intestinal epithelial monolayers similarly showed that inhibitors of clathrin-dependent and caveolin-dependent endocytosis had no effect on IgG uptake but inhibition of macropinocytosis decreased uptake of IgG (Sato et al., 2009). Coupled with the saturation behavior of IgGs, these data are consistent with a nonspecific charge-based adsorptive transport mechanism where the IgGs first adhere to the negatively charged cell surface and are subsequently endocytosed. Triguero *et al.* (1989) demonstrated increased uptake of a cationized IgG compared to native IgG in isolated bovine brain microvessels and the transport behavior observed here is consistent with this report.

Because drug transport properties are hypothesized to be altered in AD (Erickson and Banks, 2013; Schenk and Vries, 2016), we employed disease models to understand changes to IgG transport that may occur in AD. This iPSC-derived *in vitro* model responds to disease stimuli with changes to uptake and transport of molecules at the BBB, demonstrating its utility for investigating transport changes in disease. Both uptake and transport of IgGs were altered in diseased states, with the most significant increases in uptake and transport occurring with $A\beta_{1-42}$ incubation. $A\beta_{1-42}$ had a more significant effect on BBB function than $A\beta_{1-40}$, despite $A\beta_{1-40}$ typically being located

in closer proximity to blood vessels as the main component of vascular plaques (Güntert et al., 2006). Transport of IgGs was about two-fold higher after incubation with $A\beta_{1-42}$, which is consistent with a study that showed a two-fold increase in IgG transport after incubation with $A\beta_{1-42}$ in a primary murine BBB model (Wuest and Lee, 2014). These results suggest that soluble Aβ can act directly on BMECs to impair the BBB and the magnitude of this effect depends on the isoform. Additionally, disease progression may have an impact on relevant dose because these results suggest that transport of therapeutics may be altered in disease states.

We last sought to understand the relative changes in endocytic uptake routes that could be responsible for increased transcellular transport observed in the disease models. In the neuroinflammation model, there was a small but significant (13%) increase in caveolar endocytosis and in the AD model there were increases in both caveolar endocytosis (78%) and macropinocytosis (32%). Evidence for increased caveolar endocytosis at the BBB in disease is particularly strong in stroke models (De Bock et al., 2016), which have a strong inflammatory response. Increases in caveolar endocytosis are present after stroke (Haley and Lawrence, 2016; Reeson et al., 2015) and appear to be responsible for the acute increase in molecular transport as tight junction remodeling does not occur until 48-58 hours after stroke induction (Knowland et al., 2014). Another study has shown an increase in the number of vesicles in AD, thought to be caveolae based on size (Claudio, 1996). There were no changes to clathrin-mediated endocytosis of transferrin in either disease case. One study has shown increases in transferrin in the frontal cortex of patients with AD

compared to controls (Loeffler et al., 2002), however the transferrin receptor is not specific to BMECs and is expressed in neurons and other glial cell types as well (Moos and Morgan, 2000). These data reveal that there is an increase in caveolar transport at the BBB in disease, and potentially a disease-dependent increase in macropinocytosis as well.

Here we show that an *in vitro* BBB model derived from iPSCs can be used for studying the transport of immunotherapies for neurological disease. IgG transport in the model is saturable, consistent with *in vivo* IgG transport behavior. Through studies with endocytic inhibitors, we gained insight into the mechanism of IgG transport which is likely via macropinocytosis. We also demonstrate that IgG transport increases in models of neuroinflammation and AD and hypothesize that this is due to an increase in caveolar endocytosis. The indirect methods used here with fluorescently-labeled molecules and small molecule inhibitors allow for relatively high throughput and fast quantification of transport events compared with similar studies in animal models. Our previous work has shown that this iPSC-BBB model can be used to study small molecule therapeutics (Mantle et al., 2016), and here we demonstrate its utility in studying transport of biologics, understanding transport events at the cellular level, and understanding changes to the BBB in disease.

REFERENCES

Abbott NJ, Patabendige AAK, Dolman DEM, Yusof SR, Begley DJ. 2010. Structure and function of the blood-brain barrier. Neurobiol. Dis. 37:13–25.

Abbott NJ, Rönnbäck L, Hansson E. 2006. Astrocyte-endothelial interactions at the blood-brain barrier. Nat. Rev. Neurosci. 7:41–53.

Alzheimer's Association. 2017. 2017 Alzheimer's disease facts and figures. Alzheimer's Dement. 13:325-373.

Andreone BJ, Chow BW, Tata A, Lacoste B, Ben-Zvi A, Bullock K, Deik AA, Ginty DD, Clish CB, Gu C. 2017. Blood-Brain Barrier Permeability Is Regulated by Lipid Transport-Dependent Suppression of Caveolae-Mediated Transcytosis. Neuron 94:581–594.

Brosseron F, Krauthausen M, Kummer M, Heneka MT. 2014. Body Fluid Cytokine Levels in Mild Cognitive Impairment and Alzheimer's Disease: A Comparative Overview. Mol. Neurobiol. 50:534–544.

Cassidy JT, Nordby GL, Dodge HJ. 1974. Biologic variation of human serum immunoglobulin concentrations: Sex-age specific effects. J. Chronic Dis. 27:507–516.

Claudio L. 1996. Ultrastructural features of the blood-brain barrier in biopsy tissue from Alzheimer's disease patients. Ann. N. Y. Acad. Sci. 91:6–14.

Dahlgren KN, Manelli AM, Stine WB, Baker LK, Krafft GA, Ladu MJ. 2002. Oligomeric and fibrillar species of amyloid-β peptides differentially affect neuronal viability. J. Biol. Chem. 277:32046–32053.

De Bock M, Van Haver V, Vandenbroucke RE, Decrock E, Wang N, Leybaert L. 2016. Into rather unexplored terrain-transcellular transport across the blood-brain barrier. Glia 64:1097–1123.

Deane R, Bell RD, Sagare A, Zlokovic BV. 2009. Clearance of amyloid-beta peptide across the blood-brain barrier: implication for therapies in Alzheimer's disease. CNS Neurol. Disord. Drug Targets 8:16–30.

Deane R, Sagare A, Hamm K, Parisi M, LaRue B, Guo H, Wu Z, Holtzman DM, Zlokovic BV. 2005. IgG-assisted age-dependent clearance of Alzheimer's amyloid beta peptide by the blood-brain barrier neonatal Fc receptor 1. J.Neurosci. 25:11495–11503.

Erickson MA, Banks WA. 2013. Blood–Brain Barrier Dysfunction as a Cause and Consequence of Alzheimer's Disease. J. Cereb. Blood Flow Metab. 33:1500–1513.

Güntert A, Döbeli H, Bohrmann B. 2006. High sensitivity analysis of amyloid-beta peptide composition in amyloid deposits from human and PS2APP mouse brain. Neuroscience 143:461–475.

Haley MJ, Lawrence CB. 2016. The blood-brain barrier after stroke: Structural studies and the role of transcytotic vesicles. J. Cereb. Blood Flow Metab. 37:456–470.

Hartz AMS, Zhong Y, Wolf A, LeVine H, Miller DS, Bauer B. 2016. Aβ40 Reduces

P-Glycoprotein at the Blood-Brain Barrier through the Ubiquitin-Proteasome Pathway. J. Neurosci. 36:1930–1941.

Heppner FL, Ransohoff RM, Becher B. 2015. Immune attack: the role of inflammation in Alzheimer disease. Nat. Rev. Neurosci. 16:358–372.

Ito U, Ohno K, Yamaguchi T, Takei H, Tomita H, Inaba Y. 1980. Effect of hypertension on blood-brain barrier. Change after restoration of blood flow in post-ischemic gerbil brains. An electronmicroscopic study. Stroke. 11:606–611.

Knowland D, Arac A, Sekiguchi K, Hsu M, Lutz SE, Perrino J, Steinberg GK, Barres BA, Nimmerjahn A, Agalliu D. 2014. Stepwise Recruitment of Transcellular and Paracellular Pathways Underlies Blood-Brain Barrier Breakdown in Stroke. Neuron 82:603–617.

Lannfelt L, Relkin NR, Siemers ER. 2014. Amyloid-β-directed immunotherapy for Alzheimer's disease. J. Intern. Med. 275:284–295.

Lim JP, Gleeson PA. 2011. Macropinocytosis: An endocytic pathway for internalising large gulps. Immunol. Cell Biol. 89:836–843.

Lippmann ES, Al-Ahmad A, Azarin SM, Palecek SP, Shusta EV. 2014. A retinoic acid-enhanced, multicellular human blood-brain barrier model derived from stem cell sources. Sci. Rep. 4:4160.

Lippmann ES, Azarin SM, Kay JE, Nessler R a, Wilson HK, Al-Ahmad A, Palecek SP, Shusta EV. 2012. Derivation of blood-brain barrier endothelial cells from human pluripotent stem cells. Nat. Biotechnol. 30:783–791.

Loeffler DA, Connor JR, Juneau PL, Snyder BS, Kanaley L, DeMaggio AJ, Nguyen

H, Brickman CM, LeWitt PA. 2002. Transferrin and Iron in Normal, Alzheimer's Disease, and Parkinson's Disease Brain Regions. J. Neurochem. 65:710–716.

Mantle JL, Min L, Lee KH. 2016. Minimum Transendothelial Electrical Resistance Thresholds for the Study of Small and Large Molecule Drug Transport in a Human in Vitro Blood-Brain Barrier Model. Mol. Pharm. 13:4191–4198.

Moos T, Morgan EH. 2000. Transferrin and transferrin receptor function in brain barrier systems. Cell. Mol. Neurobiol. 20:77–95.

Pardridge WM. 2005. The blood-brain barrier: Bottleneck in brain drug development. NeuroRX 2:3–14.

Preston JE, Joan Abbott N, Begley DJ. 2014. Transcytosis of macromolecules at the blood-brain barrier. Adv. Pharmacol. 71:147–163.

Reeson P, Tennant KA, Gerrow K, Wang J, Novak SW, Thompson K, Lockhart KL, Holmes A, Nahirney PC, Brown CE. 2015. Delayed inhibition of VEGF signaling after stroke attenuates blood-brain barrier breakdown and improves functional recovery in a comorbidity-dependent manner. J. Neurosci. 35:5128–5143.

Sato K, Nagai J, Mitsui N, Ryoko Yumoto, Takano M. 2009. Effects of endocytosis inhibitors on internalization of human IgG by Caco-2 human intestinal epithelial cells. Life Sci. 85:800–807.

Schenk GJ, Vries HE De. 2016. Altered blood – brain barrier transport in neuro-inflammatory disorders. Drug Discov. Today Technol. 20:5–11.

Schlachetzki F, Zhu C, Pardridge WM. 2002. Expression of the neonatal Fc receptor

(FcRn) at the blood-brain barrier. J. Neurochem. 81:203–206.

Schnitzer JE, Oh P, Pinney E, Allard J. 1994. Filipin-sensitive caveolae-mediated transport in endothelium: Reduced transcytosis, scavenger endocytosis, and capillary permeability of select macromolecules. J. Cell Biol. 127:1217–1232.

Sevigny J, Chiao P, Bussière T, Weinreb PH, Williams L, Maier M, Dunstan R, Salloway S, Chen T, Ling Y, Gorman JO, Qian F, Arastu M, Li M, Chollate S, Brennan MS, Quintero-Monzon O, Scannevin RH, Arnold HM, Engber T, Rhodes K, Ferrero J, Hang Y, Mikulskis A, Grimm J, Hock C, Nitsch RM, Sandrock A. 2016. The antibody aducanumab reduces Aβ plaques in Alzheimer's disease. Nature. 537:50–56.

St-Amour I, Paŕe I, Alata W, Coulombe K, Ringuette-Goulet C, Drouin-Ouellet J, Vandal M, Soulet D, Bazin R, Calon F. 2013. Brain bioavailability of human intravenous immunoglobulin and its transport through the murine blood-brain barrier. J. Cereb. Blood Flow Metab. 33:1–10.

Stewart PA. 2000. Endothelial Vesicles in the Blood-Brain Barrier: Are They Related to Permeability? Cell. Mol. Neurobiol. 20:149–163.

Stine WB, Dahlgren KN, Krafft GA, LaDu MJ. 2003. In vitro characterization of conditions for amyloid-β peptide oligomerization and fibrillogenesis. J. Biol. Chem. 278:11612–11622.

Triguero D, Buciak JB, Yang J, Pardridge WM. 1989. Blood-brain barrier transport of cationized immunoglobulin G: enhanced delivery compared to native protein. Proc. Natl. Acad. Sci. 86:4761–5.

von Kleist L, Stahlschmidt W, Bulut H, Gromova K, Puchkov D, Robertson MJ, MacGregor KA, Tomlin N, Pechstein A, Chau N, Chircop M, Sakoff J, Von Kries JP, Saenger W, Kräusslich HG, Shupliakov O, Robinson PJ, McCluskey A, Haucke V. 2011. Role of the clathrin terminal domain in regulating coated pit dynamics revealed by small molecule inhibition. Cell 146:471–484.

Winkler EA, Nishida Y, Sagare AP, Rege SV, Bell RD, Perlmutter D, Sengillo JD, Hillman S, Kong P, Nelson AR, Sullivan JS, Zhao Z, Meiselman HJ, Wenby RB, Soto J, Abel ED, Makshanoff J, Zuniga E, De Vivo DC, Zlokovic BV. 2015. GLUT1 reductions exacerbate Alzheimer's disease vasculo-neuronal dysfunction and degeneration. Nat. Neurosci. 18:521–530.

Wuest DM, Lee KH. 2014. Amyloid-β concentration and structure influences the transport and immunomodulatory effects of IVIG. J. Neurochem. 130:136–144.

Yu J, Vodyanik MA, Smuga-Otto K, Antosiewicz-Bourget J, Frane JL, Tian S, Nie J, Jonsdottir GA, Ruotti V, Stewart R, Slukvin II, Thomson JA. 2007. Induced pluripotent stem cell lines derived from human somatic cells. Science. 318:1917–1920.

Yu YJ, Watts RJ. 2013. Developing Therapeutic Antibodies for Neurodegenerative Disease. Neurotherapeutics 10:459–472.

Zhang Y, Pardridge WM. 2001. Mediated efflux of IgG molecules from brain to blood across the blood–brain barrier. J. Neuroimmunol. 114:168–172.

Zlokovic BV., Skundric DS, Segal MB, Lipovac MN, Mackic JB, Davson H. 1990. A saturable mechanism for transport of immunoglobulin G across the blood-brain barrier of the guinea pig. Exp. Neurol. 107:263–270.

Chapter 5

CONCLUSIONS AND RECOMMENDATIONS FOR FUTURE WORK

5.1 Summary of Conclusions

Immunotherapies have the potential to be the first disease-modifying class of drugs for the treatment of Alzheimer's disease (AD), however the blood-brain barrier (BBB) largely restricts the transport of these therapeutics to their targets in the brain. *In vitro* BBB models derived from human stem cells provide a relatively high-throughput and cost-effective system to study transport of therapeutics and to gain a better understanding of the effects of disease progression. This thesis characterized and validated a stem cell-based *in vitro* BBB model and applied it to understand the effects of disease stimuli on barrier function and to understand the transport mechanism of immunotherapeutics. The fundamental information generated here can be applied to the development of therapeutics that are better able to cross the BBB and to inform treatment strategies as transport properties change with the progression of AD.

In Chapter 2, human induced pluripotent stem cells (hPSCs) were differentiated into BMECs and the resulting model exhibited physiologically-relevant barrier properties as measured by the expression and localization of brain microvascular endothelial cell (BMEC)-specific proteins, high transendothelial

electrical resistance (TEER), and polarized transport. The permeabilities of several common drugs were measured and used as a benchmarking system to determine "brain permeable" and "brain impermeable" regions in the model. The permeabilities of the four drug molecules that are FDA-approved for the treatment of AD symptoms were evaluated in the model and were some of the most highly brain permeable compounds investigated. Lastly, different TEER thresholds required for the study of small and large molecule drugs were established, serving as a universal benchmark for any *in vitro* BBB studies.

Astrocytes derived from neural stem cells (NSCs) grown in coculture with hPSC-derived BMECs improved TEER and mitigated the negative effects of inflammatory cytokines on barrier function in Chapter 3. These cytokines are able to act directly on the cells of the BBB to cause barrier dysfunction and transcellular transport breakdown occurs before paracellular permeability is affected. Importantly, the model can be used to investigate crosstalk between multiple cell types and is able to replicate cellular responses to disease stimuli at the BBB.

Chapter 4 presented insights into the transport mechanisms of IgGs across the BBB, both in health and with AD stimuli. IgG uptake is a saturable process, demonstrated both by a plateau in the amount transported with increasing concentration as well as in an inhibitory effect of a high concentration of unlabeled IgGs. The use of small molecule inhibitors of endocytic pathways demonstrated that IgG uptake is primarily via macropinocytosis. After the addition of amyloid-β (Aβ) or inflammatory cytokines, IgG uptake and transport increased and it is likely that an

increase in caveolar endocytosis is responsible for the change in transport. This work demonstrates that the stem cell-derived model can be used to investigate the transport mechanisms of potential therapeutics across the BBB in health and disease states.

5.2 hPSC Culture Lessons Learned

While the hPSC differentiation protocol is robust and has been shown to be effective across multiple cell lines and different laboratories, hPSC culture and differentiation still requires considerable experience and care. As expected when any new protocol is implemented, a considerable amount of troubleshooting was performed to achieve successful and consistent differentiation. 5.1 contains a list of factors that were investigated for their effects on hPSC culture and BMEC differentiation.

Table 5.1. Troubleshooting of hPSC culture and differentiation.

Factor	Comments
Freezing density	VERY IMPORTANT to have enough cells; 1 well ready to passage/differentiate to 1 vial
Freezing media	70% mTeSR1, 20% KOSR, 10% DMSO, 10 μM ROCK inhibitor
Freezing cryovial	No effect
Thawing ROCK inhibitor conc.	10 μM
Thawing media	mTeSR1, 10 μM ROCK inhibitor
Thawing density	Thaw 1:3 or 1:4, best to err on the side of more cells and passage earlier
Media changes after thaw	I cells are sparse, add new media daily but remove media every other day

Factor	Comments
Time to passage	Confluence and colonly health is important; if centers of colonies start to differentiate, passage at a higher density more often; wells should be ~70% full and colonies almost touching
Passaging reagent	Versene, accutase, ReleSR all OK
Passaging split ratio	Usually 1:6 however best to err on the side of more cells
Hand selection of EC regions	No effect; If hand selecting regions of interest, the differentiation was not successful
UM time	6 days
EC time	2 days best; extra day of EC does not hurt
Recombinant human sonic hedgehog during differentiation	No effect (0-2 μg/mL; D8, D8-9, D8-11)
Retinoic acid during differentiation	VERY IMPORTANT, add on D8
Human serum in EC media	Negative effect (cannot replace PDS)
Passaging reagent after differentiation	Versene or accutase OK; TrypLE or trypsin not OK
Pipetting after differentiation	Best mechanism to break up cells; Must be vigorous; No visible aggregates
Vortexing after differentiation	No/negative effect
Centrifugation after differentiation	No effect
Transwell material	PET (Corning #353095) ideal for most uses; highest TEER; PE (Corning #3470) best for small molecule permeability; will result in lower TEER; overnight collagen/fibronectin incubation; evaporate protein solution in hood (1-2h) instead of aspirating immediately before use

5.3 Recommendations for Future Work

The work presented here provides a foundation for studying the human BBB in AD and other neurodegenerative diseases. Extensions of this work could improve understanding of the contributions of the BBB to AD progression and treatment and

inform development of new disease-modifying therapeutics. Some potential applications include addition of multiple neurovascular unit (NVU) cell types to make a more complex disease model, expanding the model to three dimensions using biocompatible hydrogels, and further investigation of IgG transport mechanisms.

5.3.1 Incorporation of hPSC-Derived Pericytes, Astrocytes, and Neurons for an Improved NVU Model of AD

The hPSC-derived BMECs exhibit an *in vivo*-like phenotype in monoculture, but increasing layers of complexity can be incorporated through coculture with other cell types of the NVU. NSC-astrocytes were incorporated in this work (Chapter 3), however the model could benefit from further characterization of the differentiated population. Flow cytometry or simultaneous immunocytochemistry for NSC (nestin), neural (βIII tubulin), and astrocytic (GFAP) markers could better classify the heterogeneous population of differentiating NSCs. Alternate differentiation routes could be explored as well; Canfield et al. have demonstrated that neural progenitor-like "EZ spheres" can be generated from hPSCs, and these EZ spheres can subsequently be differentiated into astrocytes and neurons for use in the *in vitro* BBB model (Canfield et al., 2017). The work presented in Chapter 3 could also be expanded to examine the individual contributions of astrocytes to secreted cytokines and chemokines observed after the addition of TNF-α and IL-6. This experiment could

provide better insight into the endothelial-derived and astrocyte-derived factors that contribute to pro-inflammatory or anti-inflammatory environments.

Because of their importance in BBB differentiation and maintenance (Daneman et al., 2010), pericytes are often included in coculture or triple coculture BBB models (Lippmann et al., 2014; Nakagawa et al., 2007; Nakagawa et al., 2009). Additionally, pericytes regulate expression of MFSD2A (major facilitator super family domain containing 2a) in BMECs, which has been implicated in the suppression of transcytosis activity at the BBB (Ben-Zvi et al., 2014). In AD, pericyte loss and degeneration occurs in the hippocampus and cortex (Baloyannis and Baloyannis, 2012; Sengillo et al., 2013) and there is a relationship between reduction in pericyte coverage of capillaries and disruption of the BBB (Sengillo et al., 2013). *In vitro* studies have shown that prolonged exposure to high Aβ concentrations can overwhelm pericyte clearance of Aβ and can cause pericyte cell death (Sagare et al., 2013; Wilhelmus et al., 2007). To investigate relationships between pericytes, BMEC transport processes and AD stimuli, pericytes derived from hPSCs could be incorporated into the *in vitro* model. Differentiation of pericytes can be accomplished on a similar timescale as BMEC differentiation (18 days and 11 days, respectively) and involves adherent culture with different levels of serum and growth factors (Wanjare et al., 2014).

Generation of neurons from hPSCs provides an additional cell type to incorporate into the *in vitro* NVU model and would provide a means to evaluate the transport and activity of new therapeutics simultaneously. Neurons have been

differentiated from hPSC lines with different mutations in AD-related genes, including amyloid precursor protein and presenillin (Israel et al., 2012; Kondo et al., 2013; Yagi et al., 2011). Such neurons could be used to study effects of Aβ pathology on BBB dysfunction and would provide a means to evaluate the transport and activity of new therapeutics simultaneously. Other groups have focused on tau pathology, and have generated neurons from hPSCs that exhibit tau aggregation after seeding with preformed aggregated tau (Verheyen et al., 2015). Incorporation of neurons that exhibit tau pathology could be used to investigate the secondary effects of tau aggregation on barrier function. Treatment of tauopathies could be simulated by addition of a potential therapeutic to the luminal compartment and quantifying effects on neurodegeneration in the abluminal compartment.

5.3.2 Intracellular IgG Trafficking

For an immunotherapeutic to be effective at treating neurological disease, it must be transported across the BBB in to the brain. Endocytosed cargo can proceed to the abluminal membrane for release, however it can also be recycled back to the luminal membrane or sent to lysosomes for degradation. Relative quantification of each of these pathways is an extension of the work in Chapter 4 and would useful as a baseline for the design of therapeutics that can more effectively transverse the BBB.

While real time imaging of endocytic events is the gold standard, given the low density of endocytic vesicles in BMECs, short distance from luminal to abluminal

membrane (300-500 nm; Cornford *et al.* 1998), and transport events that occur with second-to-minute timescales (De Bock et al., 2016; Casley-Smith and Clark, 1972), live cell imaging of these events remains challenging. A first step towards quantifying the relative fraction of IgG in each of the intracellular trafficking pathways is using superresolution imaging of fixed cells. Fluorescently labeled IgGs can be added to culture media and cells can be fixed at different timepoints after addition. Simultaneous labeling of different endosomes such as early endosomes (EEA1), late endosomes (Rab 7), recycling endosomes (Rab 4; Rab 11), transcytotic endosomes (Rab 25) lysosomes (LAMP1) and quantification of colocalization with IgG can offer a snapshot of intracellular trafficking. One key challenge to overcome is sourcing of high quality primary antibodies against the endocytic compartments from enough different animals for secondary labeling. As a further extension of this work, it would be of interest to investigate the effects of antibody properties such as immunoglobulin type, species, Fc region sequence and glycosylation.

5.3.3 Three-Dimensional Microfluidic Model in Patterned PEGDA Hydrogels

Three-dimensional (3D) cell culture models more closely mimic the architecture of tissue found *in vivo*. The addition of shear stress via media flow can further mimic the *in vivo* BMEC environment and can improve barrier properties (Cucullo et al., 2011). One study has shown hPSC-BMECs in coculture with rat astrocytes grown on a “BBB-on-a-chip” microfluidic model have peak TEER values

above 4000 Ω·cm² that remain above 2000 Ω·cm² for ten days (Wang et al., 2017). Additionally, Katt and Xu et al. have demonstrated that hPSC-BMECs show alignment in response to high curvature at capillary-like diameters, resisting elongation wrap around to form tight junctions with themselves and neighbors (Katt et al., 2016). We have demonstrated that the hPSC-BMECs are capable of forming spontaneous 3D capillary structures with a lumen *in vitro* (Figure 5.1) however a greater degree of control is desirable.

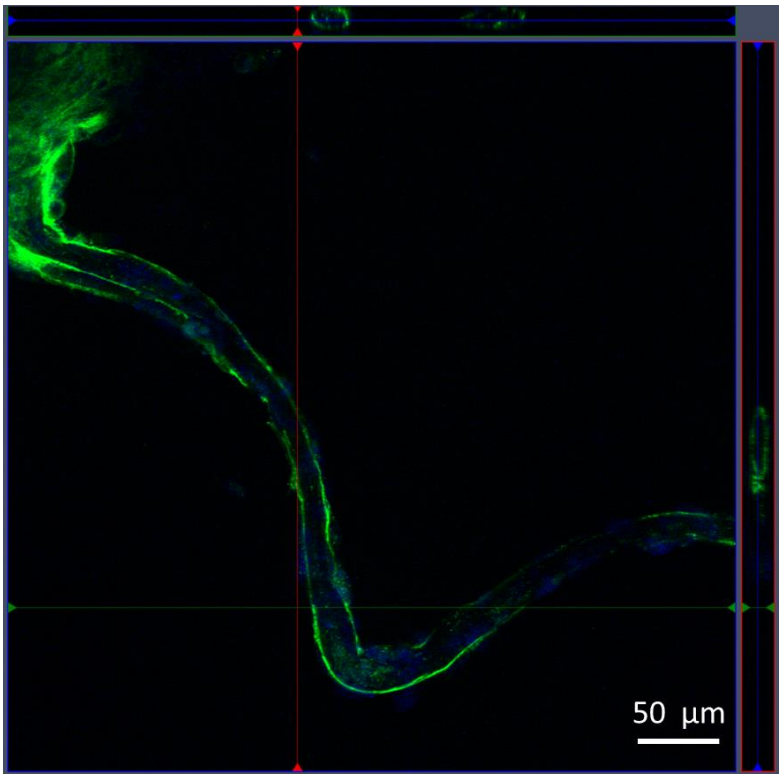

Figure 5.1. A spontaneously formed 3D capillary with a closed lumen. hPSC-BMECs are stained for GLUT1 (green) and nuclei are counterstained with DAPI (blue). Closed lumens can be seen in the cross sections, indicated by red and green bars.

One way to combine the 3D architecture with physiologically-relevant shear stress is through the methods developed by Heintz et al. to pattern biomimetic hydrogels using photoablation (Heintz et al., 2016). Poly(ethylene glycol) diacrylate (PEGDA) hydrogels are degraded using image-guided laser control and complex 3D geometries based on cerebral blood vessel architecture can be created. As preliminary steps towards creating a 3D microfluidic BBB model, hPSC-BMECs were grown on PEGDA hydrogels with 6mM of the integrin binding sequence RGDS, provided by the Slater Lab (Figure 5.2).

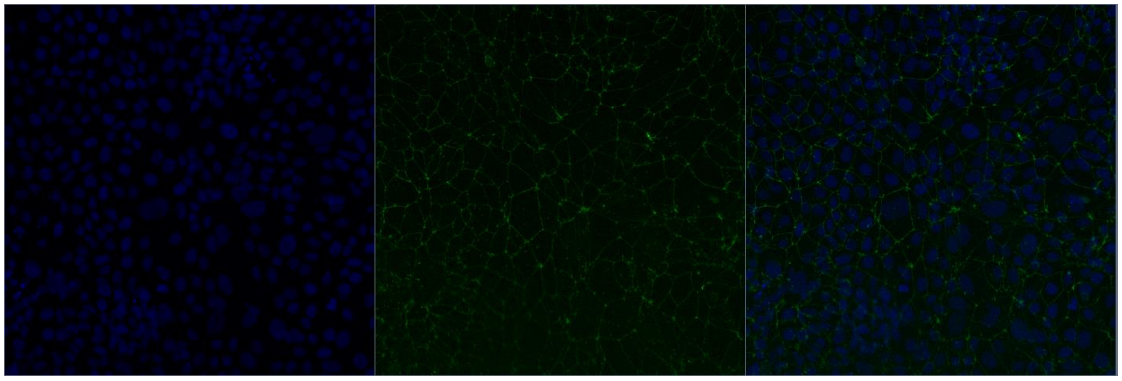

Figure 5.2. hPSC-BMECs grown on 6mM PEGDA-RDGS hydrogel. Cell nuclei are stained with DAPI (left) and tight junctions are stained with claudin-5 (middle). Overlay on the right. Images were taken with a 20x lens on a Zeiss LSM 710 inverted confocal microscope.

Additionally, as a proof of concept, immortalized mouse brain endothelial cells were grown inside photoablated channels within a PEGDA-RGDS hydrogel (Figure 5.3). Small channels were created between two open wells and bEnd.3 cells were seeded and allowed to migrate into the channels for up to 11 days.

Immunocytochemistry shows that the bEnd.3 cells grew in three dimensions around the channels (Figure 5.4). These preliminary results demonstrate the compatibility of the 3D hydrogel patterning techniques developed in the Slater lab and the growth of BMECs.

Next steps towards a 3D microfluidic BBB model include growing hPSC-derived BMECs inside the microchannels. This is not a trivial task as the hPSC-BMECs do not migrate throughout the entire channel as the bEND.3 cell line does. Some potential ways to overcome these challenges are to use different diameter channels, improve the seeding process, or experiment with different integrin binding peptides. Once hPSC-BMECs can be grown inside microchannels, the effects of geometry and flow can be examined. Additionally, there is potential for inclusion of other cell types within the hydrogels such as astrocytes (e.g. those generated in Chapter 3), pericytes and neurons. With the inclusion of multiple NVU cell types, questions such as the effects of pericyte coverage on BBB function or AD-induced neurotoxicity on BBB function can be systematically addressed.

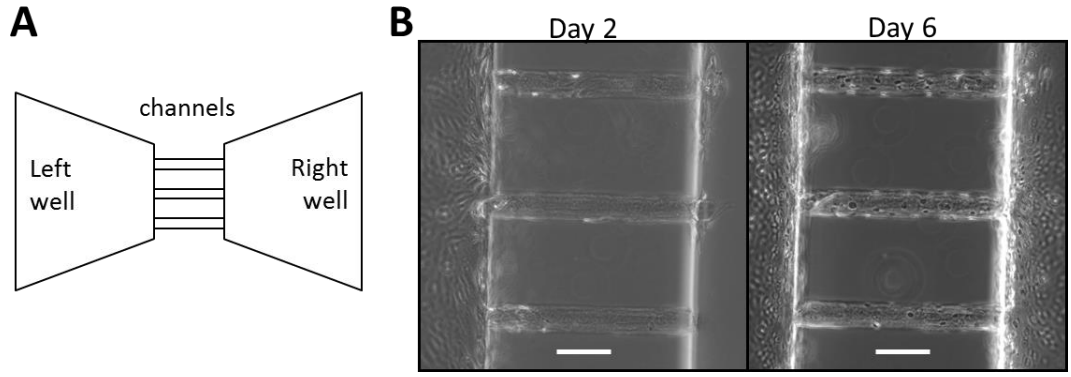

Figure 5.3. Proof of concept: Microchannels with b.End3 cells. (A) A top-down schematic (not to scale) of the 3D structure degraded in the PEGDA hydrogel. (B) Phase contrast images (scale bars = 100 μm) of b.End3 cells in microchannels over time.

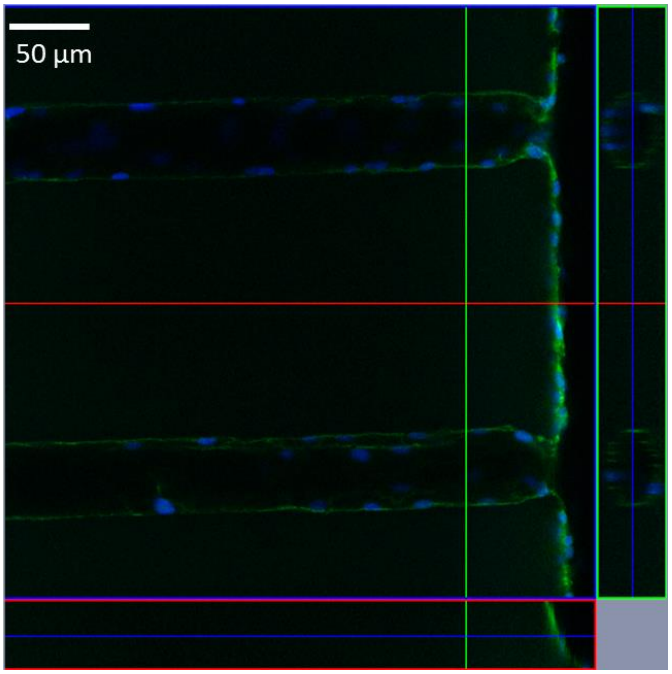

Figure 5.4. Immunocytochemistry of bEnd.3 cells grown in microchannels. Cells were stained for the tight junction protein ZO-1 (green) and nuclei were stained with DAPI (blue).

5.4 Concluding Remarks

Patients suffering from Alzheimer's and other diseases of the central nervous system would greatly benefit from disease modifying therapies. Developing therapeutics capable of overcoming the BBB is challenging, therefore human *in vitro* models are essential tools for studying drug transport and for elucidating molecular mechanisms in disease at the cellular level. This work offers key insights into the critical characteristics required of an *in vitro* BBB model and how immunotherapies are transported into the brain. Modeling the cells that make up and surround the BBB can facilitate a better understanding of disease progression, reveal new therapeutic targets, and can contribute to the development of new strategies to deliver therapeutics across the BBB into the brain in neurodegenerative disease.

REFERENCES

Baloyannis SJ, Baloyannis IS. 2012. The vascular factor in Alzheimer's disease: A study in Golgi technique and electron microscopy. J. Neurol. Sci. 322:117–121.

Ben-Zvi A, Lacoste B, Kur E, Andreone BJ, Mayshar Y, Yan H, Gu C. 2014. MSFD2A is critical for the formation and function of the blood brain barrier. Nature 509:507–511.

De Bock M, Van Haver V, Vandenbroucke RE, Decrock E, Wang N, Leybaert L. 2016. Into rather unexplored terrain-transcellular transport across the blood-brain barrier. Glia 64:1097–1123.

Canfield SG, Stebbins MJ, Morales BS, Asai SW, Vatine GD, Svendsen CN, Palecek SP, Shusta EV. 2017. An isogenic blood-brain barrier model comprising brain endothelial cells, astrocytes, and neurons derived from human induced pluripotent stem cells. J. Neurochem. 140:874–888.

Casley-Smith JR, Clark HI. 1972. The dimensions and numbers of small vesicles in blood capillary endothelium in the hind legs of dogs, and their relation to vascular permeability. J. Microsc. 96:263–267.

Cornford EM, Hyman S, Cornford ME, Landaw EM, Delgado-Escueta A V. 1998. Interictal Seizure Resections Show Two Configurations of Endothelial Glut1 Glucose Transporter in the Human Blood-Brain Barrier. J. Cereb. Blood Flow

Metab. 18:26–42.

Cucullo L, Hossain M, Puvenna V, Marchi N, Janigro D. 2011. The role of shear stress in Blood-Brain Barrier endothelial physiology. BMC Neurosci. 12:40.

Daneman R, Zhou L, Kebede A a, Barres B a. 2010. Pericytes are required for blood-brain barrier integrity during embryogenesis. Nature 468:562–566.

Heintz KA, Bregenzer ME, Mantle JL, Lee KH, West JL, Slater JH. 2016. Fabrication of 3D Biomimetic Microfluidic Networks in Hydrogels. Adv. Healthc. Mater. 5: 2153–2160.

Israel MA, Yuan SH, Bardy C, Reyna SMS, Mu Y, Herrera C, Hefferan MP, Van Gorp S, Nazor KL, Boscolo FS, Carson CT, Laurent LC, Marsala M, Gage FH, Remes AM, Koo EH, Goldstein LSB. 2012. Probing sporadic and familial Alzheimer's disease using induced pluripotent stem cells. Nature 482:216–220.

Katt ME, Xu ZS, Gerecht S, Searson PC. 2016. Human Brain Microvascular Endothelial Cells Derived from the BC1 iPS Cell Line Exhibit a Blood-Brain Barrier Phenotype. PLoS One 11.

Kondo T, Asai M, Tsukita K, Kutoku Y, Ohsawa Y, Sunada Y, Imamura K, Egawa N, Yahata N, Okita K, Takahashi K, Asaka I, Aoi T, Watanabe A, Watanabe K, Kadoya C, Nakano R, Watanabe D, Maruyama K, Hori O, Hibino S, Choshi T, Nakahata T, Hioki H, Kaneko T, Naitoh M, Yoshikawa K, Yamawaki S, Suzuki S, Hata R, Ueno SI, Seki T, Kobayashi K, Toda T, Murakami K, Irie K, Klein WL, Mori H, Asada T, Takahashi R, Iwata N, Yamanaka S, Inoue H. 2013. Modeling Alzheimer's disease with iPSCs reveals stress phenotypes associated

with intracellular Aβ and differential drug responsiveness. Cell Stem Cell 12:487–496.

Lippmann ES, Al-Ahmad A, Azarin SM, Palecek SP, Shusta EV. 2014. A retinoic acid-enhanced, multicellular human blood-brain barrier model derived from stem cell sources. Sci. Rep. 4:4160.

Nakagawa S, Deli MA, Kawaguchi H, Shimizudani T, Shimono T, Kittel Á, Tanaka K, Niwa M. 2009. A new blood-brain barrier model using primary rat brain endothelial cells, pericytes and astrocytes. Neurochem. Int. 54:253–263.

Nakagawa S, Deli MA, Nakao S, Honda M, Hayashi K, Nakaoke R, Kataoka Y, Niwa M. 2007. Pericytes from brain microvessels strengthen the barrier integrity in primary cultures of rat brain endothelial cells. Cell. Mol. Neurobiol. 27:687–694.

Sagare AP, Bell RD, Zhao Z, Ma Q, Winkler EA, Ramanathan A, Zlokovic BV. 2013. Pericyte loss influences Alzheimer-like neurodegeneration in mice. Nat. Commun. 4:2932.

Sengillo JD, Winkler EA, Walker CT, Sullivan JS, Johnson M, Zlokovic BV. 2013. Deficiency in mural vascular cells coincides with blood-brain barrier disruption in Alzheimer's disease. Brain Pathol. 23:303–310.

Verheyen A, Diels A, Dijkmans J, Oyelami T, Meneghello G, Mertens L, Versweyveld S, Borgers M, Buist A, Peeters P, Cik M. 2015. Using human iPSC-derived neurons to model TAU aggregation. PLoS One 10:1–15.

Wang YI, Abaci HE, Shuler ML. 2017. Microfluidic blood–brain barrier model provides in vivo-like barrier properties for drug permeability screening.

Biotechnol. Bioeng. 114:184–194.

Wanjare M, Kusuma S, Gerecht S. 2014. Defining differences among perivascular cells derived from human pluripotent stem cells. Stem Cell Reports 2:561–575.

Wilhelmus MMM, Otte-Höller I, van Triel JJJ, Veerhuis R, Maat-Schieman MLC, Bu G, de Waal RMW, Verbeek MM. 2007. Lipoprotein Receptor-Related Protein-1 Mediates Amyloid-β-Mediated Cell Death of Cerebrovascular Cells. Am. J. Pathol. 171:1989–1999.

Yagi T, Ito D, Okada Y, Akamatsu W, Nihei Y, Yoshizaki T, Yamanaka S, Okano H, Suzuki N. 2011. Modeling familial Alzheimer's disease with induced pluripotent stem cells. Hum. Mol. Genet. 20:4530–4539.

REFERENCES

Abbott NJ, Patabendige AAK, Dolman DEM, Yusof SR, Begley DJ. 2010. Structure and function of the blood-brain barrier. Neurobiol. Dis. 37:13–25.

Abbott NJ, Rönnbäck L, Hansson E. 2006. Astrocyte-endothelial interactions at the blood-brain barrier. Nat. Rev. Neurosci. 7:41–53.

Alzheimer's Association . 2017. 2017 Alzheimer's disease facts and figures. Alzheimer's Dement. 13:325-373.

Ametamey SM, Bruehlmeier M, Kneifel S, Kokic M, Honer M, Arigoni M, Buck A, Burger C, Samnick S, Quack G, Schubiger PA. 2002. PET studies of 18F-memantine in healthy volunteers. Nucl. Med. Biol. 29:227–231.

Andreone BJ, Chow BW, Tata A, Lacoste B, Ben-Zvi A, Bullock K, Deik AA, Ginty DD, Clish CB, Gu C. 2017. Blood-Brain Barrier Permeability Is Regulated by Lipid Transport-Dependent Suppression of Caveolae-Mediated Transcytosis. Neuron 94:581–594.

Appelt-Menzel A, Cubukova A, Günther K, Edenhofer F, Piontek J, Krause G, Stüber T, Walles H, Neuhaus W, Metzger M. 2017. Establishment of a Human Blood-Brain Barrier Co-culture Model Mimicking the Neurovascular Unit Using Induced Pluri- and Multipotent Stem Cells. Stem Cell Reports 8:894–906.

Attems J, Jellinger KA, Lintner F. 2005. Alzheimer's disease pathology influences severity and topographical distribution of cerebral amyloid angiopathy. Acta Neuropathol. 110:222–231.

Badur MG, Zhang H, Metallo CM. 2015. Enzymatic passaging of human embryonic stem cells alters central carbon metabolism and glycan abundance. Biotechnol. J. 10:1600–1611.

Baloyannis SJ, Baloyannis IS. 2012. The vascular factor in Alzheimer's disease: A study in Golgi technique and electron microscopy. J. Neurol. Sci. 322:117–121.

Bell RD, Zlokovic BV. 2009. Neurovascular mechanisms and blood-brain barrier disorder in Alzheimer's disease. Acta Neuropathol. 118:103–113.

Ben-Zvi A, Lacoste B, Kur E, Andreone BJ, Mayshar Y, Yan H, Gu C. 2014. MSFD2A is critical for the formation and function of the blood brain barrier. Nature 509:507–511.

Bernas M, Cardoso F, Daley S. 2010. Establishment of primary cultures of human brain microvascular endothelial cells: a new and simplified method to obtain cells for an in vitro model of the blood. Nat. Protoc. 5:1265–1272.

Blecharz KG, Drenckhahn D, Forster CY. 2008. Glucocorticoids increase VE-cadherin expression and cause cytoskeletal rearrangements in murine brain endothelial cEND cells. J. Cereb. Blood Flow Metab. 28:1139–1149.

Brosseron F, Krauthausen M, Kummer M, Heneka MT. 2014. Body Fluid Cytokine Levels in Mild Cognitive Impairment and Alzheimer's Disease: A Comparative Overview. Mol. Neurobiol. 50:534–544.

Broux B, Gowing E, Prat A. 2015. Glial regulation of the blood-brain barrier in health and disease. Semin. Immunopathol. 37:577–590.

Brown RC, Morris AP, O'Neil RG. 2007. Tight junction protein expression and barrier properties of immortalized mouse brain microvessel endothelial cells. Brain Res. 1130:17–30.

Butt AM, Jones HC, Abbott NJ. 1990. Electrical resistance across the blood-brain barrier in anaesthetized rats: a developmental study. J. Physiol. 429:47–62.

Buzzard JJ, Gough NM, Crook JM, Colman A. 2004. Karyotype of human ES cells during extended culture. Nat. Biotechnol. 22:381–382.

Canfield SG, Stebbins MJ, Morales BS, Asai SW, Vatine GD, Svendsen CN, Palecek SP, Shusta EV. 2017. An isogenic blood-brain barrier model comprising brain endothelial cells, astrocytes, and neurons derived from human induced pluripotent stem cells. J. Neurochem. 140:874–888.

Casley-Smith JR, Clark HI. 1972. The dimensions and numbers of small vesicles in blood capillary endothelium in the hind legs of dogs, and their relation to vascular permeability. J. Microsc. 96:263–267.

Cassidy JT, Nordby GL, Dodge HJ. 1974. Biologic variation of human serum immunoglobulin concentrations: Sex-age specific effects. J. Chronic Dis. 27:507–516.

Chen G, Gulbranson DR, Hou Z, Bolin JM, Probasco MD, Smuga-otto K, Howden SE, Nicole R, Propson NE, Wagner R, Lee GO, Teng JMC, Thomson J a. 2011. Chemically defined conditions for human iPS cell derivation and culture. Nat. Methods 8:424–429.

Claudio L. 1996. Ultrastructural features of the blood-brain barrier in biopsy tissue from Alzheimer's disease patients. Ann. N. Y. Acad. Sci. 91:6–14.

Cornford EM, Hyman S, Cornford ME, Landaw EM, Delgado-Escueta AV. 1998. Interictal Seizure Resections Show Two Configurations of Endothelial Glut1 Glucose Transporter in the Human Blood-Brain Barrier. J. Cereb. Blood Flow Metab. 18:26–42.

Cucullo L, Hossain M, Puvenna V, Marchi N, Janigro D. 2011. The role of shear stress in blood-brain barrier endothelial physiology. BMC Neurosci. 12:40.

Dahlgren KN, Manelli AM, Stine WB, Baker LK, Krafft GA, Ladu MJ. 2002. Oligomeric and fibrillar species of amyloid-β peptides differentially affect neuronal viability. J. Biol. Chem. 277:32046–32053.

Daneman R, Zhou L, Kebede AA, Barres BA. 2010. Pericytes are required for blood-brain barrier integrity during embryogenesis. Nature 468:562–566.

De Bock M, Van Haver V, Vandenbroucke RE, Decrock E, Wang N, Leybaert L. 2016. Into rather unexplored terrain—transcellular transport across the blood-brain barrier. Glia 64:1097–1123.

Deane R, Bell RD, Sagare A, Zlokovic BV. 2009. Clearance of amyloid-beta peptide across the blood-brain barrier: implication for therapies in Alzheimer's disease. CNS Neurol. Disord. Drug Targets 8:16–30.

Deane R, Sagare A, Hamm K, Parisi M, LaRue B, Guo H, Wu Z, Holtzman DM, Zlokovic BV. 2005. IgG-assisted age-dependent clearance of Alzheimer's amyloid beta peptide by the blood-brain barrier neonatal Fc receptor 1. J.Neurosci. 25:11495–11503.

Deli MA, Ábrahám CS, Kataoka Y, Niwa M. 2005. Permeability studies on in vitro blood-brain barrier models: Physiology, pathology, and pharmacology. Cell. Mol. Neurobiol. 25:59–127.

Deo AK, Theil FP, Nicolas JM. 2013. Confounding Parameters in Preclinical Assessment of Blood–Brain Barrier Permeation: An Overview With Emphasis on Species Differences and Effect of Disease States. Mol. Pharm. 10:1581–1595.

DiMasi JA, Grabowski HG, Hansen RW. 2016. Innovation in the pharmaceutical industry: New estimates of R&D costs. J. Health Econ. 47:20–33.

Draper JS, Smith K, Gokhale P, Moore HD, Maltby E, Johnson J, Meisner L, Zwaka TP, Thomson JA, Andrews PW. 2004. Recurrent gain of chromosomes 17q and 12 in cultured human embryonic stem cells. Nat. Biotechnol. 22:53–54.

Erickson MA, Banks WA. 2013. Blood–Brain Barrier Dysfunction as a Cause and Consequence of Alzheimer's Disease. J. Cereb. Blood Flow Metab. 33:1500–1513.

Förster C, Burek M, Romero IA, Weksler B, Couraud PO, Drenckhahn D. 2008. Differential effects of hydrocortisone and TNFalpha on tight junction proteins in an in vitro model of the human blood-brain barrier. J. Physiol. 586:1937–1949.

Garitaonandia I, Amir H, Boscolo FS, Wambua GK, Schultheisz HL, Sabatini K, Morey R, Waltz S, Wang YC, Tran H, Leonardo TR, Nazor K, Slavin I, Lynch C, Li Y, Coleman R, Romero IG, Altun G, Reynolds D, Dalton S, Parast M, Loring JF, Laurent LC. 2015. Increased risk of genetic and epigenetic instability in human embryonic stem cells associated with specific culture conditions. PLoS One 10.

Grammas P, Ovase R. 2001. Inflammatory factors are elevated in brain microvessels in Alzheimer's disease. Neurobiol. Aging 22:837–842.

Grammas P, Ovase R. 2002. Cerebrovascular transforming growth factor-β contributes to inflammation in the Alzheimer's disease brain. Am. J. Pathol. 160:1583–1587.

Güntert A, Döbeli H, Bohrmann B. 2006. High sensitivity analysis of amyloid-beta peptide composition in amyloid deposits from human and PS2APP mouse brain. Neuroscience 143:461–475.

El Hafney B, Chappey O, Piciottia M, Debraya M, Bovalb B, Rouxa F. 1997. Modulation of P-glycoprotein activity by glial factors and retinoic acid in an immortalized rat brain microvessel endothelial cell line. Neurosci. Lett. 236:107–111.

Haley MJ, Lawrence CB. 2016. The blood-brain barrier after stroke: Structural studies and the role of transcytotic vesicles. J. Cereb. Blood Flow Metab. 37:456–470.

Hamm S, Dehouck B, Kraus J, Wolburg-Buchholz K, Wolburg H, Risau W, Cecchelli R, Engelhardt B, Dehouck MP. 2004. Astrocyte mediated modulation of blood-brain barrier permeability does not correlate with a loss of tight junction proteins from the cellular contacts. Cell Tissue Res. 315:157–166.

Hartz AMS, Zhong Y, Wolf A, LeVine H, Miller DS, Bauer B. 2016. Aβ40 Reduces P-Glycoprotein at the Blood-Brain Barrier through the Ubiquitin-Proteasome Pathway. J. Neurosci. 36:1930–1941.

Heintz KA, Bregenzer ME, Mantle JL, Lee KH, West JL, Slater JH. 2016. Fabrication of 3D Biomimetic Microfluidic Networks in Hydrogels. Adv. Healthc. Mater. 5:2153–2160.

Helms HC, Abbott NJ, Burek M, Cecchelli R, Couraud PO, Deli MA, Förster C, Galla HJ, Romero IA, Shusta EV, Stebbins MJ, Vandenhaute E, Weksler B, Brodin B. 2016. In vitro models of the blood-brain barrier: An overview of commonly used brain endothelial cell culture models and guidelines for their use. J. Cereb. Blood Flow Metab. 36:862–890.

Helms HC, Hersom M, Kuhlmann LB, Badolo L, Nielsen CU, Brodin B. 2014. An Electrically Tight In Vitro Blood-Brain Barrier Model Displays Net Brain-to-Blood Efflux of Substrates for the ABC Transporters, P-gp, Bcrp and Mrp-1. AAPS J. 16:1046–1055.

Heppner FL, Ransohoff RM, Becher B. 2015. Immune attack: the role of inflammation in Alzheimer disease. Nat. Rev. Neurosci. 16:358–372.

Higuchi K, Kitamura A, Okura T, Deguchi Y. 2015. Memantine transport by a proton-coupled organic cation antiporter in hCMEC/D3 cells, an in vitro human blood-brain barrier model. Drug Metab. Pharmacokinet. 30:182–187.

Holmes C, Cunningham C, Zotova E, Woolford J, Dean C, Kerr S, Culliford D, Perry VH. 2009. Systemic inflammation and disease progression in Alzheimer disease. Neurology 73:768–74.

Israel M a., Yuan SH, Bardy C, Reyna SMS, Mu Y, Herrera C, Hefferan MP, Van Gorp S, Nazor KL, Boscolo FS, Carson CT, Laurent LC, Marsala M, Gage FH, Remes AM, Koo EH, Goldstein LSB. 2012. Probing sporadic and familial Alzheimer's disease using induced pluripotent stem cells. Nature 482:216–220.

Ito U, Ohno K, Yamaguchi T, Takei H, Tomita H, Inaba Y. 1980. Effect of hypertension on blood-brain barrier. Change after restoration of blood flow in post-ischemic gerbil brains. An electronmicroscopic study. Stroke. 11:606–611.

Katt ME, Xu ZS, Gerecht S, Searson PC. 2016. Human Brain Microvascular Endothelial Cells Derived from the BC1 iPS Cell Line Exhibit a Blood-Brain Barrier Phenotype. PLoS One 11.

Kiyota T, Okuyama S, Swan RJ, Jacobsen MT, Gendelman HE, Ikezu T. 2010. CNS expression of anti-inflammatory cytokine interleukin-4 attenuates Alzheimer's disease-like pathogenesis in APP+PS1 bigenic mice. FASEB J. 24:3093–3102.

Kleiderman S, Sá JV, Teixeira AP, Brito C, Gutbier S, Evje LG, Hadera MG, Glaab E, Henry M, Sachinidis A, Alves PM, Sonnewald U, Leist M. 2016. Functional and phenotypic differences of pure populations of stem cell-derived astrocytes and neuronal precursor cells. Glia 64:695–715.

Knowland D, Arac A, Sekiguchi K, Hsu M, Lutz SE, Perrino J, Steinberg GK, Barres BA, Nimmerjahn A, Agalliu D. 2014. Stepwise Recruitment of Transcellular and Paracellular Pathways Underlies Blood-Brain Barrier Breakdown in Stroke. Neuron 82:603–617.

Kondo T, Asai M, Tsukita K, Kutoku Y, Ohsawa Y, Sunada Y, Imamura K, Egawa N, Yahata N, Okita K, Takahashi K, Asaka I, Aoi T, Watanabe A, Watanabe K, Kadoya C, Nakano R, Watanabe D, Maruyama K, Hori O, Hibino S, Choshi T, Nakahata T, Hioki H, Kaneko T, Naitoh M, Yoshikawa K, Yamawaki S, Suzuki S, Hata R, Ueno SI, Seki T, Kobayashi K, Toda T, Murakami K, Irie K, Klein WL, Mori H, Asada T, Takahashi R, Iwata N, Yamanaka S, Inoue H. 2013. Modeling Alzheimer's disease with iPSCs reveals stress phenotypes associated with intracellular Aβ and differential drug responsiveness. Cell Stem Cell 12:487–496.

Kubo Y, Ohtsuki S, Uchida Y, Terasaki T. 2015. Quantitative Determination of Luminal and Abluminal Membrane Distributions of Transporters in Porcine Brain Capillaries by Plasma Membrane Fractionation and Quantitative Targeted Proteomics. J. Pharm. Sci. 104:3060–3068.

Kyrkanides S, Tallents RH, Miller JH, Olschowka ME, Johnson R, Yang M, Olschowka JA, Brouxhon SM, O'Banion MK. 2011. Osteoarthritis accelerates and exacerbates Alzheimer's disease pathology in mice. J. Neuroinflammation 8:112.

Lacombe O, Videau O, Chevillon D, Guyot A-C, Contreras C, Blondel S, Nicolas L, Ghettas A, Bénech H, Thevenot E, Pruvost A, Bolze S, Krzaczkowski L, Prévost C, Mabondzo A. 2011. In vitro primary human and animal cell-based blood-brain barrier models as a screening tool in drug discovery. Mol. Pharm. 8:651–663.

Lannfelt L, Relkin NR, Siemers ER. 2014. Amyloid-β-directed immunotherapy for Alzheimer's disease. J. Intern. Med. 275:284–295.

Lee KS, Chung JH, Lee KH, Shin M-J, Oh BH, Hong CH. 2008. Bioplex analysis of plasma cytokines in Alzheimer's disease and mild cognitive impairment. Immunol. Lett. 121:105–109.

Lim JP, Gleeson PA. 2011. Macropinocytosis: an endocytic pathway for internalising large gulps. Immunol. Cell Biol. 89:836–843.

Lim JC, Wolpaw AJ, Caldwell MA, Hladky SB, Barrand MA. 2007. Neural precursor cell influences on blood-brain barrier characteristics in rat brain endothelial cells. Brain Res. 1159:67–76.

Lipinski CA, Lombardo F, Dominy BW, Feeney PJ. 1997. Experimental and Computational Approaches to Estimate Solubility and Permeability in Drug Discovery and Development Settings. Adv. Drug Deliv. Rev. 23:3–25.

Lippmann ES, Weidenfeller C, Svendsen CN, Shusta EV. 2011. Blood-brain barrier modeling with co-cultured neural progenitor cell-derived astrocytes and neurons. J. Neurochem. 119:507–520.

Lippmann ES, Al-Ahmad A, Azarin SM, Palecek SP, Shusta EV. 2014. A retinoic acid-enhanced, multicellular human blood-brain barrier model derived from stem cell sources. Sci. Rep. 4:4160.

Lippmann ES, Azarin SM, Kay JE, Nessler RA, Wilson HK, Al-Ahmad A, Palecek SP, Shusta EV. 2012. Derivation of blood-brain barrier endothelial cells from human pluripotent stem cells. Nat. Biotechnol. 30:783–791.

Loeffler DA, Connor JR, Juneau PL, Snyder BS, Kanaley L, DeMaggio AJ, Nguyen H, Brickman CM, LeWitt PA. 2002. Transferrin and Iron in Normal, Alzheimer's Disease, and Parkinson's Disease Brain Regions. J. Neurochem. 65:710–716.

Lohmann C, Hüwel S, Galla H-J. 2002. Predicting Blood-Brain Barrier Permeability of Drugs: Evaluation of Different In Vitro Assays. J. Drug Target. 10:263–276.

Ludwig TE, Bergendahl V, Levenstein ME, Yu J, Probasco MD, Thomson JA. 2006. Feeder-independent culture of human embryonic stem cells. Nat. Methods 3:637–646.

Lue LF, Rydel R, Brigham EF, Yang LB, Hampel H, Murphy GM, Brachova L, Yan S Du, Walker DG, Shen Y, Rogers J. 2001. Inflammatory repertoire of Alzheimer's disease and nondemented elderly microglia in vitro. Glia 35:72–79.

Mantle JL, Min L, Lee KH. 2016. Minimum Transendothelial Electrical Resistance Thresholds for the Study of Small and Large Molecule Drug Transport in a Human in Vitro Blood-Brain Barrier Model. Mol. Pharm. 13:4191–4198.

Marchesi VT. 2011. Alzheimer's dementia begins as a disease of small blood vessels, damaged by oxidative-induced inflammation and dysregulated amyloid metabolism: implications for early detection and therapy. FASEB J. 25:5–13.

Mathiisen TM, Lehre KP, Danbolt NC, Ottersen OP. 2010. The perivascular astroglial sheath provides a complete covering of the brain microvessels: An electron microscopic 3D reconstruction. Glia 58:1094–1103.

Mayeux R, Ottman R, Tang MX, Noboa-Bauza L, Marder K, Gurland B, Stern Y. 1993. Genetic susceptibility and head injury as risk factors for Alzheimer's disease among community-dwelling elderly persons and their first-degree relatives. Ann Neurol 33:494–501.

Mitalipova MM, Rao RR, Hoyer DM, Johnson JA, Meisner LF, Jones KL, Dalton S, Stice SL. 2005. Preserving the genetic integrity of human embryonic stem cells. Nat. Biotechnol. 23:19–20.

Mizee MR, Wooldrik D, Lakeman KA, van het Hof B, Drexhage JA, Geerts D, Bugiani M, Aronica E, Mebius RE, Prat A, de Vries HE, Reijerkerk A. 2013. Retinoic Acid Induces Blood-Brain Barrier Development. J. Neurosci. 33:1660–1671.

Moos T, Morgan EH. 2000. Transferrin and transferrin receptor function in brain barrier systems. Cell. Mol. Neurobiol. 20:77–95.

Naik P, Cucullo L. 2012. In Vitro Blood–Brain Barrier Models: Current and Perspective Technologies. J. Pharm. Sci. 101:1337–1354.

Nakagawa S, Deli MA, Kawaguchi H, Shimizudani T, Shimono T, Kittel Á, Tanaka K, Niwa M. 2009. A new blood-brain barrier model using primary rat brain endothelial cells, pericytes and astrocytes. Neurochem. Int. 54:253–263.

Nakagawa S, Deli MA, Nakao S, Honda M, Hayashi K, Nakaoke R, Kataoka Y, Niwa M. 2007. Pericytes from brain microvessels strengthen the barrier integrity in primary cultures of rat brain endothelial cells. Cell. Mol. Neurobiol. 27:687–694.

Omidi Y, Campbell L, Barar J, Connell D, Akhtar S, Gumbleton M. 2003. Evaluation of the immortalised mouse brain capillary endothelial cell line, b.End3, as an in vitro blood-brain barrier model for drug uptake and transport studies. Brain Res. 990:95–112.

Pardridge WM. 2012. Drug Transport across the Blood–Brain Barrier. J. Cereb. Blood Flow Metab. 32:1959–1972.

Pardridge WM. 2005. The blood-brain barrier: Bottleneck in brain drug development. NeuroRX 2:3–14.

Patel R, Page S, Al-Ahmad AJ. 2017. Isogenic blood-brain barrier models based on patient-derived stem cells display inter-individual differences in cell maturation and functionality. J. Neurochem. 142:74–88.

Preston JE, Joan Abbott N, Begley DJ. 2014. Transcytosis of macromolecules at the blood-brain barrier. Adv. Pharmacol. 71:147–163.

Ransohoff RM, Schafer D, Vincent A, Blachère NE, Bar-Or A. 2015. Neuroinflammation: Ways in Which the Immune System Affects the Brain. Neurotherapeutics 12:896–909.

Reeson P, Tennant KA, Gerrow K, Wang J, Novak SW, Thompson K, Lockhart KL, Holmes A, Nahirney PC, Brown CE. 2015. Delayed inhibition of VEGF signaling after stroke attenuates blood-brain barrier breakdown and improves functional recovery in a comorbidity-dependent manner. J. Neurosci. 35:5128–5143.

Sagare AP, Bell RD, Zhao Z, Ma Q, Winkler EA, Ramanathan A, Zlokovic BV. 2013. Pericyte loss influences Alzheimer-like neurodegeneration in mice. Nat. Commun. 4:2932.

Sato K, Nagai J, Mitsui N, Ryoko Yumoto, Takano M. 2009. Effects of endocytosis inhibitors on internalization of human IgG by Caco-2 human intestinal epithelial cells. Life Sci. 85:800–807.

Schenk GJ, De Vries HE. 2016. Altered blood–brain barrier transport in neuro-inflammatory disorders. Drug Discov. Today Technol. 20:5–11.

Schlachetzki F, Zhu C, Pardridge WM. 2002. Expression of the neonatal Fc receptor (FcRn) at the blood-brain barrier. J. Neurochem. 81:203–206.

Schnitzer JE, Oh P, Pinney E, Allard J. 1994. Filipin-sensitive caveolae-mediated transport in endothelium: Reduced transcytosis, scavenger endocytosis, and capillary permeability of select macromolecules. J. Cell Biol. 127:1217–1232.

Sengillo JD, Winkler EA, Walker CT, Sullivan JS, Johnson M, Zlokovic BV. 2013. Deficiency in mural vascular cells coincides with blood-brain barrier disruption in Alzheimer's disease. Brain Pathol. 23:303–310.

Sevigny J, Chiao P, Bussière T, Weinreb PH, Williams L, Maier M, Dunstan R, Salloway S, Chen T, Ling Y, Gorman JO, Qian F, Arastu M, Li M, Chollate S, Brennan MS, Quintero-Monzon O, Scannevin RH, Arnold HM, Engber T, Rhodes K, Ferrero J, Hang Y, Mikulskis A, Grimm J, Hock C, Nitsch RM, Sandrock A. 2016. The antibody aducanumab reduces Aβ plaques in Alzheimer's disease. Nature 537:50–56.

Shayan G, Adamiak B, Relkin NR, Lee KH. 2012. Longitudinal analysis of novel Alzheimer's disease proteomic cerebrospinal fluid biomarkers during intravenous immunoglobulin therapy. Electrophoresis 33:1975–1979.

Shayan G, Choi YS, Shusta EV., Shuler ML, Lee KH. 2011. Murine in vitro model of the blood-brain barrier for evaluating drug transport. Eur. J. Pharm. Sci. 42:148–155.

Shimizu F, Nishihara H, Sano Y, Takeshita Y, Takahashi S, Maeda T, Takahashi T, Abe M, Koga M, Kanda T. 2015. Markedly increased IP-10 production by blood-brain barrier in neuromyelitis optica. PLoS One 10.

Sofroniew M V. 2015. Astrocyte barriers to neurotoxic inflammation. Nat. Rev. Neurosci. 16:249–263.

Sperling RA, Aisen PS, Beckett LA, Bennett DA, Craft S, Fagan AM, Iwatsubo T, Jack CR, Kaye J, Montine TJ, Park DC, Reiman EM, Rowe CC, Siemers E, Stern Y, Yaffe K, Carrillo MC, Thies B, Morrison-Bogorad M, Wagster M V., Phelps CH. 2011. Toward defining the preclinical stages of Alzheimer's disease: Recommendations from the National Institute on Aging-Alzheimer's Association workgroups on diagnostic guidelines for Alzheimer's disease. Alzheimer's Dement. 7:280–292.

St-Amour I, Paŕe I, Alata W, Coulombe K, Ringuette-Goulet C, Drouin-Ouellet J, Vandal M, Soulet D, Bazin R, Calon F. 2013. Brain bioavailability of human intravenous immunoglobulin and its transport through the murine blood-brain barrier. J. Cereb. Blood Flow Metab. 33:1–10.

Stebbins MJ, Wilson HK, Canfield SG, Qian T, Palecek SP, Shusta EV. 2016. Differentiation and characterization of human pluripotent stem cell-derived brain microvascular endothelial cells. Methods 101:93–102.

Stewart PA. 2000. Endothelial Vesicles in the Blood-Brain Barrier: Are They Related to Permeability? Cell. Mol. Neurobiol. 20:149–163.

Stine WB, Dahlgren KN, Krafft GA, LaDu MJ. 2003. In vitro characterization of conditions for amyloid-β peptide oligomerization and fibrillogenesis. J. Biol. Chem. 278:11612–11622.

Tarasoff-Conway JM, Carare RO, Osorio RS, Glodzik L, Butler T, Fieremans E, Axel L, Rusinek H, Nicholson C, Zlokovic BV, Frangione B, Blennow K, Ménard J, Zetterberg H, Wisniewski T, de Leon MJ. 2015. Clearance systems in the brain—implications for Alzheimer disease. Nat. Rev. Neurol. 11:457–470.

Thal DR, Griffin WST, de Vos RAI, Ghebremedhin E. 2008. Cerebral amyloid angiopathy and its relationship to Alzheimer's disease. Acta Neuropathol. 115:599–609.

Thomson JA, Ludwig TE. 2012. Primate Pluripotent Stem Cells Cultured in Medium Containing Gamma-aminobutyric Acid, Pipecolic Acid and Lithium. U.S. U.S. Patent 8,158,424.

Triguero D, Buciak JB, Yang J, Pardridge WM. 1989. Blood-brain barrier transport of cationized immunoglobulin G: enhanced delivery compared to native protein. Proc. Natl. Acad. Sci. 86:4761–4765.

Verheyen A, Diels A, Dijkmans J, Oyelami T, Meneghello G, Mertens L, Versweyveld S, Borgers M, Buist A, Peeters P, Cik M. 2015. Using human iPSC-derived neurons to model TAU aggregation. PLoS One 10:1–15.

von Kleist L, Stahlschmidt W, Bulut H, Gromova K, Puchkov D, Robertson MJ, MacGregor KA, Tomlin N, Pechstein A, Chau N, Chircop M, Sakoff J, Von Kries JP, Saenger W, Kräusslich HG, Shupliakov O, Robinson PJ, McCluskey A, Haucke V. 2011. Role of the clathrin terminal domain in regulating coated pit dynamics revealed by small molecule inhibition. Cell 146:471–484.

Wang YI, Abaci HE, Shuler ML. 2017. Microfluidic blood–brain barrier model provides in vivo-like barrier properties for drug permeability screening. Biotechnol. Bioeng. 114:184–194.

Wang Y, Jin S, Sonobe Y, Cheng Y, Horiuchi H, Parajuli B, Kawanokuchi J, Mizuno T, Takeuchi H, Suzumura A. 2014. Interleukin-1β induces blood-brain barrier disruption by downregulating sonic hedgehog in astrocytes. PLoS One 9:e110024.

Wanjare M, Kusuma S, Gerecht S. 2014. Defining differences among perivascular cells derived from human pluripotent stem cells. Stem Cell Reports 2:561–575.

Weidenfeller C, Svendsen CN, Shusta EV. 2007. Differentiating embryonic neural progenitor cells induce blood-brain barrier properties. J. Neurochem. 101:555–565.

Weksler BB, Subileau EA, Perrière N, Charneau P, Holloway K, Leveque M, Tricoire-Leignel H, Nicotra A, Bourdoulous S, Turowski P, Male DK, Roux F, Greenwood J, Romero IA, Couraud PO. 2005. Blood-brain barrier-specific properties of a human adult brain endothelial cell line. FASEB J. 19:1872–1874.

Wilhelm I, Fazakas C, Krizbai IA. 2011. In vitro models of the blood-brain barrier. Acta Neurobiol. Exp. 71:113–128.

Wilhelmus MMM, Otte-Höller I, van Triel JJJ, Veerhuis R, Maat-Schieman MLC, Bu G, de Waal RMW, Verbeek MM. 2007. Lipoprotein Receptor-Related Protein-1 Mediates Amyloid-β-Mediated Cell Death of Cerebrovascular Cells. Am. J. Pathol. 171:1989–1999.

Williams R, Yao H, Dhillon NK, Buch SJ. 2009. HIV-1 Tat co-operates with IFN-gamma and TNF-alpha to increase CXCL10 in human astrocytes. PLoS One 4:e5709.

Winkler EA, Nishida Y, Sagare AP, Rege S V, Bell RD, Perlmutter D, Sengillo JD, Hillman S, Kong P, Nelson AR, Sullivan JS, Zhao Z, Meiselman HJ, Wenby RB, Soto J, Abel ED, Makshanoff J, Zuniga E, De Vivo DC, Zlokovic BV. 2015. GLUT1 reductions exacerbate Alzheimer's disease vasculo-neuronal dysfunction and degeneration. Nat. Neurosci. 18:521–530.

Wuest DM, Lee KH. 2012. Optimization of endothelial cell growth in a murine in vitro blood-brain barrier model. Biotechnol. J. 7:409–417.

Wuest DM, Lee KH. 2014. Amyloid-β concentration and structure influences the transport and immunomodulatory effects of IVIG. J. Neurochem. 130:136–144.

Wuest DM, Wing AM, Lee KH. 2013. Membrane configuration optimization for a murine in vitro blood-brain barrier model. J. Neurosci. Methods 212:211–221.

Xia MQ, Bacskai BJ, Knowles RB, Qin SX, Hyman BT. 2000. Expression of the chemokine receptor CXCR3 on neurons and the elevated expression of its ligand IP-10 in reactive astrocytes: in vitro ERK1/2 activation and role in Alzheimer's disease. J. Neuroimmunol. 108:227–235.

Yagi T, Ito D, Okada Y, Akamatsu W, Nihei Y, Yoshizaki T, Yamanaka S, Okano H, Suzuki N. 2011. Modeling familial Alzheimer's disease with induced pluripotent stem cells. Hum. Mol. Genet. 20:4530–4539.

Yao Y, Tsirka SE. 2014. Monocyte chemoattractant protein-1 and the blood-brain barrier. Cell. Mol. Life Sci. 71:683–697.

Yu J, Vodyanik MA, Smuga-Otto K, Antosiewicz-Bourget J, Frane JL, Tian S, Nie J, Jonsdottir GA, Ruotti V, Stewart R, Slukvin II, Thomson JA. 2007. Induced pluripotent stem cell lines derived from human somatic cells. Sci. (New York, NY) 318:1917–1920.

Yu YJ, Watts RJ. 2013. Developing Therapeutic Antibodies for Neurodegenerative Disease. Neurotherapeutics 10:459–472.

Zhang Y, Pardridge WM. 2001. Mediated efflux of IgG molecules from brain to blood across the blood–brain barrier. J. Neuroimmunol. 114:168–172.

Zlokovic BV, Skundric DS, Segal MB, Lipovac MN, Mackic JB, Davson H. 1990. A saturable mechanism for transport of immunoglobulin G across the blood-brain barrier of the guinea pig. Exp. Neurol. 107:263–270.

Zlokovic BV. 2011. Neurovascular pathways to neurodegeneration in Alzheimer's disease and other disorders. Nat. Rev. Neurosci. 12:723–738.

Appendix A

REPRINT PERMISSIONS

Reprinted with permission from:

Mantle JL, Min L, Lee KH. 2016. Minimum Transendothelial Electrical Resistance Thresholds for the Study of Small and Large Molecule Drug Transport in a Human in Vitro Blood-Brain Barrier Model. Mol. Pharm. 13:4191–4198.

Appendix B

IPSC-DERIVED BRAIN MICROVASCULAR ENDOTHELIAL CELL COCULTURE WITH MURINE ASTROCYTES

B.1 Introduction

Coculture with astrocytes has been shown to be an effective way to improve barrier properties of BMECs grown in culture (Abbott et al., 2010; Helms et al., 2016). Furthermore, coculture with mixed species has been successfully employed to improve TEER and other barrier properties (Lippmann et al., 2012). In an effort to achieve a more *in vivo*-like model, coculture with murine astrocytes and culture with murine astrocyte conditioned medium were investigated.

B.2 Methods

iPSCs were differentiated into BMECs and grown on Transwell inserts as described in Chapter 2 (Section 2.3.1).

Murine astrocytes were isolated from postnatal mice pups and kindly provided by Dr. Davide Trotti (Department of Biochemistry and Molecular Biology, Thomas Jefferson University, Philadelphia, PA, USA) using established protocols (Gibb, et al. 2007). Astrocytes were grown on T-25 tissue culture flasks in DMEM/F-12 supplemented with 20% fetal bovine serum, 0.25% gentamicin, 0.2% primocin, 0.2%

fungin, and 1% antibiotic solution (100 U/mL penicillin and 100 µg/mL streptomycin) and fed every three days. Cells were maintained in a humidified cell culture incubator at 37 °C with 5% CO2 for at least one week until coculture initiation.

On Day 5 of BMEC differentiation, astrocytes were passaged to the bottom chamber of 24-well companion plates that had previously been coated with 5 g/cm2 poly-D-lysine for 12 hours at 37 °C. Astrocyte conditioned medium was collected from cells grown in T-25 flasks and centrifuged for 10 minutes at 1000 RPM. The supernatant was aspirated and stored at 4 °C until use. Coculture was initiated on Day 9 of differentiation, when the iPSC-derived BMECs were passaged onto Transwell inserts and placed into the companion plates containing astrocytes.

B.3 Results and Discussion

Monoculture and culture with murine astrocyte conditioned media yielded similar results, with a peak TEER around 1700 Ω·cm². BMECs grown in astrocyte conditioned media had elevated TEER from Day 2 to Day 3, compared to a peak on Day 2 followed by a significant drop on Day 3 (Figure B.1). BMECs grown in coculture with murine astrocytes had significantly lower TEER, which peaked at about 500 Ω·cm², however TEER remained relatively constant throughout the four days of the experiment.

From these experiments, we concluded that astrocytes do impact barrier function however murine astrocytes do not improve the TEER of human stem cell-

derived BMECs. Species differences have been observed in other model systems; Wuest et al. (2012) observed a decrease in TEER and an increase in permeability when murine BMECs were cocultured with rat astrocytes instead of murine astrocytes (Wuest and Lee, 2012). Because there was a detrimental effect on barrier tightness, murine astrocyte coculture was not pursued further and alternate sources of astrocytes were investigated. These results are discussed in Chapter 3.

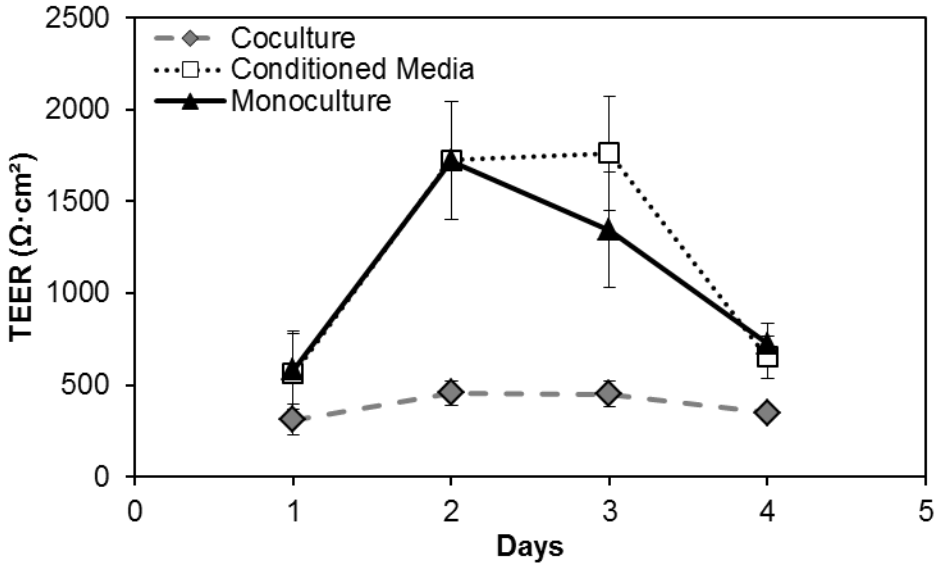

Figure B.1. TEER with mouse astrocyte coculture. TEER was measured for four days following coculture with mouse astrocytes (gray) or addition of mouse astrocyte conditioned media (white). Day 9 of differentiation is Day 0 of coculture. (n = 9; three independent experiments; error bars represent the standard error of the mean).

REFERENCES

Abbott NJ, Rönnbäck L, Hansson E. 2006. Astrocyte-endothelial interactions at the blood-brain barrier. Nat. Rev. Neurosci. 7:41–53.

Gibb, S. L., Boston-Howes, W., Lavina, Z. S., Gustincich, S. etal., A caspase-3-cleaved fragment of the glial glutamate transporter EAAT2 is sumoylated and targeted to promyelocytic leukemia nuclear bodies in mutant SOD1-linked amyotrophic lateral sclerosis. J. Biol. Chem. 2007, 282,32480–32490

Helms HC, Abbott NJ, Burek M, Cecchelli R, Couraud PO, Deli MA, Förster C, Galla HJ, Romero IA, Shusta EV, Stebbins MJ, Vandenhaute E, Weksler B, Brodin B. 2016. In vitro models of the blood-brain barrier: An overview of commonly used brain endothelial cell culture models and guidelines for their use. J. Cereb. Blood Flow Metab. 36:862–890.

Lippmann ES, Azarin SM, Kay JE, Nessler R a, Wilson HK, Al-Ahmad A, Palecek SP, Shusta EV. 2012. Derivation of blood-brain barrier endothelial cells from human pluripotent stem cells. Nat. Biotechnol. 30:783–791.

Wuest DM, Lee KH. 2012. Optimization of endothelial cell growth in a murine in vitro blood-brain barrier model. Biotechnol. J. 7:409–417.

Appendix C

EFFECTS OF AMYLOID BETA CONFORMATION ON BARRIER FUNCTION

C.1 Introduction

Aβ is produced in the brain by cleavage of amyloid precursor protein. In AD, Aβ peptide monomers aggregate into soluble oligomers, protofibrils, fibrils and eventually plaques. While plaques are a pathological hallmark of AD, there is evidence that soluble oligomers are the more cytotoxic form (Dalgren, et al., 2002). Previous work has shown that soluble oligomers are more detrimental to BBB function in a murine *in vitro* model (Wuest and Lee, 2014). As a first step towards choosing an appropriate AD model, we investigated the effects of oligomers and fibrils in the human iPSC-based BBB model.

C.2 Methods

Aliquots of human $A\beta_{1-42}$ (described in Chapter 4, Section 4.3.2) was aggregated into either oligomers or fibrils as previously described (Dalgren et al., 2002; Stine et al., 2003). $A\beta_{1-42}$ was dissolved to 5 mM in anhydrous dimethyl sulfoxide. To prepare oligomers, peptide solution was diluted to 100 μM in cold phenol-free Ham's F-12 media with L-glutamine and incubated at 4 °C for 24 hours.

To prepare fibrils, peptide solution was diluted to 100 μM in 10 mM HCl and incubated at 37 °C for 24 hours.

To confirm Aβ conformation, atomic force microscopy (AFM) analysis was performed. Aβ oligomers or fibrils were diluted to 10 μM in water. Aliquots of 50 μL were applied to freshly cleaved mica and allowed to adsorb for 5 minutes at room temperature, rinsed with water and air dried. Images were taken with a Vecco Multimode AFM with Nanoscope IIA Controller.

BMECs were passaged to Transwell inserts on Day 9, 5 μM $A\beta_{1-42}$ was added to abluminal compartments on Day 10 and experiments were performed on Day 11 after 24 hours of incubation with $A\beta_{1-42}$.

C.3 Results and Discussion

AFM analysis confirms the presence of fibrillar and oligomeric structures (Figure C.1). With the addition of $A\beta_{1-42}$, the barrier is loosened by 20% in both the oligomer and fibril cases to a final TEER value of about 2000 $\Omega \cdot cm^2$ (Figure C.2, A). Despite this reduction in TEER, the overall value remains above the transport thresholds for both small (500 $\Omega \cdot cm^2$) and large (1000 $\Omega \cdot cm^2$) molecules (Section 2.4.5). The transport rate of IgGs across the BBB doubles after the addition of oligomeric $A\beta_{1-42}$ (Figure C.2, B). This increase in transport rate of antibodies cannot be explained by a breakdown of the paracellular barrier, as TEER remains above the 1000 $\Omega \cdot cm^2$ threshold.

The results of these preliminary studies demonstrate that oligomeric Aβ has a greater effect on the integrity of the BBB and provide justification for using only the oligomeric form of Aβ in Chapter 4. Additionally, these studies provide further evidence of a breakdown in transcellular transport in pathological states before tight junction integrity is impaired.

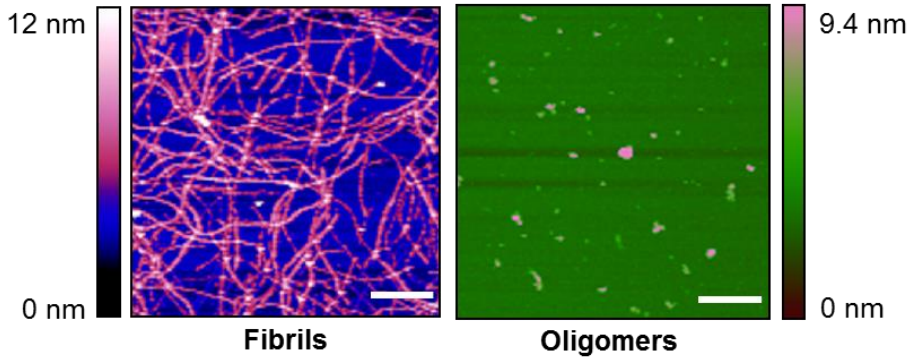

Figure C.1. Atomic force microscopy of amyloid beta conformation. Preparation of Aβ fibrils (left) and oligomers (right) were confirmed using AFM. Scale bars are 500 nm.

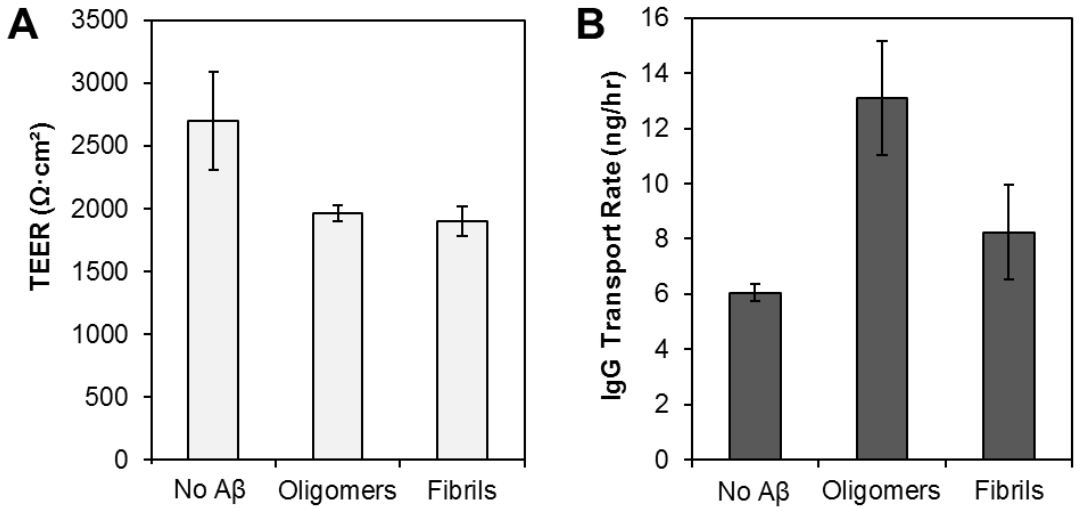

Figure C.2. Effects of Aβ conformation on barrier properties. BMECs were incubated with 5 μM $A\beta_{1-42}$ for 24 hours and (A) TEER and (B) IgG transport rate were quantified.

REFERENCES

Dahlgren KN, Manelli AM, Stine WB, Baker LK, Krafft GA, Ladu MJ. 2002. Oligomeric and fibrillar species of amyloid-β peptides differentially affect neuronal viability. J. Biol. Chem. 277:32046–32053.

Stine WB, Dahlgren KN, Krafft GA, LaDu MJ. 2003. In vitro characterization of conditions for amyloid-β peptide oligomerization and fibrillogenesis. J. Biol. Chem. 278:11612–11622.

Wuest DM, Lee KH. 2014. Amyloid-β concentration and structure influences the transport and immunomodulatory effects of IVIG. J. Neurochem. 130:136–144.

Appendix D

CYTOKINES AND CHEMOKINES SECRETED IN RESPONSE TO $A\beta_{1-42}$ IN COCULTURE AND MONOCULTURE

D.1 Preface

In Chapter 3, the cytokines and chemokines secreted by BMECs and astrocytes in response to neuroinflammation were quantified. Analogous experiments were performed with BMECs in monoculture or coculture exposed to 5 μM $A\beta_{1-42}$ for 24 hours. Only two cytokines were detected above the limit of quantitation: MCP-1 and IL-8. These results are shown in Figure D.1.

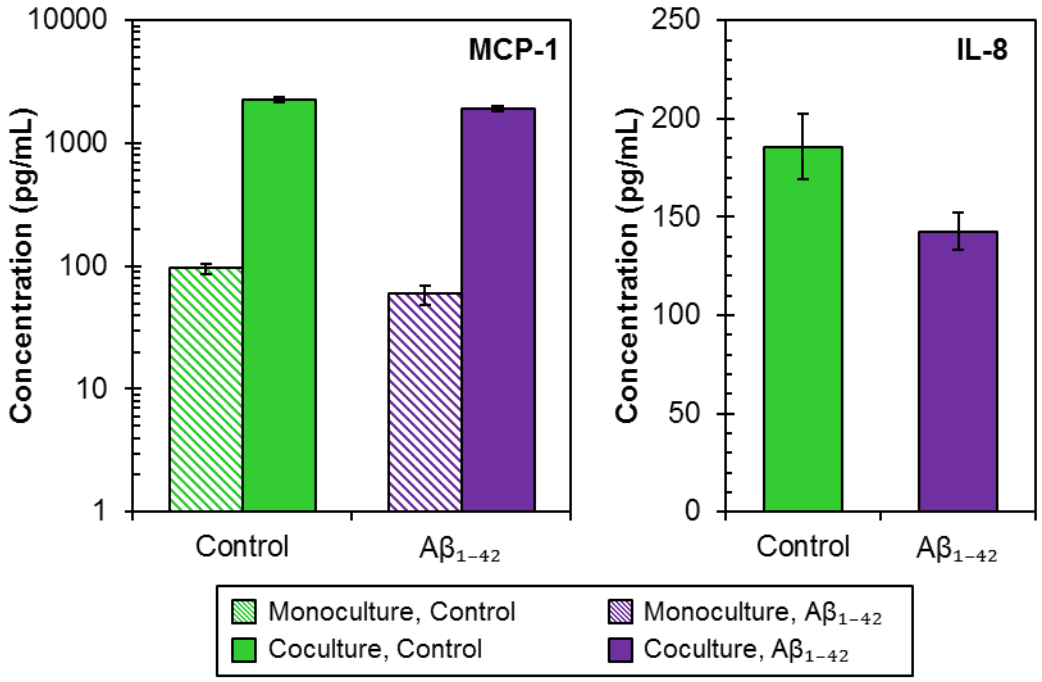

Figure D.1. Concentrations of cytokines and chemokines measured by Luminex assay after incubation with $A\beta_{1-42}$. Abluminal concentrations of 25 human cytokines and chemokines were measured after 24 hours of incubation with $A\beta_{1-42}$ or control media for cells grown in monoculture or coculture. Of the cytokines assayed, only MCP-1 and IL-8 were detected in the $A\beta_{1-42}$ cases.

Appendix E

PRELIMINARY WORK TO IDENTIFY MECHANISM OF TRANSPORT BREAKDOWN IN DISEASE: QRT-PCR OF AND MFSD2A AND FCRN

E.1 Introduction

This work provides evidence that a transcellular breakdown occurs in pathological states before there is a significant decline in tight junction integrity. There is a significant increase in NaFl permeability in inflammation without a corresponding decrease in TEER below the small molecule transport threshold of 500 $\Omega \cdot cm^2$ (Figure 3.1). There is also an increase in IgG transport in inflammation (Figure 3.5). Furthermore, in Chapter 4, there is a significant increase in IgG uptake and transport after incubation with $A\beta_{1-42}$ and with cytokines. We sought to identify a mechanism responsible for these changes in transcellular transport in pathological states and tested two hypotheses.

We first hypothesized that MFSD2A (major facilitator super family domain containing 2a; *MFSD2A*) expression decreases in disease states. In the development of the BBB, an increase in MFSD2A expression is correlated with a suppression of transcytosis activity and a sealing of the BBB (Ben-Zvi et al., 2014). Furthermore, Andreone et al. recently demonstrated that suppression of caveolar endocytosis specifically is responsible for the sealing of the barrier during development (Andreone

et al., 2017). Because the BBB develops a paracellular barrier first and a transcellular barrier second, and in disease breakdown occurs in the reverse order, we hypothesized that MFSD2A might be involved in BBB breakdown as well.

Our second hypothesis was that FcRn (neonatal Fc receptor; *FCGRT*) expression decreases in disease. FcRn extends serum half-life of IgGs in other endothelial cells by rescuing it from degradation and recycling the IgG back to the blood stream (Roopenian and Akilesh, 2007). FcRn is present at the BBB and may be involved in reverse transcytosis of IgGs out of the brain (Zhang and Pardridge, 2001; Schlachetzki et al., 2002). Furthermore, the iPSC-BMECs express FcRn (Figure 4.1). Because IgGs are more readily transported across the BBB in the disease models, we hypothesized that a lower expression of FcRn and therefore less recycling back to the blood compartment could be responsible for these observed changes in transport.

These two hypotheses were investigated by quantifying relative gene expression of *MFSD2A* and *FCGRT* in disease models compared to control cells. Gene expression via qRT-PCR was chosen as an initial screening technique because it is relatively quick and simple, compared to other methods that quantify gene or protein expression.

E.2 Methods

On Day 9 of differentiation, BMECs were passaged to 24 well plates. To mimic neuroinflammation, 10 ng/mL of IL-6 and 10ng/mL TNF-α were added to the

appropriate wells on Day 10. To mimic AD, 5mM $A\beta_{1-42}$ was added to the appropriate wells on Day 10. On Day 12, half the wells were collected for western blot analysis. Cells were rinsed with DPBS, 300 µL trypsin-EDTA was added for 10 minutes and 700 µL EC- media was added to neutralize trypsin. Three wells were pooled per 1.5 mL tube and cells were centrifuged at 350xg for 5 minutes at room temperature. Culture medium was aspirated, cells were washed with DPBS and centrifuged again. Cell was aspirated and the cell pellets were stored at -80 ℃. On Day 12, the other half of the wells were collected for qRT-PCR. RNA was isolated using the RNeasy Mini Kit (Qiagen) according to the manufacturer's protocol. RNA concentration was quantified using a NanoDrop ND-1000 UV-Vis Spectrophotometer. Samples were stored at -80 ℃.

Probes and primers were purchased from IDT (Table F.2) and TaqMan RNA-to-C_T 1-Step Kit was purchased from ThermoFisher Scientific. qRT-PCR was performed according to the TaqMan RNA-to-C_T 1-Step Kit protocol. The reaction plate was run on an AB7500 thermocycler with the following steps: 1) Hold 48 °C for 15 minutes, 2) Hold 95 °C for 10 minutes, 3) Cycle (40 cycles) 95 °C for 15 seconds followed by 60 °C for 1 minute. Data were analyzed by relative standard curve and the $\Delta\Delta C_T$ methods.

Table F.2. Probes and primers for qRT-PCR.

Gene	***MFSD2A***	***FCGRT***	***GAPDH***
Reason	Expression correlated with in transcytosis suppression	Responsible for IgG recycling	Housekeeping gene
IDT Prod. #	Hs.PT.58.2075445	Hs.PT.58.26878788.g	Hs.PT.39a.22214836
Probe	/56-FAM/CCG GCC CAG /ZEN/GTG AAG AAA GAA CC/3IABkFQ/	/56-FAM/CCC CTT GGA /ZEN/TCT CCC TTC GTG G/3IABkFQ/	/56-FAM/AAG GTC GGA /ZEN/GTC AAC GGA TTT GGT C/3IABkFQ/
Primer 2	GCA TCC TCC AAA GCA CTG AA	TGT AGG AGG AGC TCT GTT GT	ACA TCG CTC AGA CAC CAT G
Primer 1	CAA GTG CAT AGC AAA GCT TGT	ACA TCC TTC AAA TCA GCA TCC T	ACA TCC TTC AAA TCA GCA TCC T

E.3 Results

Differences in gene expression of *MFSD2A* between disease models and the control were not statistically significant (Figure E.1, A). Differences in gene expression of *FCGRT* between the disease models and the control were not statistically significant (Figure E.1, B).

These results are inconclusive. This work could benefit from using additional techniques to test these hypotheses, such as MRM to quantify peptide levels or western blot to quantify protein expression level. MRM requires significant work to select appropriate transitions to develop a functional assay. Western blots are semi-quantitative and greatly depend on the quality of antibodies selected.

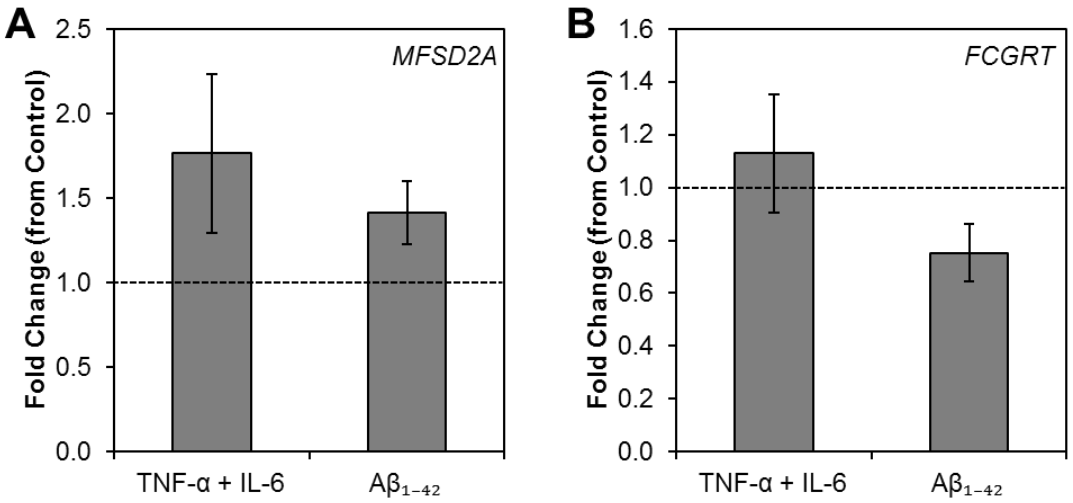

Figure E.1. Gene expression levels in inflammation and AD models. Expression of (A) MFSD2A and (B) FCGRT after 24h incubation with TNF-α and IL-6 or $A\beta_{1-42}$, relative to expression levels in the control. Data shown were analyzed by the $\Delta\Delta C_t$ method to calculate a fold change over the control (n = 3; three independent experiments; three technical replicates performed for each biological replicate; error bars represent standard error of the mean)

REFERENCES

Andreone BJ, Chow BW, Tata A, Lacoste B, Ben-Zvi A, Bullock K, Deik AA, Ginty DD, Clish CB, Gu C. 2017. Blood-Brain Barrier Permeability Is Regulated by Lipid Transport-Dependent Suppression of Caveolae-Mediated Transcytosis. Neuron 94:581–594.

Ben-Zvi A, Lacoste B, Kur E, Andreone BJ, Mayshar Y, Yan H, Gu C. 2014. MSFD2A is critical for the formation and function of the blood brain barrier. Nature 509:507–511.

Roopenian D, Akilesh S. 2007. FcRn: the neonatal Fc receptor comes of age. Nat. Rev. Immunol. 7:715–725.

Schlachetzki F, Zhu C, Pardridge WM. 2002. Expression of the neonatal Fc receptor (FcRn) at the blood-brain barrier. J. Neurochem. 81:203–206.

Zhang Y, Pardridge WM. 2001. Mediated efflux of IgG molecules from brain to blood across the blood–brain barrier. J. Neuroimmunol. 114:168–172.